AD710769

This document has been approved for public release and sale; its distribution is unlimited.

LMSC Technical Report N-3L-70-1

Project Number
NR-025-390
ARPA Order No. 925

ATOMIC LINE TRANSITIONS AND RADIATION FROM HIGH TEMPERATURE AIR

by

R. R. Johnston, O. R. Platas, and L. M. Tannenwald
Lockheed Palo Alto Research Laboratory
1970 July 15

Research supported by the U. S. Advanced Research Projects Agency through the U. S. Office of Naval Research under Contract N00014-68-C-0481.

ABSTRACT

The status of the current investigation into the radiant emission from high temperature air is described. A treatment of emission by molecular species and some new results in line broadening is included.

Results are presented for air at temperatures 0.5 to 5.0 eV and densities from 1.0 to 10^{-4} times normal.

TABLE OF CONTENTS

I. Introduction

The previous report distributed under this program (Ref. 1) described our approach toward a theoretical prediction of the spectral radiant emission from high temperature atomic air and included some preliminary results. This report describes an extension of the previous results toward lower temperatures at which radiation from molecular species must be included.

The atomic transitions dominating the integrated emissivity are generally of reasonably well-known strength, width, and energy (Ref. 2 and 3). Thus we expect our estimates of the spectral air absorption coefficient to be quite reliable where the absorption coefficient is large. Indeed, our integrated emissivities agreed well with other reported values (Ref. 4, 5) which, in turn, generally agree with experimental observations.

For radiation transport calculations, however, results are often dominated by values of the spectral absorption coefficient where it is small - the Rosseland mean free path employed in radiation diffusion theory is an inverse mean of the absorption coefficient (Ref. 1, Eq. 36). Such values of the absorption coefficient generally include many small contributions - including transitions with small occupation numbers and wings from distant lines. Experimental observation and theoretical prediction of many of these contributions is difficult. (Much of the uncertainty in the magnitude of the N^- cross section involves estimates of such contributions.) Accordingly, much of our effort this past year has been aimed toward an improved prediction of the absorption coefficient where it is small by isolating

individual contributions and attempting improved theoretical estimates thereof.

In Section II we review our definitions of radiation quantities, and Section III treats some improvements in line width estimates, including a discussion of the line profile in the line wings. Section IV describes our molecular emissivity model, with Section V summarizing our results. For calculation of autoionization cross sections and for numerical configuration-interaction Hartree-Fock calculations the integration of the electron-electron matrix elements between many-particle states of differing orbital occupation is a tedious exercise in Racah algebra. Considerable simplicity is gained with techniques of second quantization (Ref. 6), our treatment of which constitutes Appendix A.

Some of this work was included in our semi-annual report (Ref. 7) - of limited distribution. We repeat it here for completeness with our currently "best" results.

II. The Radiative Emissivity

The total power radiated per unit surface area by a uniform isothermal plasma of temperatures T, density ρ, may be written approximately (Ref. 1, Eq. 30 et seq.)

$$\overline{J} \approx \pi \int_0^\infty B(\omega) \left[1 - e^{-\mu'(\omega) L}\right] d\omega \ (\text{watts/cm}^2) \qquad (1)$$

in terms of the black body function

$$B(\omega)\, d\omega = \frac{15}{\pi^4} \frac{(\sigma T^4)}{\pi} \frac{u^3 du}{e^u - 1} \ (\text{watts/cm}^2/\text{sterad.}) \qquad (2)$$

Here the photon energy ω and temperature T are in eV, $u = \omega/T$ (dimensionless), and $\sigma = 1.028 \times 10^5$ watts/cm^2 eV^4. L(cm) is a geometric parameter characterizing the spatial extent of the radiating plasma:

(i) Plane slab, thickness a: $L = 2a(cm)$

(ii) Circular cylinder, radius r: $L = 2r(cm)$

and

$$\mu'(\omega) = \mu(\omega)\,(1 - e^{-\omega/T})$$

in terms of the absorption coefficient $\mu(\omega)$ (cm^{-1}) for photons of energy ω in air at the temperature T, density ρ.

For a <u>thick</u> source, ($\mu'L \gg 1$ for most ω) $\bar{J} = \sigma T^4$, the black body result obtains. It is convenient to describe the energy emitted as a fraction of the black body emission at the same temperature. We thus define a dimensionless emissivity $\epsilon(T,\rho,L)$ depending on temperature T, density ρ, and geometric parameter L, according to

$$\bar{J}(T,\rho,L) \equiv \epsilon(T,\rho,L)(\sigma T^4) \quad . \tag{3}$$

That is,

$$\epsilon(T,\rho,L) = \frac{15}{\pi^4 T^4} \int_0^\infty \omega^3 \, d\omega \, \frac{e^{-\omega/T}}{(1-e^{-\omega/T})} \left[1-e^{-\mu'(\omega)L}\right] \quad . \tag{4}$$

If $(\mu'L) \ll 1$ for most ω the Planck mean opacity is a convenient result,

$$\bar{\mu}_P = \frac{15}{\pi^4 T^4} \int_0^\infty \omega^3 \, e^{-\omega/T} \, \mu(\omega) \, d\omega \ (cm^{-1}) \tag{5}$$

in terms of which

$$\epsilon(T,\rho,L \to 0) = \bar{\mu}_P \, L \quad . \tag{6}$$

The physics problem is the determination of the basic absorption coefficient $\mu(\omega)$ and is described in Ref. 1 and in subsequent sections of this report. The numerical problem of the evaluation of the integral (Eq. 4) over the photon energy ω is the topic of Appendix B.

III. The Absorption Line Profile

The results presented in Ref. 1 assumed the atomic lines to be broadened only due to the interactions of the radiating atoms with free electrons - Stark broadening. At higher temperatures or lower densities the Doppler width may dominate the Stark width, and at lower temperatures and high density the resonance and Van der Waals atom-atom interactions become important. The results presented here include both these effects, our treatment of which is described in subsections A and B.

The Baranger-Griem classical path impact theory for line widths of neutral radiators has been amply verified experimentally (Ref. 8). Our version of this theory is reported in Ref. 1. For ion lines, however, the corresponding theory generally predicts widths too small by factors of two or more. Some recent theoretical (Ref. 9) and experimental (Ref. 10) results suggest the modifications described in subsection C, where we include for comparison our estimates, alternative theoretical values, and experimental results.

At high temperatures or low densities the multitude of contributing atomic and ionic lines in most all spectral intervals tends to preclude emission dominance at any frequency from far wings of lines. At lower temperatures and high densities the opposite may be true. Our previous results for normal

density air at kT = 1.0 eV provides such an example (Fig. 1 - a more recent version of Fig. 8 of Ref. 1). The continuum absorption coefficient for photons of energy $\omega = 5.0$ eV is $\mu_c = 1.05 \times 10^{-2}$ cm^{-1}; the Lorentz wing of the dominating NI line ($2p^3(^4S) \rightarrow 2p^2(^3P)3s(^4P)$) at the same energy contributes $\mu(\text{line}) = 2.02 \times 10^{-2}$ cm^{-1}, although the line center and width are 10.33 eV and 3×10^{-3} eV, respectively. That is, assuming a pure Lorentz profile, the continuum is dominated by a line located over 1000 half-widths away.

The inapplicability of the simple Baranger-Griem impact theory to such circumstances is well known. The possible magnitude of the error resulting from ignoring the appropriate validity criteria is a new result. In subsection D we describe some new line wing approximations we intend to incorporate into our codes so as to predict the absorption coefficient in such wings more reliably.

IIIA. Doppler Broadening and the Voigt Line Shape

Due to thermal motions of the radiating atoms an infinitely sharp spectral line at photon energy ω_o takes on the Doppler shape (Ref. 11)

$$b_D(\omega) = \frac{1}{\sqrt{\pi}\, W_D} \exp\left[-\left(\frac{\omega - \omega_o}{W_D}\right)^2\right] \tag{7}$$

where the Doppler width W_D is given by

$$W_D = \omega_o \sqrt{\frac{2kT}{Mc^2}} \quad . \tag{8}$$

M is the mass of the radiating species.

For air atoms:

$$W_D/\omega_o \cong 1.2 \times 10^{-5} \sqrt{T_{eV}}$$

For air molecules: (diatomic)

$$W_D/\omega_o \approx 0.85 \times 10^{-5} \sqrt{T_{eV}} \quad .$$

The collision width of Ref. 1 depends on the relative velocity of the radiator and perturber. For electron perturbers the radiator thermal velocities are much smaller than electron velocities and the Lorentz and Doppler broadening mechanisms may be independently treated. For atomic perturbers, however, the comparability of thermal and collisional velocities should couple the Lorentz and Doppler broadening (Ref. 3, 12). At the lower temperatures when atom-atom perturbations are expected to be important, resonance broadening is velocity independent (see Section B below), but Van der Waals broadening varies as $\langle v^{3/5} \rangle$, where v is the relative velocity, so a coupled approach may be expected to modify the line shape somewhat.

The results reported here assume Lorentz and Doppler broadening mechanisms are independent, the resulting line profile being the Voigt profile (Ref. 13).

$$b_\nu(\omega) = \frac{1}{\pi^{3/2} W_D} \int_{-\infty}^{\infty} \frac{dy}{1 + y^2} \exp\left[-\left(\frac{x-y}{\kappa}\right)^2\right] \qquad (9)$$

$$x = \left(\frac{\omega - \omega_o}{W_C}\right), \quad \kappa = W_D/W_C$$

and W_C is the Lorentz collision width of Ref. 1. We approximate this function as follows:

(i) ($\kappa < 0.2$ or $|x| > 5\kappa$): (Modified Lorentz limit, Ref. 14)

$$b_V(\omega) = \frac{1}{2\pi W_C}\left[\frac{1}{1 + (x + \kappa/\sqrt{2})^2} + \frac{1}{1 + (x - \kappa/\sqrt{2})^2}\right] \qquad (9a)$$

(ii) ($|x| \leq 5\kappa$ and $\kappa > 5.0$): (Modified Doppler limit)

$$b_V(\omega) = \frac{1}{\sqrt{\pi}\, W_D} e^{-\left(\frac{\omega - \omega_o}{W_D}\right)^2}\left[1 + \frac{1}{\kappa^2}\left(1 - 2\frac{x^2}{\kappa^2}\right)\right] + \frac{1}{\kappa} f\left(\frac{|x|}{\kappa}\right)\} \qquad (9b)$$

where $f(y)$ is the slowly varying function tabulated in Table I.

(iii) ($|x| \leq 5\kappa$ and $0.2 \leq \kappa \leq 5.0$) Tabulated values from Ref. 14 (reproduced in Ref. 15, Pg. B-14)

As discussed in Ref. 1 estimates of the emissivity contributions of individual lines are useful for identifying critical transitions as well as providing a monitor to the more detailed (and presumably more accurate) numerical integration. For a purely Lorentz line shape, the Ladenburg-Reiche approximation applies (Ref. 1, Eq. 39). For the Voigt profile no such simple approximation obtains. Recently, extensive numerical tabulations of "equivalent widths" for Voigt profiles have been published (Ref. 16) which should be useful for detailed work. For our purpose a simpler approximation is sufficient. We employ the Curtis approximation - quoted in Ref. 17 (p. 72) - according to which the emissivity of an isolated

spectral line with Voigt shape may be approximated

$$\epsilon_V = \epsilon_{LR} + \epsilon_D - \frac{\epsilon_{LR}\epsilon_D}{(\bar{\mu}_p L)} = \epsilon_{LR}\left(1 - \frac{\epsilon_D}{\bar{\mu}_p L}\right) + \epsilon_D \qquad (10)$$

ϵ_{LR} is the Ladenburg-Reiche result and ϵ_D is the isolated line emissivity for a pure Doppler profile,

$$\epsilon_D = \bar{\mu}_p L \sum_{n=0}^{\infty} \frac{(-x_D)^n}{\sqrt{n+1}\,(n+1)!} \approx \bar{\mu}_p L \times \begin{cases} e^{-\frac{1}{2}\sqrt{x_D}} & (x_D < 26) \\ \frac{2}{x_D}\sqrt{\frac{\ln x_D}{\pi}} & (x_D > 26) \end{cases} \qquad (11)$$

where

$$x_D = \pi\left(\frac{W_C}{W_D}\right)\mu_L(\omega_C)$$

in terms of the absorption coefficient at line center, $\mu_L(\omega_C)$, assuming purely Lorentz collision broadening.

Our computer program employs the Curtis approximation (Eq. 10) with the Doppler approximations (Eq. 11). Comparison with our detailed line integration results, in cases where one expects an isolated line approximation to be valid, indicates these approximations are generally valid to better than ten per cent accuracy.

IIIB. Resonance and Van der Waals Broadening

At high density and low temperatures the number density of free electrons becomes sufficiently small that atom-atom broadening becomes important. The theory of such broadening has been worked out by Griem (Ref. 3) in a perturbation theory approach with a "strong collision" cutoff chosen to satisfy unitarity (analogous to the Stark broadening treatment of Ref. 1). Here we merely reproduce his results in the form employed in our calculations.

The line absorption coefficient for ground state atoms is broadened by the resonance exchange collisions of the excited (final state) atom with other ground state atoms. If N_g is the number density of the ground state atoms, f_R and ω_R the absorption oscillator strength and energy, respectively, of the resonance line under consideration, the line width is

$$W_{Res} = 3\pi \sqrt{\frac{g_1}{g_2}} \left(\frac{e^2\hbar^2}{M\omega_R}\right) f_R N_g$$

$$= 12\pi \sqrt{\frac{g_1}{g_2}} \left(\frac{Ryd.}{\omega_R}\right) f_R (N_g a_o^3) \quad (Ryd.) \qquad (12)$$

(g_1 and g_2 are statistical weights of the lower and upper states, respectively.)

Except for resonance exchange collisions atom-atom perturbations are dominated by Van der Waals interactions. If N_n is the total number density of neutral perturbers, Griem (Ref. 3) estimates the broadening as due to strong collisions alone,

$$W_V = (\pi\rho_{Min}^2)\, h\langle v\rangle\, N_n ,$$

where the polarizability entering ρ_{Min} is estimated by a closure approximation similar to Ref. 1.

$$\rho_{Min} = \left(\frac{9\pi\hbar^5\overline{r^2}}{16m^3vE_P^2}\right)^{1/5}$$

$$= \left(\frac{c}{v}\right)^{1/5} \left[\frac{9\pi}{4}\alpha \left(\frac{Ryd.}{E_P}\right)^2 \overline{r^2}\right]^{1/5} a_o .$$

Here $\overline{r^2}$ is the mean squared atomic radius of the upper state in atomic units (Ref. 1, Eq. 22) and E_p is a representative excitation energy - taken to be the energy of the strongest resonance line. For neutral oxygen and nitrogen E_p = 10 eV = 0.74 Ryd agrees within 20% with the experimental values, which is likely within the validity limits of the closure approximation itself. With these approximations we obtain

$$W_V = 6.87 \times 10^{-22} N_n \left(\frac{kT}{Mc^2}\right)^{3/10} \left[\left(\frac{Ryd}{E_p}\right)^2 \overline{r^2}\right]^{2/5} \quad (eV)$$

$$= 8.0 \times 10^{-25} N_n(cm^{-3}) (T_{eV})^{3/10} (\overline{r^2})^{2/5} \quad (eV) \qquad (13)$$

for air. Observing that $\overline{r^2} \sim 5\nu^4/2$ in terms of the "effective quantum number" ν of the upper state (Ref. 1) and writing $N_n = 5.37 \times 10^{19}(\rho/\rho_o)$,

$$\underline{\text{Van der Waals}}: \quad W_V \approx 6.4 \times 10^{-5}(\rho/\rho_o)\, T_{eV}^{3/10}\, \nu^{8/5} \quad (eV) \qquad (14a)$$

For comparison, we list the corresponding expressions for

$$\underline{\text{Doppler}}: \quad W_D = 1.2 \times 10^{-5}\, \omega_{eV} \sqrt{T_{eV}} \quad (eV) \qquad (14b)$$

$$\underline{\text{Resonance}}: \quad W_{Res} \approx 5.6 \times 10^{-2} (F_g \rho/\rho_o) \sqrt{\frac{g_1}{g_2}}\, (f_R/\omega_R(eV)) \quad (eV) \qquad (14c)$$

$$\underline{\text{Adiabatic Stark}}: \quad W_S \approx 1.0 \times 10^{-3} (F_i \rho/\rho_o) T_{eV}^{1/6}\, \nu^{8/3} \quad (eV) \qquad (14d)$$

where the approximations of eq. 14a have been applied to eq. 21 of Ref. 1. F_g is the fraction of the atoms in the ground state, and F_i is the fractional ionization of the plasma (assuming singly-charged ions only). (All the numerical values above are for air atoms only.)

The results presented in this report assume the collision width, W_C, to be given by

$$W_C = W_S + W_V(+ W_R)$$

where W_S is from Ref. 1, W_V (Eq. 13, above), and W_R, where applicable, from Eq. 12 (above). The resulting W_C is combined with the Doppler width as described in Section A above.

IIIC. Electron Impact Broadening of Ion Lines

Numerous attempts have been made to explain the discrepancy between classical path impact theory and experiment for ion line widths (see, for example, Ref. 18-20). Although the resulting discrepancies were sometimes decreased, they were sometimes increased. Overall differences as much as factors of two generally remained.

In view of these uncertainties in theoretical prediction we chose to follow the semi-empirical approach familiar in astrophysical applications (Ref. 1 and Ref. 21, for example), an approach independently suggested by Griem (Ref. 22). The line width is written

$$w_i = \frac{h}{2} < n_e v \ \sigma_j (v) >_{Av} \qquad (15)$$

as a thermal average over the n_e electrons (cm^{-3}) of the total inelastic scattering cross section, which we write

$$\begin{aligned} \sigma_j(v) &= \sum_k \sigma_{j\to k}(v) \\ &= \sum_k \frac{2(2\pi Ryd)^2}{\sqrt{3}\omega_{jk}} f_{jk}\, g(\omega_{jk}, \epsilon) a_0^2 \ . \end{aligned} \qquad (16)$$

ϵ is the energy of the incident electron, ω_{jk} and f_{jk} the energy difference and f-number, respectively, between states j and k, and the "effective Gaunt factor" $g(\omega_{jk}, \epsilon)$ is chosen to reproduce collisional excitation experiments. (Note: if $\omega_{jk} > 0$, f_{jk} is the absorption f-number; if $\omega_{jk} < 0$, it is the emission f-number.) Performing the thermal average indicated in Eq. 15, we obtain

$$w_j(\text{eV}) = 5.22 \times 10^{-21} \frac{n_e(\text{cm}^{-3})}{\sqrt{T(\text{eV})}} \sum_k \frac{f_{jk}}{\omega_{jk}(\omega)} G(\omega_{jk}, T) \qquad (17)$$

in terms of the thermal-averaged Gaunt factor

$$G(\omega,T) = \int_0^\infty e^{-y} dy \; g(\omega, yT) \; .$$

Our previous results followed van Regemorter (Ref. 23), whose Gaunt factor we approximated (Ref. 24, Eq. 4-142)

$$\begin{aligned} g_{BBW}(\omega, \epsilon) &= 0.20 && (\epsilon < 2\omega) \\ &= 0.052 \ln x && (\epsilon \geq 2\omega, \; 0 < \ln x \leq 1.45) \\ &= g_1 \equiv 0.30 (\ln x - 1.2) \\ &= g^c(\eta_i, \eta_f) \end{aligned} \Bigg\} \begin{array}{l} \text{Interpolated for } (1.45 \leq \\ \ln x \leq 6) \\ \ln x \geq 6 \end{array} \qquad (18a)$$

where

$$x = \left(\frac{k+k'}{|k-k'|}\right) , \quad k^2 = \left(\frac{\epsilon}{\text{Ryd}}\right) a_0^{-2} , \quad (k')^2 = \left(\frac{\epsilon-\omega}{\text{Ryd}}\right) a_0^{-2} \; .$$

$g^c(\eta_i, \eta_f)$ is the Coulomb Gaunt factor (Ref. 25)

We interpolate linearly (in ln x) between g_1 and g^c for $(1.45 \leq \ln x \leq 6)$.

Recently, Bely and Griem (Ref. 9) employed t-matrices for Mg^+ evaluated by

close-coupling calculations to evaluate the line width of the resonance transition. They express their results in terms of an "effective Gaunt factor" (through Eq. 15, 16 above) and find results comparable to those of van Regemorter near threshold and approximately a factor of two greater than his at higher energies. We fit their results as follows:

$$g_{BG}(\omega, \epsilon) = 0.160 + \frac{1}{2}\frac{\epsilon}{\mathrm{Ryd}} \qquad (\epsilon \leq \omega)$$

$$= g_o + \frac{\ln x}{1.65}(0.41 - g_o) \qquad (0 \leq \ln x \leq 1.65) \qquad (18b)$$

$$= g_1 \equiv 0.13 + 0.17 \ln x \qquad (1.65 \leq \ln x \leq 3.0)$$

$$g_o = g_{BG}(\omega,\omega) = 0.160 + \frac{1}{2}\frac{\omega}{\mathrm{Ryd}} \ .$$

For $\omega \ll \epsilon$ general considerations lead one to expect $g(\omega, \epsilon) \rightarrow g^c(\eta_i,\eta_f)$, the Coulomb Gaunt factor. Thus a suitable extrapolation procedure between g_{BG} and g^c is necessary. For our calculations, we choose

$$g_R(\omega,\epsilon) = g_{BG}(\omega,\epsilon) \qquad (\ln x \leq 1.65)$$

$$= \left(\frac{3.0 - \ln x}{1.35}\right) g_1 + \left(\frac{\ln x - 1.65}{1.35}\right) g^c(\eta_i,\eta_f) \qquad (1.65 \leq \ln x \leq 3) \qquad (18c)$$

$$= g^c(\eta_i,\eta_f) \qquad (\ln x \geq 3)$$

In Figure 2 are the thermal-averaged Gaunt factors obtained from these alternative approximations, for temperature kT = 2.0 eV. Using these Gaunt factors we have evaluated the line widths of some recently measured NII lines (Ref. 10). The results are in Table II, including our previous results and some earlier theoretical values as well as the observed experimental values. Comparing the

Bely-Griem (Eq. 18b) and Bely-Griem-Coulomb (18c) Gaunt factors of Figure 2, it is evident that good agreement depends as much on a suitably chosen interpolation to the coulomb limit as on threshold details.

The Gaunt factor of Eq. 18c has been included in our present code. Figure 3 presents the associated thermal averaged Gaunt factor at several temperatures.

IIID. Line Wing Absorption

As described in the introduction to this chapter, photon absorption in the far wings of strong, isolated lines may contribute substantially to the valleys in the total absorption coefficient, especially at the lower temperatures and higher densities. Baranger and Stewart (Ref. 27) early considered the absorption in windows between spectral lines of ions and introduced the "one-electron" approximation. Griem (Ref. 28-30) has extensively studied the line wings of hydrogen in the one-electron approximation. When the atom-perturber interactions - as measured by the impact theory widths - are of the order of the splitting of the atomic levels with the same principal quantum number Griem's hydrogen results should apply. We are principally concerned here, therefore, with isolated lines.

Near the line center the impact approximation is generally valid for electrons, and the line profile obtains from averaging over the large number of contributing weak interactions. Assumptions regarding lack of correlation among the perturbers during the perturbation "time," or equivalently, non-overlapping (in time) of the atom-single perturber interactions, allows the average over the product of the perturber interactions to be expressed as

the product of the averages and the usual Lorentz profile obtains.

If $\Delta\omega$ is the displacement of the photon energy of interest, ω, from the energy of the unperturbed line, ω_{ij}

$$\Delta\omega = \omega - \omega_{ij} = \omega - (\epsilon_i - \epsilon_j) \ , \tag{19}$$

and w_j is the impact theory line width, the Lorentz wing profile is

$$b_{ij}(\omega) \xrightarrow[\Delta\omega \gg w_j]{} \frac{1}{\pi(\Delta\omega)^2} \ w_j \ , \tag{20}$$

where the collision part of the width is given by (Ref. 1, Eq. 18)

$$w_j^c = n_e \int_0^\infty dv \ f(v) h v \left[\frac{4\pi}{3} \lambda^2 \sum_k R_{jk} \int_{\rho_{Min}}^\infty \frac{d\rho}{\rho} A\left(\frac{\rho \ \omega_{jk}}{hv}\right) \right] \ . \tag{21}$$

$f(v)$ is the Maxwell velocity distribution of the $n_e(cm^{-3})$ perturbers of mass m, $\lambda = \frac{\hbar}{mv}$, $R_{jk} = \overline{|\langle k|\vec{r}|j\rangle|^2}$, averaged and summed over magnetic substates, and $A(Z)$ is expressed in terms of Bessel functions of imaginary argument

$$A(Z) = Z^2 \left[K_0^2(|Z|) + K_1^2(Z)\right] \ . \tag{22a}$$

Comparing with Eq. 16, noting $R_{jk} = 3\left(\frac{Ryd}{\omega_{jk}}\right) f_{jk}$, we see the function

$$a(Z) = \int_Z^\infty \frac{dZ'}{Z'} A(Z') \tag{22b}$$

plays the role of an "effective Gaunt factor" for electron-atom collisions. This classical path impact theory is valid if $\rho_{Min} \gg \lambda^2$, if $kT \gg \omega_{jk}$ contributing importantly to Eq. 21, and $\Delta\omega \ll \omega_p$ = ($\hbar$ x Plasma frequency).

Far from the line center, the perturbation "time" $\tau = \hbar/\Delta\omega$ will become short enough that perturber motion may be neglected. Then the quasi-static

approximation is valid. The line profile may then be described in terms of the static field distribution function W(F). For isolated states non-degenerate in orbital angular momentum, the quadratic Stark shift applies, according to which energy levels, $\epsilon_j(F)$, in a field F are shifted from their unperturbed values ϵ_j by

$$\epsilon_j(F) = \epsilon_j + C_j F^2$$

where

$$C_j = 2a_0^3 \sum_k \left(\frac{Ryd}{\omega_{jk}}\right)^2 f_{jk} . \tag{23}$$

The line profile is then given by

$$b_{ij}^{QS}(\omega) = \int_0^\infty dF W(F)\, \delta(\Delta\omega + C_j F^2) \tag{24}$$

$$= \frac{1}{2\sqrt{C_j \Delta\omega}} W\left(\sqrt{\frac{\Delta\omega}{C_j}}\right) ,$$

if only the upper state is significantly perturbed. (Inclusion of the lower state replaces C_j by $(C_j - C_i)$.) For the simple Holtsmark distribution (Ref. 26)

$$W(F)\, dF \approx \frac{3}{2}\left(\frac{F_0}{F}\right)^{3/2} \frac{dF}{F}$$

and

$$b_{ij}^{Holts.}(\omega) = \frac{3}{4\Delta\omega}\left(\frac{\Delta\omega_0}{\Delta\omega}\right)^{3/4} \tag{25}$$

where

$$\Delta\omega_0 = (13.6\bar{Z}^2)(Na_0^3)^{4/3}\left(\frac{C_j}{a_0^3}\right)(Ryd)$$

for N quasi-static perturbers (cm^{-3}) of mean charge $\bar{Z}$. The quasi-static

distribution is expected to apply for frequencies (Ref. 29, Eq. 8)

$$\Delta\omega > \frac{kT}{\sqrt{r_j^2/a_0^2}} \tag{26}$$

In the intermediate region, $w_j \ll \Delta\omega \lesssim \frac{kT}{\sqrt{r_j^2/a_0^2}}$, the one-electron approximation is valid if the impact approximation is valid at the line center. As discussed by Baranger (Ref. 11), the one-electron theory treats the photon absorption as a three-body collision,

$$e + h\nu + (\text{Atom}) \rightarrow e' + (\text{Atom})^* ,$$

where the spectator electron provides overall energy conservation. Thus, in the red wing, $\Delta\omega < 0$, the electron must provide energy $\Delta\omega$, while it absorbs $\Delta\omega$ in the blue wing. This results in a line asymmetry as $\Delta\omega \rightarrow kT$ due to the population depletion of electrons with energy $\epsilon \gtrsim \Delta\omega$, hence a suppression of the red wing.

Clearly such an energy-conserving picture requires that the interaction be completed in the time $\tau \sim \hbar/\Delta\omega$. In terms of classical path impact parameters, only electrons with velocities v and impact parameters ρ satisfying $\rho \lesssim (\frac{\hbar v}{\Delta\omega})$ may contribute, the so-called Lewis cutoff (Ref. 31). Our intention in this section is to provide a formulation of the line wing absorption profile which varies continuously from the impact to quasi-static limits, delineates the appropriate limiting conditions, and incorporates the above-mentioned line asymmetry due to electron population depletion.

From standard time-dependent perturbation theory one easily obtains the line profile function (see, for example, Ref. 3, Eq. 4-21, or Ref. 11, Eq. 9-23).

$$L(\omega) = \frac{1}{\pi} \mathrm{Re} \sum_{\alpha\beta\beta'\sigma} \rho_\alpha \langle \alpha | d_\sigma | \beta \rangle \langle \beta' | d_\sigma | \alpha \rangle \int_0^\infty ds e^{-\frac{i}{\hbar}(\omega-\omega_{\alpha\beta})s} \{ \langle \beta | U(s,0) | \beta' \rangle \}_{Av}$$

where we have made the usual classical path approximation and have assumed only the upper state to be significantly perturbed. ρ_α is the density matrix - assumed diagonal - for (unperturbed) lower atomic state α, $\vec{d}$ is the electron dipole moment operator, $U(s,0)$ is the interaction representation time-evolution operator of the atomic states β - due solely to perturber interactions - and the average $\{\ldots\}_{Av.}$ is taken over all perturber classical paths. Expressing the time-evolution operator in terms of the time-dependent potential due to the classical perturber trajectories, and retaining only the second-order (lowest non-trivial) term, one obtains (after interchanging orders of integration)

$$L(\omega) = \frac{1}{\pi} \mathrm{Re} \sum_{\alpha\beta\beta'\sigma} \rho_\alpha \langle \alpha | d_\sigma | \beta \rangle \langle \beta' | d_\sigma | \alpha \rangle \sum_{\beta_2} \left(\frac{-i}{\hbar}\right)^2 \int_0^\infty dt e^{\frac{-i}{\hbar}(\omega-\omega_{\alpha\beta})t} \int_0^\infty dt_1 e^{\frac{-i}{\hbar}(\omega-\omega_{\alpha\beta_2})t_1} \cdot$$

$$\int_0^\infty dt_2 e^{\frac{-i}{\hbar}(\omega-\omega_{\alpha\beta'})t_2} \{ \langle \beta | V(t_1+t_2) | \beta_2 \rangle \langle \beta_2 | V(t_2) | \beta' \rangle \}_{Av} .$$

In the one-electron approximation the average is to be taken over all classical paths of a single perturber. Assuming the statistical distribution of perturbers is stationary

$$\{ f(t+\tau) f(t) \}_{Av} = \{ f(\tau) f(0) \}_{Av} ,$$

we obtain (Ref. 29, Eq. 12)

$$L(\omega) = \frac{1}{\pi} \mathrm{Re} \sum_{\alpha\beta\beta'\sigma} \rho_\alpha \frac{\langle \alpha | d_\sigma | \beta \rangle \langle \beta' | d_\sigma | \alpha \rangle}{(\omega-\omega_{\alpha\beta})(\omega-\omega_{\alpha\beta'})} \sum_{\beta_2} \int_0^\infty dt_1 e^{\frac{-i}{\hbar}(\omega-\omega_{\alpha\beta_2})t_1}$$

$$\{ \langle \beta | V(t_1) | \beta_2 \rangle \langle \beta_2 | V(0) | \beta' \rangle \}_{Av}$$

and $\omega \neq \omega_{\alpha\beta}$ or $\omega_{\alpha\beta'}$.

Substituting the classical potentials

$$\langle \beta \mid V(t) \mid \beta' \rangle = e^2 \sum_{\nu=1}^{3} \frac{r_\nu(t)}{|\vec{r}(t)|^3} \langle \beta \mid R_\nu \mid \beta' \rangle$$

$$\vec{r}(t) = \vec{\rho} + \vec{v}(t-t_0), \quad \vec{\rho}\cdot\vec{v} = 0$$

and performing the one-electron average

$$n_e \int_0^\infty dv\, f(v) \int_{(4\pi)} \frac{d^2\Omega_v}{4\pi} \int_{\rho_{Min}}^{\rho_{Max}} 2\pi\rho d\rho \int_{-\infty}^{\infty} v dt_0 \,(\ldots)$$

one easily obtains

$$\{ \langle \beta \mid V(t_1) \mid \beta_2 \rangle \langle \beta_2 \mid V(0) \mid \beta' \rangle \}_{Av} = \frac{n_e e^4}{3} \int_0^\infty f(v)dv \int_{\rho_{Min}}^{\rho_{Max}} 2\pi\rho d\rho \int_{-\infty}^{\infty} v dt_0$$

$$\left[\sum_\nu \langle \beta \mid R_\nu \mid \beta_2 \rangle \langle \beta_2 \mid R_\nu \mid \beta' \rangle\right] \cdot \frac{[\rho^2 - v^2 t_0 (t_1 - t_0)]}{[\rho^2 + v^2(t_1-t_0)^2]^{3/2} [\rho^2 + v^2 t_0^2]^{3/2}} .$$

Then, with substitutions $x_1 = \frac{vt_0}{\rho}$, $x_2 = \frac{v}{\rho}(t_0 - t_1)$

$Z_{\alpha\beta_2} = \frac{\rho}{\hbar v}(\omega_{\alpha\beta_2} - \omega)$, the time-integrations result in

$$L(\omega) = \frac{1}{\pi} \mathrm{Re} \sum_{\alpha\beta\beta'\sigma} \rho_\alpha \frac{\langle \alpha \mid d_\sigma \mid \beta \rangle \langle \beta' \mid d_\sigma \mid \alpha \rangle}{(\omega - \omega_{\alpha\beta})(\omega - \omega_{\alpha\beta'})} \frac{n_e e^4}{3} \sum_{\beta'',\nu} \langle \beta \mid R_\nu \mid \beta'' \rangle \langle \beta'' \mid R_\nu \mid \beta' \rangle .$$

$$\cdot \int_0^\infty f(v)vdv \int_{\rho_{Min}}^{\rho_{Max}} 2\pi\rho d\rho \left(\frac{2}{\rho^2 v^2}\right) C\left[\frac{\rho}{\hbar v}(\omega_{\alpha\beta''} - \omega)\right]$$

where $C(X) = A(X) + iB(X)$ is defined in Ref. 1. (Note, $A(X)$ is even in X.)

In the line wings, we approximate $\beta' = \beta$ and extract the line shape function

$$b(\omega) = \frac{1}{\pi(\Delta\omega)^2}\left\{ n_e \int_0^\infty dv\, f(v)\, h\nu \left[\frac{4\pi}{3}\lambda^2 \sum_k R_{jk} \int_{\rho_{Min}}^{\rho_{Max}} \frac{d\rho}{\rho} A\left(\frac{\rho}{h\nu}(\omega-\omega_{ik})\right)\right.\right. \qquad (27)$$

which compares exactly with Eq. 20, 21 in terms of the same A-function (Eq. 22a) but evaluated with a frequency-dependent argument,

$$\omega-\omega_{ik} = \omega-\omega_{ij}-\omega_{jk} = \Delta\omega - \omega_{jk} .$$

Equation (27) is our basic result; it remains to evaluate the ρ-limits.

The completed collision criteria requires that

$$\rho_{Max} = \rho_2 \equiv \text{Min}\left\{\frac{h\nu}{\omega_p}, \frac{h\nu}{\Delta\omega}\right\} \equiv \frac{h\nu}{\omega_2} . \qquad (28)$$

The unitary condition requires

$$\rho_{Min}^2 \lesssim \frac{2}{3}\lambda^2 \sum_k R_{jk} \left| A\left[\frac{\rho_{Min}}{h\nu}(\Delta\omega-\omega_{jk})\right] + i\, B\left[\frac{\rho_{Min}}{h\nu}(\Delta\omega-\omega_{jk})\right]\right|$$

From the definition of ρ_{Max}, the largest value

$$\frac{\rho_{Min}}{h\nu}(\Delta\omega-\omega_{jk}) = \left(\frac{\Delta\omega-\omega_{jk}}{\omega_2}\right) \leq 1, \text{ and from tabulated values,}$$

$|A(x) + i\,B(x)| \sim 1$ for $0 \leq x \leq 1$, so we take

$$\rho_{Min}^2 \lesssim \frac{2}{3}\lambda^2 \left(\sum_k R_{jk}\right) = \frac{2}{3}\lambda^2 \left(\overline{r_j^2}\right) \approx \frac{n^4}{Z^2}\lambda^2 \qquad (29)$$

This choice of ρ_{Min} evidently satisfies the validity condition for the classical path approximation.

Near the line center, $\Delta\omega \to 0$, $\rho_2 \to \infty$ and the impact theory approximation obtains. Thus the validity conditions for impact theory must include $\Delta\omega \ll \omega_{jk}$, where k is the state lying nearest in energy to the state j and connected with it by a dipole-allowed transition. Collecting these results, our frequency-dependent "line width" becomes

$$w_j(\omega) = \frac{4\pi}{3}\,\frac{h^3}{m^2}\,n_e \int_0^\infty \frac{dv}{v}\, f(v) \sum_k R_{jk} \int_{\rho_1}^{\rho_2} \frac{d\rho}{\rho}\, A\left[\frac{\rho}{hv}\,(\Delta\omega - \omega_{jk})\right]$$

$$= \frac{8\pi}{3}\,\alpha\,(n_e a_0^3)\sqrt{\frac{2mc^2}{\pi kT}}\;W\,(\mathrm{Ryd}) \qquad (30)$$

where

$$W(\mathrm{Ryd}) = \sum_k R_{jk} \int_{y_M}^\infty dy e^{-y} \int_{Z_1(y)}^{Z_2} \frac{dZ^1}{Z^1}\, A(Z^1)$$

$$Z_2 = \left(\frac{\Delta\omega - \omega_{jk}}{\Delta\omega}\right),\quad Z_1 = \frac{y_M}{y}\,Z_2,\quad y_M = \sqrt{\frac{r_j^2}{6}}\;\left(\frac{h\Delta\omega}{kT}\right).$$

Perturbers of energy $\epsilon \leq y_M\, kT$ have been removed from the one-electron theory. According to Eq. 26, they should be added to the quasi static profile.

Generalizing the effective thermal Gaunt factor (Ref. 1, Eq. 21 and Fig. 1)

$$\alpha\,(X, \gamma) = \int_{\gamma X}^\infty dt e^{-t}\, a(X/t) - e^{-\gamma X}\, a\,(\tfrac{1}{\gamma}) \qquad (31)$$

we write

$$W(\mathrm{Ryd}) = \sum_k R_{jk}\, \alpha\left[\sqrt{\frac{r_j^2}{6}}\left(\frac{\Delta\omega - \omega_{jk}}{kT}\right),\ \frac{\Delta\omega}{\Delta\omega - \omega_{jk}}\right]. \qquad (32)$$

The function $\alpha(X, \gamma)$ is presented in Fig.54 for $0 \leq \gamma \leq 1.8$. Near the line center, $\Delta\omega \to 0$ and $\alpha(X,0)$ reproduces $\alpha(X)$ of Ref. 1. Far into the line wings, $\gamma \to 1$.

To incorporate the red wing electron depletion effect into our profile, the classical path theory is no longer adequate, as it ignores the change in

perturber energy during the interaction. It is well known from coulomb excitation theory (Ref. 32) that a classical coulomb Gaunt factor with symmetrized energy argument $\bar{\epsilon} = \frac{1}{2}(\epsilon_i + \epsilon_f)$ frequently provides an adequate representation of the quantum mechanical result. We similarly symmetrize our Gaunt factor, obtaining

$$W(\mathrm{Ryd}) = \sum_k R_{jk} \left\{ e^{-\frac{\Delta\omega}{kT}} \alpha\left[\sqrt{\frac{\overline{r_j^2}}{6}} \left(\frac{\Delta\omega - \omega_{jk}}{kT} \right), \frac{\Delta\omega}{\Delta\omega - \omega_{jk}} \right] - \right.$$

$$\left. (1 - e^{-\Delta\omega/kT})\, e^{-\left(\sqrt{\frac{\overline{r_j^2}}{6}} \frac{\Delta\omega}{kT} \right)} a\left(\frac{\Delta\omega - \omega_{jk}}{\Delta\omega} \right) \right\}. \qquad (33)$$

The strong collision impact theory term must be similarly treated. We find

$$w_j^s(\omega) = 2\pi\alpha\,(n_e a_0^3) \sqrt{\frac{2mc^2}{\pi kT}} \left[\sum_k R_{jk} \left(\frac{kT}{\Delta\omega - \omega_{jk}} \right) \right]^{2/3} e^{-y_M} \left(\frac{\pi}{3} \right)^{2/3} \Gamma\left(\frac{5}{3} \right) \qquad (34)$$

and the total one-electron width is the sum of Eq. 34 and 30, with W from Eq. 33. Finally, the number density, N, in the quasi static term (Eq. 25) must be increased by the number of electrons removed from the one-electron term

$$N \rightarrow N + n_e \int_0^{y_M} \frac{2}{\sqrt{\pi}}\, y^{1/2}\, e^{-y}\, dy \qquad (35)$$

With these expressions we have obtained a computationally feasible formulation of the absorption line profile varying continuously from the impact theory line center to the quasi-static far line wing. These equations have not yet been incorporated into our radiative mean computer programs, but will be shortly.

IV. The Molecular Absorption Coefficient and Emissivity

For temperatures below kT = 1.0 eV, absorption by molecular species becomes of primary importance. Avilova et al. (Ref. 4) recently summarized molecular contributions to the air absorption coefficient. Comparison with earlier work (Ref. 51 and 53) indicated some large differences, toward the resolution of which most of the work here described has been directed. In almost all cases our results will be found to be in general agreement with Avilova (Ref. 4).

In subsection A, below, we define our notation and write down our representation of the absorption coefficient of a single molecular line. We have employed both the "smeared band" model of Avilova (Ref. 4) and a more detailed three-branch "PQR-model," as described in subsection B. The molecular bands we have studied and the associated data constitute subsection C, and in subsection D we describe some emission band models we have studied. Finally, in subsection E, we briefly describe our molecular absorption coefficient computer program ABSMOL.

Our notation closely follows Herzberg (Ref. 38) and Nicholls (Ref. 52), and we shall frequently follow the convention of choosing wave number κ as our energy variable, noting that a wave number $10^4 cm^{-1}$ corresponds to an energy 1.240 eV.

IVA. The Absorption Coefficient of a Molecular Line

Molecular states are labeled according to their electronic state e, the component of electronic angular momentum along the internuclear axis Λ, and the rotation and vibration quantum numbers J and v, respectively. Upper states are singly primed (') and lower states are doubly primed (").

We consider a transition from a lower state $i \equiv (v'',J'',e'',\Lambda'')$, one of d_m states of energy ϵ_m, to an upper state $j \equiv (v',J',e',\Lambda')$ of energy ϵ_n and degeneracy d_n. The f-number for such a transition is (Ref. 38, 52)

$$f_{m\to n} = \frac{1}{3}\left(\frac{\epsilon_{mn}}{Ryd}\right) q_{v'v''} S^{J'\Lambda'}_{J''\Lambda''} \frac{R_e^2(\bar{r}_{v'v''})}{d_m} , \qquad (36)$$

in terms of which we may express the absorption coefficient as

$$\mu_{m\to n}(\kappa) = \pi r_o N_m f_{m\to n} b_{mn}(\kappa) \quad (cm^{-1}) . \qquad (37)$$

$$(r_o = e^2/mc^2 = 2.818 \times 10^{-13} \text{ cm})$$

$N_m(cm^{-3})$ is the number density of molecules in the (lower) state m, and $b_{mn}(\kappa)$ (cm) is a line shape factor, normalized according to

$$\int_0^\infty d\kappa\, b_{mn}(\kappa) = 1 .$$

In eq. 36, $\varepsilon_{mn} = (\epsilon_n - \epsilon_m)$ is the transition photon energy, $q_{v'v''}$ the Franck-Condon factor, $S^{J'\Lambda'}_{J''\Lambda''}$ the Hönl-London factor, and $R_e^2(\bar{r}_{v'v''})$ the electronic transition moment in atomic units. In writing down eq. 36 we have assumed the validity of the Born-Oppenheimer approximation, and we shall further assume R_e^2 to be a smoothly varying function of its argument $\bar{r}_{v'v''}$, the r-centroid (Ref. 52)

To relate N_m to the species number density N, we introduce the partition function Q and decompose the state energy into electronic, vibrational, and rotational parts,

$$\epsilon_m = \epsilon_{e''} + \epsilon_{v''} + \epsilon_{J''} ,$$

or, in wave number units,

$$\frac{1}{hc}\epsilon_m = T_{e''} + G_{v''} + F_{J''} \ (cm^{-1}) .$$

$T_{e''}$ is the electronic energy of the state (measured to the minimum of the

potential curve) and we approximate (Ref. 38)

$$G_v = G(o) + G_o(v) = G(o) + \omega_o v - \omega_o x_o v^2 + \omega_o y_o v^3 + \ldots$$

$$F_J = B_v J(J+1)$$

$$B_v = B_e - \alpha_e(v + \tfrac{1}{2})$$

Then

$$N_m = N\left(\frac{d_m}{Q}\right) e^{-\epsilon_m/kT}$$

$$d_m = (2J'' + 1)\, d_{e''} \quad , \quad d_{e''} = (2S'' + 1)(2 - \delta_{\Lambda'',0})$$

and the usual approximations - assuming $kT \gg hcB_v$ - result in

$$Q = Q_V Q_R Q_{el}$$

$$Q_V = e^{-G(o)/\theta}\left(1 - e^{-\omega_o/\theta}\right)^{-1}$$

$$Q_R = \theta/B_v \ ,$$

where $\theta = kT/hc$ is the temperature in cm^{-1}. Gilmore (Ref. 40) tabulates

$$f_{e''}(T) = \frac{d_{e''}}{Q_{el}} e^{-\epsilon_{e''}/kT}$$

for most molecules of interest to us. Writing $N_{e''} = f_{e''}(T)N$, we finally obtain

$$N_m = N_{e''}\left(\frac{B_{v''}}{\theta}\right)\left(1 - e^{-\omega_o''/\theta}\right)(2J'' + 1)\, e^{-[G_o(v'') + F_{J''}]/\theta} \ . \qquad (38)$$

Combining the above expressions our final form of the absorption coefficient is

$$\mu_{m\to n}(\kappa) = \frac{\pi r_o}{3} N_{e''}\left(\frac{B_{v''}}{\theta}\right)\left(1 - e^{-\omega_o''/\theta}\right) e^{-[G_o(v'') + F_{J''}]/\theta}$$

$$\times \left(\frac{\kappa_{mn}}{Ryd}\right) q_{v'v''}\, S^{J'\Lambda'}_{J''\Lambda''} \left[\frac{R_e^2(\bar{r}_{v'v''})}{d_{e''}}\right] b_{mn}(\kappa) \quad (cm^{-1}) \qquad (39)$$

[Note: Many authors (ex. Ref. 4) include the electronic statistical factor $d_{e''}$ in their definition of the electronic transition moment, so care should be taken when comparing numerical values.]

We write the transition energy κ_{mn} variously as

$$\begin{aligned}\kappa_{mn} &= (T_{e'} - T_{e''}) + (G_{v'} - G_{v''}) + (F_{J'} - F_{J''}) \\ &= \kappa_{oo} + [G_o(v') - G_o(v'')] + (F_{J'} - F_{J''}) \\ &= \kappa_{v'v''} + (F_{J'} - F_{J''})\end{aligned}$$

where κ_{oo} is the energy of the transition $[e',v' = o,J' = o,\Lambda'] \longleftrightarrow [e'',v'' = o,J'' = o,\Lambda'']$, the so-called "o-o" transition.

IVB. Molecular Band Models

In applications we are generally interested in an averaged molecular absorption coefficient - averaged over an energy interval $\Delta\kappa$ much greater than a molecular line width W and generally large enough to contain many individual lines. That is, for a particular pair of electronic states (e',e'') we define

$$\bar{\mu}_{e'e''}(\kappa) = \frac{1}{\Delta\kappa} \int_{\kappa}^{\kappa+\Delta\kappa} d\kappa' \{ \sum_{\substack{v''J'' \\ v'J'}} \mu_{mn}(\kappa') \} \qquad (40)$$

$$= \sum_{\substack{v''J'' \\ v'J'}} [\frac{\mu_{mn}}{b_{mn}\Delta\kappa}]$$

summed over all values of v'',J'',v',J' for which κ_{mn} is in the interval $\Delta\kappa$ about κ. To this end the $(J' - J'')$ selection rules must be considered.

In general, $J' = J''$, $J'' \pm 1$, leading to the three branches (Ref. 38, Eq. IV, 32-34):

$$\begin{aligned}
&\text{"Q-branch"} \quad (J' = J'') && \kappa^{Q}_{mn} = \kappa_{v'v''} + (B_{v'} - B_{v''})\ J''(J''+1) \\
&\text{"R-branch"} \quad (J' = J'' + 1) && \kappa^{R}_{mn} = \kappa^{Q}_{mn} + 2B_{v'}\ (J''+1) \\
&\text{"P-branch"} \quad (J' = J'' - 1) && \kappa^{P}_{mn} = \kappa^{Q}_{mn} - 2B_{v'}\ (J''+1)
\end{aligned} \tag{41}$$

For electronic angular momentum $\Lambda \neq 0$, details of the Λ - J coupling may lead to further splitting of these branches. For simplicity we have ignored such coupling; our Hönl-London factors are those of a rotating top and are tabulated by Herzberg (Ref. 38, p. 208). Care should be taken with Herzberg's formulae, as, for $\Delta \Lambda \neq 0$, they must be multiplied by a factor of two in order to satisfy the sum rule (Ref. 52)

$$\sum_{J'} S^{J'' \Lambda''}_{J' \Lambda'} = (2J'' + 1)\ . \tag{42}$$

Explicitly writing the rotational sum terms of Eqs. 39 and 40:

$$\mathcal{A}_{v'v''} = \sum_{J'J''} \frac{\kappa_{mn}}{\Delta\kappa} S^{J'\Lambda'}_{J''\Lambda''}\, e^{-B_{v''}J''(J''+1)/\theta} \tag{43a}$$

The maximum value of J'' we choose to be the smallest of the following:

$$J_1 = \left\{ \frac{1}{B_{v''}} \left[D''_e - G''(0) - \omega_0 v'' + \omega_0 x_0 v''^2 \right] \right\}^{1/2}$$

(and the same with (') replacing (''))

$$J_2 = 5.0 \sqrt{\theta / B_{v''}}$$

J_1 refers to the Morse-Potential dissociation limit, and J_2 is effectively an occupation number cutoff.

Equations (39-43) explicitly define our "PQR-Branch" model. All the molecular absorption coefficients presented in this report were generated by this model.

At higher temperatures, $\theta = \frac{kT}{hc}$ ($\sim 10^3$ cm^{-1}) becomes much greater than $B_{v''}$ (~ 1 cm^{-1}), and we clearly wish to replace the sums over J' and J" in Eq. 43 by integrals. Since $\bar{J} \sim \sqrt{\theta/B_{v''}} \sim 10^2$ for T = 1.0 eV, we are interested primarily in Hönl-London factors for $J \gg 1$ and $J \gg \Lambda$ (Ref. 38, p.208).

	R-branch	Q-branch	P-branch
$\Delta\Lambda = 0$:	$S_J^R \sim J$	$S_J^Q \sim \frac{2\Lambda^2}{J} \sim 0$	$S_J^P \sim J$
$= +1$:	$J/2$	J	$J/2$
$= -1$:	$J/2$	J	$J/2$

These approximations exhibit the familiar effect (Ref. 38, Pg. 207) that the Q-branch intensity is approximately twice the R- or P-branch intensity (for $\Delta\Lambda \neq 0$). Further, the P- and R-branch energies differ from the Q-branch energy only by a term of order $B_{v''}/J''\Delta B$, where $\Delta B = (B_{v'} - B_{v''})$. For the principal air bands this factor is less than $10/J''$, resulting in an energy displacement of order ten percent for $J'' \sim \bar{J}$. For these reasons, plus computational convenience, high temperature models usually assume Q-branch energy dependence only (Ref. 4).

Assuming a Q-branch energy dependence defines our " Smeared Band" Model.

$$\kappa_{mn} = \kappa_{v'v''} + \Delta B J''(J''+1),$$

Using Eq. 42 $\sum_{J'} S^{J'\Lambda'}_{J''\Lambda''} = (2J''+1)$ and expressing the sum in Eq. 43a as an integral, we obtain

$$\mathcal{A}_{v'v''} = \frac{1}{\Delta\kappa\ \Delta B}\int_{\kappa}^{\kappa+\Delta\kappa} d\kappa'\,\kappa' e^{-B_{v''}\left(-\frac{\kappa'-\kappa_{v'v''}}{\Delta B}\right)/\theta} \quad \text{for } (\kappa-\kappa_{v'v''})\Delta B \geq 0$$
$$= 0 \text{ otherwise.} \qquad (43b)$$

Our final expression for the Smeared Band averaged absorption coefficient then becomes

$$\bar{\mu}(\kappa) = \frac{4\pi^2}{3}\alpha a_o^2 N_{e''}(1 - e^{-\omega_o''/\theta}) \sum_{v'v''} \left(\frac{B_{v''}}{\theta}\right) q_{v'v''} \left(\frac{R_e^2}{d_{e''}}\right) e^{-G_o(v'')/\theta}\, \mathcal{A}_{v'v''}(cm^{-1}) \qquad (44)$$

$$\left(\frac{4\pi^2}{3}\alpha a_o^2 = 2.68 \times 10^{-18}\ cm^2\right)$$

which agrees with the result of Ref. 4.

We note that the sum rule guarantees the total oscillator strength conservation; our Q-branch model errs only in an energy redistribution of oscillator strength, an effect of less importance at higher temperatures and larger averaging interval $\Delta\kappa$.

All the band systems we have treated have been evaluated in both the "PQR-Branch" and "Smeared Band" Models. For detailed comparison with experiments of high energy resolution only the PQR-Branch model is suitable. Furthermore, for the purpose of developing energy-dependent distribution functions of the line strength - for our band-emissivity and opacity studies - the more detailed line-by-line treatment is necessary. For evaluation of the mean absorption coefficient, however, averaged over an interval $\Delta\kappa \gtrsim 0.1$ eV, the results of the two models are essentially in agreement for temperatures $T \geq 6000^{\circ}K$.

IVC. Molecular Band Systems Contributing to Air Radiation

The molecular species we have examined are N_2, O_2, N_2^+ and NO. In Table II we list each molecular band we have studied, its spectroscopic

designation and name, and the energy interval in which the band radiates. This table also includes our chosen values of the electronic transition moment R_e^2 (Eq. 36), and the source of our Frank-Condon factors and r-centroids. The oscillator strength is listed for the Rydberg states of NO and finally the energy averaging interval $\Delta\kappa$ (Eq. 40), determining the spectral details of our average absorption coefficient. The maximum value of $\Delta\kappa$ used in our calculations was 0.10 eV, chosen large enough to resolve the vibrational structure, generally of the order 0.124 - 0.248 eV.

The spectroscopic constants T_e, ω_e, $\omega_e x_e$, $\omega_e y_e$, B_e, α_e, r_e depend only on the electronic state e and the values we used are listed in Table IV, with the source for these constants.

In Table V we list the Line Planck-Mean per molecule for N_2, O_2, NO and N_2^+ (in units of 10^{-18} cm^2) for the temperatures 4000, 6000, 8000, 10000, 12000, 18000, 24000 (^oK).

1. N_2 Systems

For the N_2 systems we include the bands:

	Transition	Spectral Inverval (eV)
a)	$A\ ^3\Sigma_u^+ \rightarrow B\ ^3\pi_g$ (First Positive)	0.4 - 2.7
b)	$B\ ^3\pi_g \rightarrow C\ ^3\pi_u$ (Second Positive)	2.2 - 4.8
c)	$X\ ^1\Sigma_g^+ \rightarrow b'\ ^1\Sigma_u^+$ (Birge-Hopfield 1)	5.0 - 13.3
d)	$X\ ^1\Sigma_g^+ \rightarrow b\ ^1\pi_u$ (Birge-Hopfield 2)	5.9 - 13.1

(a) N_2 (First Positive)

For this band system we used the Frank-Condon factors of Ref. 37, $v' = 0\text{-}17$, $v'' = 0\text{-}13$. The values of R_e^2 were calculated from

$$R_e^2 = 0.500 - 2.95X + 8.73\ X^2 \quad (1.16\ \text{Å} < r < 1.61\ \text{Å})$$

where $X = (\bar{r}_{v'v''} - r_{e''})$ in terms of the r-centroid $\bar{r}_{v'v''}$ (Ref. 52) and $r_{e''}$, the equilibrium internuclear distance of the lower state. The coefficients of the R_e^2 fit were obtained from Ref. 47 and the r-centroid data from Ref. 36.

The resultant cross sections agree well with the results of Avilova (Ref. 4). (The values given earlier (Ref. 53) are erroneously higher.)

(b) N_2 (Second Positive)

We used the Frank-Condon factors of Ref. 37, $v' = 0\text{-}4$, $v'' = 0\text{-}12$. The values of R_e^2 were calculated from

$$R_e^2 = 4.0 - 41.20\ X^2 + 10.1\ X^4,$$

where $X = (\bar{r}_{v'v''} - r_{e''})$.

The coefficients in R_e^2 were obtained from Ref. 49, and the r-centroids from Ref. 35.

(c) N_2 (Birge-Hopfield 1)

The Frank-Condon factors are from Ref. 37, $v' = 0\text{-}6$, $v'' = 0\text{-}28$. The value of R_e^2 were obtained from Ref. 4.

(d) N_2 (Birge-Hopfield 2)

We used the Frank-Condon factors of Ref. 37, $v' = 0\text{-}7$, $v'' = 0\text{-}28$. The value of R_e^2 came from Ref. 4.

2. O_2 System

In the figures presented here (Fig. 11-17) we have included only line transitions

	Spectral Interval (eV)
$X\ ^3\Sigma_g^- \rightarrow B\ ^3\Sigma_u^-$ (Schumann-Runge)	1.0 - 7.0

The Frank-Condon factors were obtained from Nicholls (Ref. 33) for $v' = 0\text{-}21$ and $v'' = 1\text{-}21$ and for $v' = 0\text{-}21$, $v'' = 0$ we used the values of Jarmain (Ref. 34). The r-centroids and coefficients used in calculating R_e^2 were obtained from Ref. 45.

$$R_e^2 = 3.0625 - 5.25\ X + 2.25\ X^2$$

where $X = \bar{r}_{v'v''} - r_{e''}$.

For the energy interval ≥ 7.0 eV we used the Schumann-Runge continuum results of Avilova (Ref. 4) in our emissivity calculations. Our results for the Schumann-Runge band agree quite well with those of Avilova et al. (Ref. 4), but differ from those of Churchill (Ref. 51) whose data on Frank-Condon factors was incomplete.

3. N_2^+ Systems

In this system we included

	Transition	Spectral Interval (eV)
a)	$X\ ^2\Sigma_g^+ \rightarrow B\ ^2\Sigma_u^+$ (First Negative)	1.5 - 4.9
b)	$X\ ^2\Sigma_g^+ \rightarrow A\ ^2\pi_u$ (Meinel)	0.5 - 4.7

(a) N_2^+ (First Negative)

The Frank-Condon factors came from Ref. 37, $v' = 0\text{-}20$, $v'' = 0\text{-}20$. The value of R_e^2 was obtained from

$$R_e^2 = 0.9 + 22.14\ X^2 + 136.16\ X^4$$

where $X = (\bar{r}_{v'v''} - r_{e''})$. The coefficients of R_e^2 were obtained from Ref. 49 and the r-centroids from Ref. 36.

(b) N_2^+ (Meinel)

We used the Frank-Condon factors of Ref. 37, v' = 0-20, v" = 0-20. The value of R_e^2 was obtained from Ref. 44.

4. NO Systems

This system was divided into two separate groups

GROUP A

	Transition	Spectral Interval (eV)
a)	$X\ ^2\pi \rightarrow B\ ^2\pi\ (\beta)$	1.0 - 7.8
b)	$X\ ^2\pi \rightarrow A\ ^2\Sigma^+\ (\gamma)$	3.0 - 7.9
c)	$X\ ^2\pi \rightarrow C\ ^2\pi\ (\delta)$	4.0 - 7.8
d)	$X\ ^2\pi \rightarrow D\ ^2\Sigma^+\ (\varepsilon)$	4.0 - 8.5

GROUP B

This system consists of the Rydberg series and the Ogawa 2 band system.

GROUP B

	Transition		Spectral Interval (eV)
a)	$K\ ^2\pi \rightarrow D\ ^2\Sigma^+$		0.920 - 1.370
b)	$H'\ ^2\pi \rightarrow C\ ^2\pi$ (Ry)		1.245 - 1.445
c)	$H\ ^2\pi \rightarrow C\ ^2\pi$ (Ry)	(Feast-Heath-Lagerquist)	1.22 - 1.445
d)	$F\ ^2\Delta \rightarrow C\ ^2\pi$ (Ry)		0.920 - 1.220
e)	$H'\ ^2\pi \rightarrow D\ ^2\Sigma^+$ (Ry)	(Feast-Heath)	1.120 - 1.345

GROUP B (Cont'd)

	Transition		Spectral Interval (eV)
f)	$H\ ^2\Sigma^+ \rightarrow D\ ^2\Sigma^+$ (Ry)	(Feast-Heath)	1.070 - 1.295
g)	$D\ ^2\Sigma^+ \rightarrow A\ ^2\Sigma^+$ (Ry)	(Feast 1)	1.020 - 1.245
h)	$E\ ^2\Sigma^+ \rightarrow C\ ^2\pi$ (Ry)		0.920 - 1.295
i)	$C\ ^2\pi \rightarrow A\ ^2\Sigma^+$ (Ry)	(Heath)	0.920 - 1.070
j)	$a\ ^4\pi \rightarrow b\ ^4\Sigma^-$ (Ogawa 2)		0.470 - 1.970

(a) NO (β)

The Frank-Condon factors were obtained from Ref. 37, v' = 0-19, v" = 0-23. We calculated R_e^2 from

$$R_e^2 = 0.03844 + 0.124\ X + 0.1\ X^2$$

where $X = (\bar{r}_{v'v''} - r_{e''})$.

The coefficients for R_e^2 were obtained from Ref. 49 and the r-centroids from Ref. 36.

(b) NO (γ)

For this band system we used the Frank-Condon factors of Ref. 37 for V' = 0-5, v" = 0-23. For v' = 6-23, V" = 0-23 we used our calculated values (subsection E below). We fit the data of Callear et al. (Ref. 60):

$$\begin{aligned} R_e &= 0.350 \quad (\bar{r} \leq 1.0\ \text{Å}) \\ &= -19.90 + 39.0\ \bar{r} - 18.75\ \bar{r}^2 \quad (1.0 \leq \bar{r} \leq 1.04\ \text{Å}) \\ &= -334.267 + 924.768\ \bar{r} - 850.2\ \bar{r}^2 + 260.0\ \bar{r}^3 \quad (1.04 \leq \bar{r} \leq 1.14\ \text{Å}) \\ &= 0.250 \quad (\bar{r} > 1.14\ \text{Å}) \end{aligned}$$

The resulting f-numbers agree with recent experiments (Ref. 48 (1967)) to within ten percent.

(c) NO (δ)

For this band system we used the Franck-Condon factors of Ref. 37, v' = 0-4, v" = 0-23. The value of R_e^2 came from Avilova (Ref. 4).

(d) NO (ϵ)

The Franck-Condon factors were obtained from Ref. 37, v' = 0-7, v" = 0-23. The value of R_e^2 was obtained from Avilova (Ref. 4), and the resulting f-numbers agree within ten percent with experiment (Ref. 59).

Group B

(a) - (j) NO-Rydberg Series

For the NO (Rydberg) series the Franck-Condon factors are from Ref. 37 and our calculations. We use Wray's experimentally fit oscillator strengths (Table 4 of Ref. 42).

Our calculated values of the radiation intensity per particle as a function of wave length for the Rydberg series agrees well with the values presented by Wray (Figures 9-14 of Ref. 42).

(j) NO (Ogawa 2)

For this band system we used the Frank-Condon factor v' = 0-22, v" = 0-23 of Nicholls (43) extended by our calculations. The value of R_e^2 was obtained from Avilova (Ref. 4).

IVD. Molecular Emissivity

The averaged absorption coefficient of Eq. 40 above is fed into the atomic radiation code RATRAC (Ref. 1) as an additional contribution to the continuum

absorption coefficient. In this approximation we neglect the increased self-absorption of the individual molecular lines in the line centers where the absorption coefficient is much greater than $\bar{\mu}$. To attempt to correct for this omission we exploit the high density of the molecular lines and the approximately constant width (Ref. 54); we treat the band emissivity statistically (Ref. 55, 56).

In our band models rotational lines originating from a given band (v',v'') are distributed with a prescribed spacing and a strength exponentially decreasing from the band head. When $\bar{\mu}(\kappa)$ is large and $\Delta\kappa$ not too small several bands generally contribute in any interval $\Delta\kappa$. In most of our numerical applications $\Delta\kappa = 807\ cm^{-1}$ (0.1 eV) and we typically find 500-4000 lines contributing in an interval, the large number generally applying to intervals where $\bar{\mu}$ is large and self-absorption more important.

Considering the extensive variation of the Franck-Condon factors with (v',v'') and the large numbers of (v',v'') contributing to a given $\Delta\kappa$, we assume the n_κ individual lines in $\Delta\kappa$ may be treated as if uniformly distributed in energy and continuously distributed in strength, with the probability of a strength S in dS being $P_\kappa(S)$. Our molecular absorption coefficient computer program ABSMOL (subsection E, below) evaluates a histogram of the line strength distribution about the mean line strength in every energy interval $\Delta\kappa$. From such a detailed energy-dependent line strength distribution function we expect to be able to obtain more reliable estimates of band emissivities and opacities. This work is still in progress.

For the short path lengths and lower densities of interest here, however, the molecular line self-absorption is not a large effect, and we have approximated the line strengths as being exponentially distributed. That is,

$P(S) = S_0^{-1} \exp(-S/S_0)$ in terms of a mean line strength $S_0(\kappa)$,

$$S_0(\kappa) = \frac{\Delta\kappa}{n_\kappa} \bar{\mu}(\kappa) = d_\kappa \bar{\mu}(\kappa) \tag{45}$$

d_κ is the mean line spacing. Comparison with our detailed histograms indicates this approximation to be generally satisfactory for the majority of the lines, but a small number of lines - of order 10 - 20% of the total - appear to lie in a distribution roughly symmetric about a strength a few times the mean S_0. As these lines are most strongly self-absorbed the exponential distribution can only provide a rough indication of the true self-absorption corrections.

For a known line strength distribution, $P(S)$, and a uniform distribution in energy, a simple approximation for the emissivity obtains (Ref. 56).

$$\Delta\epsilon(\kappa) = \left(\frac{\pi}{\sigma\theta}\right) \int_\kappa^{\kappa+\Delta\kappa} d\kappa' B(\kappa')\left[1 - e^{-\mu'(\kappa')L}\right]$$

$$\cong \left(\frac{\pi}{\sigma\theta}\right) B(\kappa)\Delta\kappa \left[1 - e^{-\bar{W}_\kappa(L)/d_\kappa}\right] \tag{46}$$

where $\bar{W}_\kappa(L)$ is the average equivalent width of a single line in $\Delta\kappa$,

$$\bar{W}_\kappa(L) = \int_0^\infty dS\ P_\kappa(S) \int_0^\infty d\kappa' \left[1 - e^{-Sb(\kappa')L}\right] .$$

For a Lorentz profile of width W (Ref. 1, eq. 11) and an exponential strength distribution, the result is easily obtained,

$$\bar{W}_\kappa(L) = \int_0^\infty \frac{S_0 b(\kappa')L}{1+S_0 b(\kappa')L}\, d\kappa'$$

$$= \frac{S_0(\kappa)L}{\sqrt{1+S_0(\kappa)L/\pi W}} = \frac{\bar{\mu}(\kappa)Ld_\kappa}{\sqrt{1+\left(\frac{d_\kappa}{W}\right)\frac{\bar{\mu}(\kappa)L}{\pi}}}$$

The molecular emissivity in the band $\Delta\kappa$ is then approximately

$$\Delta\epsilon(\kappa) \approx \frac{\pi B(\kappa)}{\sigma\theta^4}\,\Delta\kappa\,\{1 - \exp[\frac{-\bar{\mu}(\kappa)L}{\sqrt{1+(\frac{d_\kappa}{W})\bar{\mu}(\kappa)L/\pi}}]\} \tag{47}$$

Treating the molecular emission as an additional contribution $\bar{\mu}(\kappa)$ to the RATRAC continuum (Ref. 1) results in an emissivity

$$\Delta\epsilon_c(\kappa) = \frac{\pi}{\sigma\theta^4}\,B(\kappa)\,\Delta\kappa\,\{1 - \exp[-\bar{\mu}(\kappa)L]\}\ . \tag{48}$$

It is interesting to consider Eq. 47 in the limit $\bar{\mu}(\kappa)L \ll 1$, for which

$$\Delta\epsilon(\kappa) \simeq \frac{\pi}{\sigma\theta^4}\,B(\kappa)\,\Delta\kappa[\frac{\bar{\mu}(\kappa)L}{\sqrt{1+(\frac{d_\kappa}{W})\bar{\mu}(\kappa)L/\pi}}]\ .$$

This agrees with (48) only if $W \geq d_\kappa$ - the line width is greater than the spacing - or $[\bar{\mu}(\kappa)L/W] \ll 1$ - the peak of the absorption coefficient at the line center is small compared to L^{-1}. If, on the other hand, $W \ll d_\kappa$, we obtain

$$\Delta\epsilon(\kappa) \simeq \frac{\pi}{\sigma\theta^4}\,B(\kappa)\,\Delta\kappa\,\sqrt{\pi(\frac{W}{d_\kappa})\,\bar{\mu}(\kappa)L}\ ,$$

corresponding to the isolated line Ladenburg - Reiche approximation (Ref. 1, Eq. 39).

For the O_2 Schumann-Runge system at normal density and temperatures 6000-10,000°K we have computed the self-absorption corrections $(\Delta\epsilon(\kappa)/\Delta\epsilon_c(\kappa))$ of Eq. 47 and 48 above. Purely Lorentz broadening was assumed, and we have used the line widths of Breene (Ref. 54, 1968, Vol. II). For path lengths L = 1.0 cm, the maximum reduction in the band emissivity is found to be ten percent at 6000°K

and less than one percent at 8000°K. The results presented here ignore self-absorption effects in the molecular bands.

IVE. Molecular Absorption Computer Programs

For the purpose of generating and analyzing the molecular absorption coefficients presented herein, three separate computer programs have been developed.

1. The computer program MORSE evaluates Franck-Condon factors $q_{v'v''}$ and "r-centroids" $\bar{r}_{v'v''}$ (Eq. 36), assuming MORSE potentials. These results have been used to extend existing tabulations and the extensive tables of RKR-values kindly provided us by Capt. John Generosa of the Air Force Weapons Laboratory (Ref. 37).

The formulation of Nicholls is closely followed (Ref. 43). For large values of the vibrational quantum number, however, increased numerical accuracy is achieved by replacing his recursion relation for Laguerre polynomials (Ref. 37, Eq. 11) by a relation we derived for the ratio of polynomials of successive order. With $L_v(Z) \equiv L^{K-2v-1}_{K-v-1}(Z)$, the associated Laguerre polynomials, we obtain

$$\mathcal{L}_v \equiv \frac{L_v}{L_{v-1}} = Z - (K-2v)\sum_{r=0}^{v-1} T_r, \quad \mathcal{L}_0 = 1.$$

where $T_0 = 1$,

$$T_r = 2(v-r)\left(\frac{2r-1}{r+1}\right)\frac{T_{r-1}}{\mathcal{L}_{v-r}}$$

Employing these relations, the code MORSE obtains results agreeing with existing MORSE potential tabulations (Ref. 41, 36, 43). (The Franck-Condon factors and r-centroids are punched on cards suitable for input to code ABSMOL.)

2. The computer program ABSMOL evaluates the averaged absorption coefficient of Eq. 40 for a particular band system in both the "PQR-Branch" and "Smeared-Band"

models. The temperature and spectral constants of Tables III and IV are entered from punched cards, as are the Franck-Condon factors and r-centroids. If employed, we also enter parameters defining the dependence of the electronic transition moment $R_e^2(\bar{r}_{v'v''})$ on the r-centroid $\bar{r}_{v'v''}$.

The band-head energy and f-number for each vibrational transition and the spectral absorption coefficient and cummulative Planck-Mean generated by both band models are evaluated and listed. The histogram of line strength for the "PQR-Branch" model is accumulated and output on punched cards, and the corresponding absorption coefficient is output both graphically and on punched cards suitable for input into RATRAC or COMBDS.

3. The COMbined BanDS computer program, COMBDS, was developed to compress the single band output of ABSMOL into an absorption coefficient and histogram for a single molecular species. The output are both punched cards suitable for RATRAC and graphic; the molecular absorption coefficients of Fig. 4-38 were obtained from this code.

Although the combining of the contributing absorption coefficient is trivial, combining the separate histograms is complicated. This is because each histogram describes the line strength distribution of a single band in each spectral interval relative to the mean strength in that interval for that band. Combining several bands of differing mean strength into a distribution about the resulting mean strength is a non-trivial exercise in computing and it is solved in the present program.

V. Results and Conclusions

A. Molecular Absorption Coefficient

The results of our studies are presented in both graphical and tabular form. The molecular bands we have treated and their spectroscopic constants are in Tables III and IV. Table V contains the Planck Mean per molecule (in units 10^{-18} cm^2) for each individual band system (Eq. 5) - a function of temperature only. Molecular continua are not included in this table.

To indicate the relative contributions of individual species to air radiation we present in Tables VI - X the total Planck Mean - lines and continua for temperatures 6000 - 24,000°K, densities normal to 10^{-4} normal and broken down by species.

The molecular absorption coefficients generated according to our "PQR-Branch" model of Chapter IV are in Figures 4-38. The quantity graphed is an effective cross section (absorption coefficient per molecule) in units (10^{-18} cm^2), averaged according to Eq. 40 over the energy interval $\Delta\kappa$ of Table III. These cross sections are functions of temperature only. These graphs were generated by the computer program COMBDS (Section IVE) and combine the individual band results obtained by ABSMOL. (Similar graphs for the individual band contributions are available but are too numerous for inclusion in this report.)

B. Negative Atomic Ions

To the molecular absorption coefficients illustrated we have added the absorption due to the atomic negative ions O^- and N^-. The O^- cross section is from Churchill, et al. (Ref. 51), and the N^- cross section is from Kobzev (Ref. 57) - an absorption process of considerable controversy. Avilova, et al. (Ref. 4) use an N^- cross section an order of magnitude greater than we employ here. (We followed Avilova's results in our earlier report (Ref. 7).) Some recent

Russian experimental work (Ref. 57) obtain values approximately twice those we employ here. (The latter reference reviews most earlier work.)

In all cases the experimental procedure is one of subtraction. The emission intensity is observed in spectral intervals between listed spectral lines, compared with a synthesized intensity, and the difference is attributed to N^-. The variation of the excess radiation with thermodynamic variables is consistent with a binding energy of $\sim$ 1.0 eV; only the large magnitude of the resulting cross section has been difficult to explain.

As we have several times emphasized in this report, a synthesis of the absorption coefficient where it is large seems quite reliable, but very questionable where it is small. As noted in Ref. 57 the experimentally accessible region is rich in spectral lines. The line atlases we employ contain many more lines in this region than do most line locators - mostly lines of large principal quantum number and hence considerable width. Asinovskii, et al. (Ref. 57) demonstrate the sensitivity of their results to the shift of nearby photoionization edges - an effect roughly accounting for the presence of these broad lines.

Furthermore, all the so-employed synthetic spectra with which we are familiar approximate the line emission by an isolated line approximation (Ref. 1). Such treatments can in no way approximate emission from the wings of lines, which we find may be of considerable importance at the temperatures and densities of interest. Finally, free-free on neutral species and molecular contributions must be more carefully assessed. For these reasons, we are not yet ready to accept the magnitude of the experimental N^- cross section (Ref. 57).

The term diagram of N^- is in Figure 53. Schaeffer and Harris (Ref. 58) have estimated the ^1D state to be bound by 0.844 eV and the ^4S state to be unbounded. We shift Kobzev's estimate (Ref. 57, Fig. 12, Curve (2)) to this

binding energy and discard his ^4S cross section. When we have included the line wing formulation of this report in our computer program RATRAC we hope to study these questions further.

C. Emissivity Results

The emissivity results obtained from our RATRAC code are presented in Figures 39-48 for path lengths 10^{-2} - 1.0 cm, temperatures 0.5 to 5.0 eV and densities 1.0 to 10^{-4} normal. The molecular contribution is included as described in Section IVD, above. Finally, Figures 49-51 present the emissivity at a path length L = 1.0 cm and pressures 1.0, 0.5, and 0.1 atmospheres as a function of temperature.

REFERENCES

1. R. R. Johnston and O. R. Platas, LMSC Technical Report N-3L-69-1 (July 15, 1969)

2. W. Wiese, M. Smith, and B. Glennon, "Atomic Transition Probabilities," NSRDS-NBS4 (1966)

3. H. R. Griem, "Plasma Spectroscopy," (McGraw-Hill, New York, 1964)

4. I. Avilova, L. Biberman, G. Norman, et al., JQSRT 9, 89 (1969)

5. K. H. Wilson and R. Greif, JQSRT 8, 1061 (1968)

6. B. R. Judd, "Second Quantization and Atomic Spectroscopy," (Johns Hopkins Press, Baltimore, 1967)

7. R. R. Johnston and O. R. Platas, LMSC Technical Report N-3L-69-1-A (Jan 15, 1970)

8. W. L. Wiese, in "Plasma Diagnostic Techniques," (R. H. Huddlestone and S. L. Leonard, Editors, Academic Press, New York, 1965), Chapter 6

9. O. Bely and H. R. Griem, Phys. Rev. A, 1, 97 (1970)

10. N. W. Jalufka and J. P. Craig, Phys. Rev. A, 1, 221 (1970)

11. M. Baranger, "Spectral Line Broadening in Plasmas," in"Atomic and Molecular Processes," (D. Bates, Editor, Academic Press, New York, 1962)

12. B. Bezzerides, JQSRT 7, 353 (1967)

13. B. H. Armstrong, JQSRT 7, 61 (1967)

14. V. N. Faddeyeva and N. M. Terentev, "Tables of the Probability Integral for Complex Argument," (Pergamon Press, New York, 1961)

15. B. H. Armstrong, R. R. Johnston and P. S. Kelly, "Opacity of High Temperature Air," Air Force Weapons Laboratory Report AFWL-TR-65-17 (Nov 1965)

16. P. A. Jansson and C. L. Korb, JQSRT 8, 1399 (1968)

17. C. D. Rodgers and C. D. Walshaw, Quart. J. Roy. Meteorol. Soc. 92, 67 (1966)

18. H. R. Griem, Phys. Rev. Lett. 17, 509 (1966)

19. S. Brechot, Physics Letters 24A, 476 (1967)

20. J. Cooper and G. K. Oertel, Phys. Rev. Lett 18, 985 (1967)

21. D. H. Sampson, Astrophys. J. 155, 575 (1969)

22. H. R. Griem, Phys. Rev. 165, 258 (1968)

23. H. van Regemorter, Astrophys. J 136, 906 (1962)

24. J. Bond, K. M. Watson, and J. A. Welch, "Atomic Theory of Gas Dynamics," (Addison-Wesley, Reading, Mass., 1965)

25. I. Grant, Mon. Nat. Roy. Astron. Soc. 118, 241 (1958)

26. H. Margenau and M. Lewis, Revs. Mod. Phys. 31, 569 (1959)

27. M. Baranger and J. C. Stewart, "The Photon Absorption Coefficient in the Windows Between Spectral Lines," General Atomic Report GAMD-996 (September 1959)(Unpublished)(Summarized in Ref. 11, Section 5.2)

28. H. Griem, Astrophys. J. 132, 883 (1960)

29. H. Griem, Astrophys. J. 136, 422 (1962)

30. H. Griem, Astrophys. J. 147, 1092 (1967)

31. M. Lewis, Phys. Rev. 121, 501 (1961)

32. K. Alder, A. Bohr, T. Huus, B. Mottelson, and A. Winther, Revs. Mod. Phys. 28, 432 (1956)

33. R. W. Nicholls, Can. J. Phys. 38, 1705 (1960)

34. W. Jarmain, Can.J. Phys. 41, 1928 (1963)

35. M. Cann and P. Dickerman, "Molecular f-Numbers from High Resolution Spectroscopy," Air Force Weapons Laboratory Report AFWL-TR-67-76 (1968)

36. T. Wentink, L. Isaacson, and R. Spindler, "Research in the Opacity of Low Temperature Air: Oscillator Strengths and Transition Moments of Band Systems of N_2, O_2, and NO," Air Force Weapons Laboratory Report AFWL-TR-65-139 (December 1965)

37. J. Generosa, Unpublished results from the Air Force Weapons Laboratory

38. G. Herzberg, "Molecular Spectra and Molecular Structure. I Spectra of Diatomic Molecules," Second Edition (Van Nostrand, Princeton, 1950)

39. A. Douglas, Astrophys. J. 117, 384 (1953)

40. F. Gilmore in "Thermal Radiation Phenomena," Vol. I (Lockheed Report DASA 1971-1, May 1967) Tables 95-101

41. R. Nicholls, J. Research Natl. Bur. Standards 68A, 535 (1964)

42. K. Wray, JQSRT 7, 255 (1968)

43. R. Nicholls, J. Research Natl. Bur. Standards 65A 451 (1961)

44. E. Kuprianova, V. Kolesnikov, and N. Sobolev, JQSRT 9, 1025 (1969)

45. G. Marr, Can. J. Phys. 42, 382 (1964)

46. H. Ory, J. Chem. Phys. 40, 562 (1964)

47. M. Jeunehomme, J. Chem. Phys. 45, 1805 (1966)

48. E. Antropov and N. Sobolev, Opt. i Spect. 16, 208 (1964), 17, 654 (1964), 22, 109(1967)

49. J. Keck, R. Allen, and R. Taylor, JQSRT 3, 335 (1963)

50. R. Nicholls, Annales de Géophysique 20, 144 (1964)

51. D. Churchill, B. Armstrong, R. Johnston, and K. Müller, JQSRT 6, 371 (1966)

52. R. Nicholls and A. Stewart, "Allowed Transitions," in "Atomic and Molecular Processes," (D. Bates, Editor, Academic Press, 1962)

53. H. Aroeste and J. Magee, in "Thermal Radiation Phenomena," Vol. III (Lockheed Report DASA 1971-3, May 1967)

54. R. G. Breene, et al., Air Force Weapons Laboratory Reports AFWL-TR-66-35, Vol. I-III, August 1966, and AFWL-TR-67-77, Vol. I-III, Jan 1968

55. R. M. Goody, Quart. J. Roy. Meteorol. Soc. 78, 165 (1962)

56. G. Plass, J. Opt. Soc. Am. 48, 690 (1958)

57. E. Asinovskii, A. Kirilbin, and G. Kobzev, JQSRT 10, 143 (1970)

58. H. F. Schaeffer and F. Harris, Phys. Rev. Lett 21, 1561 (1968)

59. J. E. Hesser, J. Chem. Phys. 48, 2518 (1968)

60. A. B. Callear, M. J. Pilling, and I. W. M. Smith, Trans. Faraday Soc. 62, 2997 (1966)

APPENDIX A

APPLICATION OF SECOND QUANTIZATION TO RACAH ALGEBRA OF EQUIVALENT PARTICLES

AI. Introduction

The use of second quantization in atomic spectroscopy has been increasing rapidly in recent years. In deriving new relations, and rederiving old ones, this method is often more straightforward and more powerful in taking account of the Pauli exclusion principle than working with an antisymmetrized configuration space wave function approach. Consequently, it is hoped that the explicit evaluation of off-diagonal matrix elements of multi-electron atoms (necessary, for example, for calculating the autoionization cross section) is more quickly handled by a computer if the programming is based on second quantization rather than on fractional parentage coefficients (FPC) and configuration space formulae.

An exposition of the most pertinent formulae is given below, and in the last section these are applied to a matrix element whose value has been in dispute.

AII. Second Quantization Formalism for Fermions

This section will begin with a brief review of equivalence of the second quantization (SQ) method and the configuration space (CS) approach in atomic problems where the number of particles is a constant of the motion. The origins

of SQ method will not be described here, but they can be found in a sizeable number of textbooks on the theory of quantized wave fields (Ref. 1).

The CS method uses, in practice, sets of single-particle states, and the SQ method requires them even in principle. In this connection, it is crucial that the Pauli Principle is obeyed.

The CS state function of the "particles" generally consists of a superposition of determinantal wave functions

$$\Psi(x_1 x_2 x_3 \ldots x_N) = \frac{1}{\sqrt{N!}} \times \begin{vmatrix} \varphi_1(x_1)\ \varphi_1(x_2)\ \varphi_1(x_3) \ \ldots\ \varphi_1(x_N) \\ \varphi_2(x_1)\ \varphi_2(x_2) \ \ldots \\ \\ \varphi_N(x_1) \ \ldots\ldots \quad \varphi_N(x_{N-1})\varphi_N(x_N) \end{vmatrix} \quad \text{(A.1)}$$

where the $\varphi_1(x)$, $\varphi_2(x)$ ... are a complete orthonormal set of Pauli eigen functions of a suitable single-particle problem. For applications to atomic spectroscopy the $\{\varphi\}$ are the solutions to the wave equation with a screened central field coulomb potential (possibly non-local due to exchange), i.e.

$$\varphi_\alpha(\vec{x}) = R_{n\ell}(r)\ Y_{\ell m}(\vartheta, \varphi)\chi_{m_s}$$

where $R_{n\ell}$ is the radial wave function, $Y_{\ell m}$ is a spherical harmonic, and χ_{m_s} is a Pauli spinor.

In the SQ method the state function carries only occupation number information regarding the states $\varphi_1(x)$, $\varphi_2(x)$ ... . For particles obeying the Pauli Principle (Fermions) the occupation number N_α of any non-degenerate, single-particle state α cannot exceet $N_\alpha = 1$. Thus, there exists a creation

operator such that

$$a_\alpha^+ | \alpha > = 0$$
$$a_\alpha^+ | 0 > = | \alpha > \qquad (A.2)$$

where $| 0 >$ and $| \alpha >$ denote, respectively, the states with $N_\alpha = 0$ and 1. In order to assure the correspondence of the state $| \alpha,\beta, \ldots \lambda\mu \ldots> = a_\alpha^+ a_\beta^+ \ldots a_\gamma^+ a_\mu^+ \ldots | 0 >$ of SQ with the CS determinental state (A.1), which is antisymmetric under exchange of states, it is furthermore required that

$$a_\lambda^+ a_\mu^+ + a_\mu^+ a_\lambda^+ = 0 \qquad (A.3)$$

The Hermitian conjugate of a^+ is the annihilation operator, with the properties

$$a_\alpha | \beta > = 0 \qquad \text{if } \beta \neq \alpha \qquad (A.4)$$
$$a_\alpha | \alpha > = | 0 >$$

and

$$a_\alpha a_\beta + a_\beta a_\alpha = 0 \qquad (A.5)$$

The equations (A.2) and (A.4) therefore imply

$$a_\alpha^+ a_\alpha | 0 > = 0$$
$$a_\alpha^+ a_\alpha | \alpha > = | \alpha >$$

which makes $a_\alpha^+ a_\alpha$ the occupation number operator for state α.

Moreover, in order to maintain the equality of

$$\langle \alpha\,\beta \,|\, \gamma\,\delta \rangle = \frac{1}{2}\int d^3x_1\, d^3x_2 \begin{vmatrix} \varphi_\alpha^*(x_1) & \varphi_\alpha^*(x_2) \\ \varphi_\beta^*(x_1) & \varphi_\beta^*(x_2) \end{vmatrix} \begin{vmatrix} \varphi_\gamma(x_1) & \varphi_\gamma(x_2) \\ \varphi_\delta(x_1) & \varphi_\delta(x_2) \end{vmatrix}$$

$$= \delta_{\alpha\gamma}\,\delta_{\beta\delta} - \delta_{\alpha\delta}\,\delta_{\beta\gamma}$$

and

$$\langle \alpha\,\beta \,|\, \gamma\,\delta \rangle = \langle 0 \,|\, a_\beta\, a_\alpha\, a_\gamma^+\, a_\delta^+ \,|\, 0 \rangle,$$

it is required that

$$a_\alpha^+ a_\beta + a_\beta\, a_\alpha^+ = \delta_{\alpha\beta} \tag{A.6}$$

Next, operators and their matrix elements will be compared in the CS and SQ approaches. If the "particles" are identical, operators must be symmetric under exchange of particle labels in the CS representation. Operators considered are made up of a sum of individual particle operators of the same form,

$$F = \sum_i f(x_i)$$

and operators consisting of a sum of pair contributions of the same form

$$G = \sum_{ij} g(x_i, x_j)$$

If operators of the F and G type are used to compute CS matrix elements with fully-antisymmetrized wave functions (A.1), then the same values will be found in SQ by using

$$\mathcal{F} = \sum_{\rho} a_{\rho}^{+} < \rho \mid f \mid \sigma > a_{\sigma}$$

$$2\mathcal{G} = \sum_{\rho\sigma\tau\upsilon} a_{\rho}^{+} a_{\sigma}^{+} < \rho\sigma \mid g \mid \tau\upsilon > a_{\upsilon} a_{\tau} \qquad \text{(A.7)}$$

and the corresponding normalized state vector $a_1^+ a_2^+ \ldots a_N^+ \mid 0 >$.

In (A.7) the matrix elements are defined as

$$< \rho \mid f \mid \sigma > \equiv \int d^3x \, \varphi_{\rho}^{*}(x) \, f(x) \, \varphi_{\sigma}(x)$$

and

$$< \rho\sigma \mid g \mid \tau\upsilon > \equiv \int d^3x_1 \, d^3x_2 \, \varphi_{\rho}^{*}(x_1) \, \varphi_{\sigma}^{*}(x_2) \, g(x_1,x_2) \, \varphi_{\tau}(x_1) \, \varphi_{\upsilon}(x_2)$$

The sums $\rho,\sigma,\tau,\upsilon$ extend over a complete set of single-particle states. Thus, in SQ the Pauli Principle is satisfied by using the anti-commutation properties of the a^+ and a operators.

It is worth noting that the equivalence of the two approaches is formally rooted in the correspondence of the Ψ of (A.1) and

$$\psi(x) = \sum a_{\sigma} \varphi_{\sigma}(x)$$

In other words if the Ψ and Ψ^* in CS matrix elements are replaced by the operators $\psi(x)$ ans $\psi^*(x)$, and the matrix elements with respect to the occupation number state vectors are taken, the result will be the same as the CS calculation.

AIII. Rotational Transformation Properties

In order to be able to exploit rotational symmetry, a discussion of it in the context of second quantization will be given in this section.

Consider two coordinate systems, "prime" and "unprime" related to each other through a rotation specified by a set of parameters R such as the three Euler angles. In order that the form of the equations of motion and the anti-commutation relations be preserved in the two coordinate system, there must exist a unitary operator U such that

$$a'^{+}_{\kappa} = U\, a^{+}_{\kappa}\, U^{-1}$$

Another way of relating a'_{κ} and a_{μ} is to examine the commutation relations of a^{+} and the orbital angular momentum operator

$$\mathcal{L}_j = \sum a^{+}_{\rho} < \rho \mid L_j \mid \sigma > a_{\sigma}. \tag{A.8}$$

Let the greek subscripts denote the principal quantum number, n, total orbital angular momentum, ℓ, total spin angular momentum 1/2, z component of the orbital angular momentum, m_ℓ, and z component of the spin angular momentum, m_s. Then, using (A.3), (A.5), (A.6), and (A.8), we obtain commutation relations

$$\begin{aligned} [\mathcal{L}_z,\ a^{+}_{\gamma}] &= m_\ell\ a^{+}_{\gamma} \\ [\mathcal{L}_{\pm},\ a^{+}_{\gamma}] &= [\ell(\ell+1) - m_\ell(m_\ell \pm 1)]^{1/2} a^{+}_{\gamma_{\pm}} \end{aligned} \tag{A.9}$$

where $\mathcal{L}_{\pm} = (\mathcal{L}_x \pm i\mathcal{L}_y)/\sqrt{2}$ and $\gamma_{\pm} = \{n,\ \ell,\ m_\ell \pm 1,\ m_s\}$. Thus, the commutation relations of $\mathcal{L}_j$ and a^{+} are the same as those of L_j and $Y_{\ell m}$. Since the

commutation relations generate the local values of a'^{+} we know their values in the large, just as with the $Y_{\ell m}$. For the latter

$$Y_{\ell m}(\vartheta',\varphi') = \sum D^{\ell}_{mm'}(R)\, Y_{\ell m}(\vartheta,\varphi)$$

where $D^{\ell}_{mm'}(R)$ is the matrix element of the ℓ-dimensional irreducible representation of the rotation R for the three-dimensional rotation group. If spin is now considered by introducing the spin angular momentum operator

$$\mathcal{S}_j = \sum a^{+}_{\rho} < \rho \mid s_j \mid \tau > a_{\tau}$$

and its commutation relations with a^{+}, one readily sees that a^{+} transforms according to a s = 1/2 representation in its spin quantum numbers. Therefore,

$$U\, a^{+}_{\alpha'} U^{-1} = \sum_{m_\ell m_s} D^{\ell}_{m_j m'_l}(R)\, D^{1/2}_{m_s m'_s}(R)\, a^{+}_{\alpha} \qquad \text{(A.10)}$$

Because

$$D^{*}_{mp}(R) = D_{pm}(R^{-1})$$

the relation complex conjugate to (A.10) becomes

$$U\, a_{\alpha'} U^{-1} = \sum D^{\ell}_{m'_\ell m_\ell}(R^{-1})\, D^{1/2}_{m'_s m_s}(R^{-1})\, a_{\alpha} \qquad \text{(A.11)}$$

In other words, a_{α} does not transform according to $D^{\ell}_{a'a}(R)\, D^{1/2}_{b'b}(R)$.

Relations (A.10) and (A.11) are useful in establishing the transformation properties of more complicated quantities built up from sets of products of a^{+} and/or a, as, for example, multi-particle creation operators.

If the spin-orbit interaction is neglected, as will be the case throughout this appendix, each stationary state of a system of bound atomic electrons will have an integral value of the total orbital angular momentum, L, and a half-integral or integral value of the total spin angular momentum S. We show how to combine products of the a^{+}'s to form such states.

In combining two angular momenta j_1 and j_2 so as to form an eigenstate of their total angular momentum J (with z components, m_1, m_2, and M, respectively), the vector coupling coefficient $< j_1\ m_1\ j_2\ m_2 \mid J\ M >$ appears according to

$$| j_1 j_2\ JM > = \sum_{m_1 m_2} < j_1 m_1\ j_2 m_2 \mid JM > | j_1 m_1 > | j_2 m_2 > \qquad (A.12)$$

The explicit form of the vector coupling coefficient is given in numerous books, e.g., Brink and Satchler (Ref. 1), and Judd (Ref. 4). However, for present purposes the following relations (Ref. 1) will suffice.

$$\sum_{JM} < j_1 m_1\ j_2 m_2 \mid JM > < JM \mid j_1 m_1'\ j_2 m_2' > = \delta(m_1, m_1')\ \delta(m_2, m_2') \qquad (A.13)$$

$$\sum_{m_1 m_2} < JM \mid j_1 m_1\ j_2 m_2 > < j_1 m_1\ j_2 m_2 \mid J'M' > = \delta(MM')\delta(J, J')$$

$$< j_1 m_1\ j_2 m_2 \mid JM > = (-1)^{j_1 + j_2 - J} < j_2 m_2\ j_1 m_1 \mid JM > \qquad (A.14)$$

If j_1 and j_2 refer to the angular momentum of identical Fermions, then (A.12) must be brought into accord with the Pauli Principle. This is done by

constructing states

$$| j_1 j_2 \; JM >_a = \sum_{m_1 m_2} <j_1 m_1 \; j_2 m_2 | \; JM > a^+_{j_1 m_1} \; a^+_{j_2 m_2} | 0 > \qquad (A.15)$$

$$\equiv O^J_M | 0 >$$

To prove that the state $| j_1 j_2 \; JM >_a$ actually has the eigen value J we examine the behavior of O^J_M under rotation. The rotational behavior of the creation operators is given by (A.10), written explicitly as

$$U a^+_{jm'} U^{-1} = \sum_m D^j_{mm'}(R) \; a^+_{jm} \qquad (A.16)$$

Hence,

$$U \; O^J_M \; U^{-1} = \sum_{m_1 m_2} U \; a^+_{j_1 m_1} a^+_{j_2 m_2} U^{-1} < j_1 m_1 \; j_2 m_2 | \; JM >$$

$$= \sum_{n_1 m_1 n_2 m_2} D^{j_1}_{n_1 m_1} \; D^{j_2}_{n_2 m_2} < j_1 m_1 \; j_2 m_2 | \; JM > a^+_{jn_1} \; a^+_{jn_2} \qquad (A.17)$$

But

$$D^{j_1}_{n_1 m_1} \; D^{j_2}_{n_2 m_2} = \sum < j_1 m_1 \; j_2 m_2 | \; JN' > D^J_{N'N} < JN | \; j_1 m_1 \; j_2 m_2 > \qquad (A.18)$$

(Ref. 1).

Using the orthogonality relation (A.13) and (A.18), Eq. (A.17) becomes

$$U \; O^J_M \; U^{-1} = \sum < j_1 m_1 \; j_2 m_2 | \; JM' > a^+_{j_1 m_1} \; a^+_{j_2 m_2} \; D^J_{M'M}$$

$$= \sum_{M'} O^J_{M'} \; D^J_{M'M}$$

Thus, O^J_M transforms according to the J-dimensional irreducible representation of the rotation group.

From eq. (A.15) on we have treated only angular momenta j_1 and j_2 of two identical particles. In the present approach, where L-S coupling is ignored, each single-particle state is an eigenstate of spin and orbital angular momentum (total and z components). This causes only a minor complication. Since spin and orbital motion are uncoupled, they transform separately, according to (A.19). The relation equivalent to (A.19) becomes

$$U\, O^{LS}_{mt}\, U^{-1} = \sum_{m't'} D^L_{m'm}\, D^S_{t't}\, O^{LS}_{m't'}$$

where

$$O^{LS}_{mt} = \sum < \ell m_\ell,\ \ell' m'_\ell \mid LM > < 1/2\ m_s\ \tfrac{1}{2}\ m'_s \mid St > a^+_\nu\, a^+_{\nu'} \qquad (A.20)$$

States of more than two particles having a certain total L and S can thus be built up from pairs of particles with given transformation properties (and a single particle) if the number of particles is even (odd). For example, a four-electron state of particular L and S can be constructed from pairs of two-electron eigenstates as follows

$$| \ell_1 s_1\ \ell_2 s_2\ (L'S'),\ \ell_3 s_3\ \ell_4 s_4\ (L''S'');\ LS > =$$

$$\sum < L'M'\ \ L''M'' \mid LM > < S'T'\ \ S''T'' \mid ST > O^{L'S'}_{M'T'}\ O^{L''S''}_{M''T''} \mid 0 >$$

with the operators given by (A.20); some of the z component labels, as well as the normalization constant, have been suppressed.

For the presentation of elementary angular momentum coupling relations, such as those above, the vector coupling coefficient notation suffices. However, for problems involving a great many angular momenta (as in the following section), it is simpler to exploit the symmetries of the 3-j symbol, which is defined by the relation

$$< a\ \alpha\ b\ \beta \mid c\text{-}\gamma > (-1)^{a-b-\gamma} = \sqrt{2c+1} \begin{pmatrix} a & b & c \\ \alpha & \beta & \gamma \end{pmatrix} \tag{A.21}$$

As a result of (A.21) the 3-j symbol has the following very useful properties. For non-cyclical permutations of columns,

$$\begin{pmatrix} j_1 j_2 j_3 \\ m_1 m_2 m_3 \end{pmatrix} = (-1)^{j_1+j_2+j_3} \begin{pmatrix} j_3 j_2 j_1 \\ m_3 m_2 m_1 \end{pmatrix} \tag{A.22}$$

and

$$\begin{pmatrix} j_1 j_2 j_3 \\ -m_1 -m_2 -m_3 \end{pmatrix} = (-1)^{j_1+j_2+j_3} \begin{pmatrix} j_1 j_2 j_3 \\ m_1 m_2 m_3 \end{pmatrix} \tag{A.23}$$

Numerous authors have introduced their own transformation symbol analogous to (A.21). As a result, errors in phase, due to different conventions, can easily be made by the beginner. A good example of this is the different uses of the same symbol V by Racah (Ref. 5), and de Shalit and Talmi (Ref. 7). Probably the most complete listing of the various transformation symbols is collected in Yutsis, et al. (Ref. 8). The 3-j symbol, however, seems to be becoming the most widely used.

IV. Off-Diagonal Matrix Elements for the Electron-Electron Interaction

As is commonly done, the eigenfunctions $\varphi_\alpha(x)$ of (A.1) will be taken to be those of a Hartree-Fock Hamiltonian. The electron-electron interaction which is thereby neglected must be approximated. It is, therefore, necessary to evaluate matrix elements of the form

$$< A | \mathcal{V} | B > \tag{A.24}$$

where $< A |$ and $| B >$ refer to multi-electron states having certain values for the quantum numbers $L_A = L_B$ and $S_A = S_B$ and different occupation numbers for individual particle quantum numbers,

$$| C > = | 1s^2(^1S)2s^2(^1S)2p^2(^3P) >$$

$\mathcal{V}$ has the form of $\mathcal{G}$ in (A.7). The two-particle matrix element to be evaluated has the form

$$< \alpha\, \beta | V | \gamma\, \delta > = \int \varphi^*(1)\, \varphi^*(2)\, \frac{e^2}{r_{12}}\, \varphi_\gamma(1)\, \varphi_\delta(2)\, d^3x_1\, d^3x_2 \tag{A.25}$$

If the addition theorem for spherical harmonics

$$(2\ell+1)P_\ell(\cos\vartheta_{12}) = 4\pi \sum_{m=-\ell}^{m=\ell} Y_{\ell m}(\vartheta_1,\varphi_1)(-1)^m\, Y_{\ell -m}\,(\vartheta_2,\varphi_2)$$

is applied to

$$\frac{1}{r_{12}} = \sum \frac{r_<^K}{r_>^{K+1}}\, P_K(\cos\vartheta_{12})$$

which in turn is substituted into (A.25), and one obtains

$$< a\ b \mid V \mid c\ d > = \sum C_K (\ell_a m_a, \ell_c m_c) C_K (\ell_d m_d, \ell_b m_b) \times$$

$$\times R^K(u_a \ell_a, u_b \ell_b, u_c \ell_c, u_d \ell_d) \delta(m_a + m_b, m_c + m_d) \times \qquad \text{(A.26)}$$

$$\times \delta(m_s(\alpha), m_s(\gamma))\ \delta(m_s(\beta), m_s(\delta)).$$

Definitions introduced in (A.25) are the following:

$$C_K(\ell\ m\ \ell' m') = \frac{2}{2K+1} \int_0^{\pi} d\vartheta \sin\vartheta\ \Theta_{\ell m}\ \Theta_{Km-m'}\ \Theta_{\ell' m'}$$

where

$$Y_{\ell m} = \frac{1}{\sqrt{2\pi}} e^{im\varphi}\ \Theta_{\ell m}$$

and

$$R^K(u_a \ell_a, u_b \ell_b, u_c \ell_c, u_d \ell_d) = e^2 \int_0^{\infty}\int_0^{\infty} \frac{r_<^K}{r_>^{K+1}} R_a(1)\ R_b(2)\ R_c(1)\ R_d(2) r_1^2 r_2^2 dr_1 dr_2$$

with the R subscript $e = \{n_e, \ell_e\}$.

It can be shown that

$$C_K(\ell m, \ell' m') = (-1)^{m'} \{(2\ell+1)(2\ell'+1)\}^{1/2} \begin{pmatrix} \ell & \ell' & K \\ 0 & 0 & 0 \end{pmatrix} \begin{pmatrix} \ell & \ell' & K \\ m & -m' & m'-m \end{pmatrix} \qquad \text{(A.27)}$$

and thus the angular integrations are disposed of. The evaluation of R^K will not be discussed further because the evaluation of these integrals is not related to the influence of the Pauli Principle on the rotational properties of matrix elements.

The task of finding the non-vanishing parts of the various products of annihilation and creation operators in (A.24) can be systematically carried out with Wick's Theorem (Ref. 6), or by matching directly creation and annihilation operator pairs so that there are no non-vanishing matrix elements. It seems that this procedure is not hard to do on a computer.

To some extent, this investigation arose from a discrepancy in the value of

$$X = \langle 2s^2\,(^1S)\,2p^2\,(^3P);\ ^3P \mid V \mid 2s3d(^1D),\ 2p^2(^3P);\ ^3P \rangle$$

calculated in two attempts to apply the CS approach based on FPC. A computer program gave $X = X_+$, where

$$X_{\pm} = \frac{1}{3} R^1 (2s,\ 2p,\ 2p,\ 3d) \pm \frac{2}{5} R^2(2s,\ 2p,\ 3d,\ 2p)$$

while an application of Fano's prescription (Ref. 3) gave $X=X_-$. It was decided to evaluate X by an independent method, i.e. by the use of SQ. The main steps of this approach will be sketched next.

The eigenvalue of the z component of the orbital and spin angular momenta we denoted by $\sigma = 0$ and σ_σ for an s electron, π and σ_π for a p electron, and Δ and σ_Δ for a d electron.

Due to (A.15) and (A.21), the normalized ket is given by

$$| B \rangle = \frac{1}{\sqrt{2}} \sum B^{(S)}_{\sigma\pi\pi'\Delta}\, B^{(L)}_{\sigma\pi\pi'\Delta}\ a^+_\sigma\, a^+_\Delta\, a^+_\pi\, a^+_{\pi'}\, | 0 \rangle$$

where, for simplicity, the spin σ labels have been omitted on the creation operators as well as on $A^{(s)}$ and $B^{(s)}$.

$$B^{(L)}_{\sigma\pi\pi'\Delta} = 3\sqrt{5}\begin{pmatrix}0 & 2 & 2\\ 0 & \Delta & -\Delta\end{pmatrix}\begin{pmatrix}1 & 1 & 1\\ \pi & \pi' & -(\pi+\pi')\end{pmatrix}\begin{pmatrix}2 & 1 & 1\\ \Delta & \pi+\pi' & -(\Delta+\pi+\pi')\end{pmatrix}$$

$$B^{S}_{\sigma\pi\pi'\Delta} = 3\begin{pmatrix}\frac{1}{2} & \frac{1}{2} & 0\\ \sigma_\sigma & \sigma_\Delta & -(\sigma_\sigma+\sigma_\Delta)\end{pmatrix}\begin{pmatrix}\frac{1}{2} & \frac{1}{2} & 1\\ \sigma_\pi & \sigma_{\pi'} & -(\sigma_\sigma+\sigma_{\pi'})\end{pmatrix}\begin{pmatrix}0 & 1 & 1\\ 0 & \sigma_\pi+\sigma_{\pi'} & -(\sigma_\pi+\sigma_{\pi'})\end{pmatrix}$$

Similarly, the normalized bra is given by

$$\langle A| = \frac{1}{2}\sum \langle 0|\, a_\sigma a_{-\sigma} a_{\pi''} a_{\pi'''}\, A^{(S)}_{\sigma\pi''\pi'''}\, A^{(L)}_{\sigma\pi''\pi'''}$$

with

$$A^{S}_{\sigma\pi''\pi'''} = 3\begin{pmatrix}\frac{1}{2} & \frac{1}{2} & 0\\ \sigma & -\sigma & 0\end{pmatrix}\begin{pmatrix}\frac{1}{2} & \frac{1}{2} & 1\\ \sigma_{\pi''} & \sigma_{\pi'''} & -(\sigma_{\pi''}+\sigma_{\pi'''})\end{pmatrix}\begin{pmatrix}0 & 1 & 1\\ 0 & \sigma_{\pi''}+\sigma_{\pi'''} & -(\sigma_{\pi''}+\sigma_{\pi'''})\end{pmatrix}$$

$$A^{L}_{\sigma\pi''\pi'''} = \begin{pmatrix}1 & 1 & 1\\ \pi'' & \pi''' & -(\pi''+\pi''')\end{pmatrix}\begin{pmatrix}0 & 1 & 1\\ 0 & \pi''+\pi''' & -(\pi''+\pi''')\end{pmatrix}$$

and

$$\mathcal{V} = \frac{e^2}{2}\sum a^+_\alpha\, a^+_\beta \langle \alpha\beta|V|\gamma\delta\rangle a_\delta\, a_\gamma$$

Non-vanishing contributions of V to X occur if the two creation operators involve an s and p electron, and if the two annihilation operators refer to d and p electrons. The contribution to the electron-electron coulomb energy matrix element X vanishes if particles other than p electrons are both "created and annihilated" in V. Thus, it turns out that the total number of non-vanishing

$< A \mid a^+_\alpha a^+_\beta a_\delta a_\gamma \mid B >$ elements is sixteen.

After carrying out all contractions of a^+ and a, X may be written in the form

$$X = 2^{3/2} (II - I)$$

where

$$II = \sum A^S_{\sigma\bar{\pi}\pi'} A^L_{\sigma\bar{\pi}\pi'} < \bar{\pi}, -\sigma \mid V \mid \pi, \Delta > B^S_{\sigma\Delta\pi\pi'} B^L_{\sigma\Delta\pi\pi'}$$

$$I = \sum A^S_{\sigma\bar{\pi}\pi'} A^L_{\sigma\bar{\pi}\pi'} < \bar{\pi}, -\sigma \mid V \mid \Delta, \pi > B^S_{\sigma\Delta\pi\pi'} B^L_{\sigma\Delta\pi\pi'} \qquad (A.31)$$

Only a single term in both $< \bar{\pi}, -\sigma \mid V \mid \pi, \Delta >$ and $< \bar{\pi}, -\sigma \mid V \mid \Delta, \pi >$ expansions does not vanish (see A.26), as can be seen from the explicit values of the 3-j symbols (Ref. 1) occurring in (A ·) and (A.27), thus

$$< \bar{\pi}, -\sigma \mid V \mid \Delta, \pi > = \frac{2}{3} (-1)^{\bar{\pi}} \delta(\sigma_{\bar{\pi}}, \sigma_\Delta) \delta(\sigma_{-\sigma}, \sigma_\pi) \delta(\bar{\pi}, \pi+\Delta) R^1$$

$$< \bar{\pi}, -\sigma \mid V \mid \pi, \Delta > = \frac{\sqrt{6}}{5} (-1)^{\bar{\pi}} \delta(\sigma_{\bar{\pi}}, \sigma_\pi) \delta(\sigma_{-\sigma}, \sigma_\Delta) \delta(\bar{\pi}, \pi+\Delta) R^2$$

A further simplification takes place at this stage because X is diagonal in the z components of the total spin and orbit angular momentum - in fact, X is independent of both. Therefore, both of these components may be taken equal to zero.

Then one finally finds that the sums of (A.31) give

$$I = -R^1/6\sqrt{2}$$

$$II/I = 6/5 \cdot R^2/R^1$$

Therefore,

$$X = X_{\sim} = \frac{1}{3} R^1(2s,\ 2p,\ 2p\ 3d) - \frac{2}{5} R^2(2s,\ 2p,\ 3d,\ 2p)$$

which is the result obtained by Fano's treatment.*

---

* Dr. Paul Bagus, Private Communication, IBM Research Laboratory, San Jose, Calif.

REFERENCES

1. D. M. Brink and G. R. Satchler, "Angular Momentum," (Clarendon Press, Oxford) 1962

2. P. A. M. Dirac, "The Principles of Quantum Mechanics," Fourth Edition, (Clarendon Press, Oxford) 1958

3. U. Fano, Phys. Rev. 140, A 67 (1965)

4. B. R. Judd, "Operator Techniques in Atomic Spectroscopy," (McGraw-Hill Book Co., New York) 1963

5. G. Racah, Phys. Rev. 62, 438 (1942)

6. S. S. Schweber, "An Introduction to Relativistic Quantum Field Theory," (Row, Peterson and Co., Evanston, Illinois) 1961

7. A. deShalit and I. Talmi, "Nuclear Shell Theory," (Academic Press, New York) 1963

8. A. P. Yutsis, I. B. Levinson and V. V. Vanagas, "Theory of Angular Momentum," NASA TT F-98, 1962

APPENDIX B

ON THE NUMERICAL INTEGRATION OVER DETAILED SPECTRAL LINE PROFILES

The preliminary emissivity results reported in Ref. 1 have been found to be numerically unstable for varying choices of the photon energy mesh interval at densities below 10^{-3} normal. At such low densities collisional line widths may become less than 10^{-5} eV and any computationally practical mesh interval $\Delta\omega$ may contain a large, but unknown, number of strong narrow lines. To treat these in the evaluation of the contribution to Eq. 4 from the photon interval $[\omega, \omega + \Delta\omega]$, we write

$$\mu'(\omega) = f(\omega) + g(\omega)$$

where $f(\omega)$ consists of all of the contributions to $\mu'(\omega)$ which vary slowly in the neighborhood of ω.

Then

$$\Delta\epsilon\ (\omega) = \int_{\omega}^{\omega+\Delta\omega} d\omega' \left[\frac{\pi B(\omega')}{\sigma T^4}\right]\left[1 - e^{-\mu'(\omega')L}\right]$$

$$\cong \frac{\pi B(\omega)}{\sigma T^4}\,\Delta\omega\,\left\{1 - e^{-f(\omega)L}\,\frac{1}{\Delta\omega}\int_{\omega}^{\omega+\Delta\omega} d\omega' e^{-g(\omega')L}\right\}$$

As described in Section IV E of Ref. 1, $f(\omega)$ includes continuous absorption, "broad" lines (width $W > \Delta\omega$), "weak" lines (absorption at line center less than continuum absorption), and the wings of "strong narrow" lines (with line centers lying <u>outside</u> the interval $[\omega - \Delta\omega, \omega + 2\,\Delta\omega]$).

We visualize the situation as in Fig. 1. The lines numbered (1) through (6) are all "strong narrow" lines by the above criteria. The integration over the interval $[\omega, \omega + \Delta\omega]$ is performed by subdividing $\Delta\omega$ into unequal subintervals sufficient to resolve in $[\omega, \omega + \Delta\omega]$ all the "strong narrow" lines whose centers lie in the larger interval $[\omega - \Delta\omega, \omega + 2\,\Delta\omega]$, accumulating at this submesh the total absorption coefficient due to all lines in the larger interval (plus $f(\omega)$) and integrating by trapezoidal integration.

The earlier numerical instability referred to above was due to an unsuitable prescription for defining the energy submesh. With extensive computer experimentation we have obtained a prescription which is efficient and accurate for all cases we have tested (densities down to 10^{-7} normal and temperatures 0.5 eV to 100 eV).

Two passes are made through the contributing strong narrow lines. Every such line whose absorption coefficient at line center lies below the wing of any other line is removed from the mesh-defining considerations. In the example of Fig. 1, only lines (1), (3), and (4) will define the submesh. The minimum in the absorption coefficient due solely to adjacent pairs of these remaining dominant lines is evaluated, assuming Lorentz wing profiles - resulting in the energy values x_2 and x_4 in the figure. The width of each dominant line then is employed to subdivide the mesh between its two adjacent minima - line (1) governs the interval $[x_o = \omega, x_2]$ and line (3) the interval $[x_2, x_1 = \omega + \Delta\omega]$. Specifically, the interval $[x_2, x_1]$ is subdivided by the energies ω_3, $\omega_3 \pm B_n$, where $B_o = 0.25\ W_3$ and $B_n = 1.6\ B_{n-1} (n = 1,2,\ldots)$, ω_3 being the line center of line (3) and W_3 its width. The energy submesh so obtained is then ordered, the absorption coefficient due to all lines evaluated over it, and the integration is performed.

The submesh defined in this fashion by definition resolves the dominant lines and by experience is sufficiently fine grained to resolve the non-dominant ones. Results included in this report were evaluated by this procedure.

y	f(y)
0.0	-1.128
0.2	-1.040
0.4	-.803
0.6	-.486
0.8	-.168
1.0	+.086
1.2	.245
1.4	.314
1.6	.316
1.8	.280
2.0	.232
2.2	.185
2.4	.146
2.6	.117
2.8	.095
3.0	.079
3.2	.067
3.4	.057
3.6	.050
3.8	.044
4.0	.039
4.2	.035
4.4	.032
4.6	.029
4.8	.026
5.0	.024

Table I

Auxiliary Function f(y) in Modified Doppler Limit to Voigt Profile

Table II. SOME NII LINE WIDTHS

(a) Multiplet	Transition	λ(Å)	$\lambda_{1/2}$(Å) (b) Griem	(c) Griem	(d) Cooper-Oertel	(e) RATRAC	(f) This Report	(g) Experiment
(5)	$3s(^3P)$-$3p(^3P)$	4630	0.28	0.25	0.24	0.21	0.31	0.35
(12)	$3s(^1P)$-$3p(^1D)$	3995	0.17	0.20	0.17	0.16	0.25	0.30
(15)	$3p(^1P)$-$3d(^1D)$	4447	-	0.26	-	0.21	0.27	0.28
(18)	$3p(^1P)$-$4s(^1P)$	3007	0.32	0.24	0.32	0.33	0.59	0.60
(29)	$3p(^3P)$-$3d(^3P)$	5496	0.50	0.43	0.72	0.60	0.49	0.58
(30)	$3p(^3P)$-$4s(^3P)$	3838	0.40	0.42	0.42	0.53	0.95	1.0

(a) Ref. 2
(b) Ref. 18 (higher order classical path)
(c) Ref. 22 (semi-emperical)
(d) Ref. 20

} (Quoted in Ref. 10)

(e) Ref. 1
(f) Eq. 17 with Bely-Griem-Coulomb Gaunt factor (Fig. 3)
(g) Ref. 10

Table III. MOLECULAR BANDS IN AIR RADIATION

MOLECULE	TRANSITION	NAME SPECTRUM BAND	R_e^2 (b)	References R_e^2	Reference Frank-Condon factors	Reference $\bar{r}_{v'v''}$	f (c)	$\Delta\kappa$(ev)
N_2	$A^3\Sigma_u^+ - B^3\Pi_g$	FIRST POSITIVE 0.4-3.0	0.25, 1.01	47	37	36	5.8-3	0.10
	$B^3\Pi_g - C^3\Pi_u$	SECOND POSITIVE 2.0-5.0	1.95, 4.20	49	37	35	5.4-2	0.10
	$X^1\Sigma_g^+ - b^1\Sigma_u^+$	BIRGE HOPFIELD No. 1 5.0-13.5	1.0	4	37	-	.23	0.10
	$X^1\Sigma_g^+ - b^1\Pi_u$	BIRGE HOPFIELD No.2 5.0-13.5	1.0	4	37	-	.31	0.10
O_2	$X^3\Sigma_g^- - B^3\Sigma_u^-$	SCHUMANN RUNGE 1.0-7.5	0.60, 3.93	45	33,34	45	.113	0.05
N_2^+	$X^2\Sigma_g^+ - B^2\Sigma_u^+$	FIRST NEGATIVE 1.5-5.0	0.90, 1.43	49	37	36	3.8-2	0.05
	$X^2\Sigma_g^+ - A^2\Pi_u$	MEINEL 0.5-5.0	0.60	44	37	-	8.2-3	0.05
NO	$X^2\Pi - B^2\Pi$	BETA 0.5-8.75	0.038,0.15	49	37,(a)	(a)	1.9-3	0.10
	$X^2\Pi - A^2\Sigma^+$	GAMMA 3.0-8.0	0.0625,0.145	48,60	37,(a)	(a)	2.6-3	0.10
	$X^2\Pi - C^2\Pi$	DELTA 4.0-8.0	0.40	4	37,(a)	(a)	1.6-2	0.10
	$X^2\Pi - D^2\Sigma^+$	EPSILON 4.0-8.75	0.32	4	37,(a)	-	1.3-2	0.10
	$K^2\Pi - D^2\Sigma^+$	RYDBERGS 0.92-1.5	4.8	42	(a)	-	0.08	0.025
	$H'\ ^2\Pi - C\ ^2\Pi$	RYDBERGS 0.92-1.5	19.	42	(a)	-	0.15	0.025
	$H\ ^2\Sigma^+ - C\ ^2\Pi$	RYDBERGS 0.92-1.5	15.	42	(a)	-	0.12	0.025

Continued

Table III. Continued

MOLECULE	TRANSITION	NAME SPECTRUM BAND	R_e^2(b)	References R_e^2	Reference Frank-Condon factors	Reference $r_{v'v''}$	f(c)	$\Delta\nu$(ev)
	$F\ ^2\Delta\text{-}C\ ^2\Pi$	RYDBERGS 0.92-1.5	30.	42	(a)	-	0.22	0.025
	$H'\ ^2\Pi\text{-}D\ ^2\Sigma^+$	FEAST-HEATH 0.92 - 1.5	35.	42	37,(a)	-	0.50	0.025
	$H\ ^2\Sigma^+\text{-}D\ ^2\Sigma^+$		18.	42	37,(a)	-	0.25	0.025
	$D\ ^2\Sigma^+\text{-}A\ ^2\Sigma^+$	FEAST 0.92-1.5	13.	42	37,(a)	-	0.18	0.025
	$E\ ^2\Sigma^+\text{-}C\ ^2\Pi$	RYDBERGS 0.92-1.5	4.7	42	37,(a)	-	0.03	0.025
	$C\ ^2\Pi\text{-}A\ ^2\Sigma^+$	HEATH 0.92-1.5	56.	42	37,(a)	-	0.70	0.025
	$a\ ^4\Pi\text{-}b\ ^4\Sigma^-$	OGAWA 2 0.42-2.0	0.80	4	(a)	-	2.8-3	0.025

(a) Computed by program Morse, see subsection E below.

(b) When two numbers are given, the value of R_e^2 lies in $X_1 \leq R_e^2 \leq X_2$.

(c) f-number from (0-0) transition ($f = f(0,0)/q(0,0)$)

Table IV. MOLECULAR SPECTROSCOPIC CONSTANTS *

Molecule	State	T_e	ω_e	$\omega_e x_e$	$\omega_e y_e$	B_e	α_e	r_e	Reference
O_2	$B\ ^3\Sigma_u^-$	49802.1	700.36	8.002	-.3753	0.819	0.011	1.60_4	40
	$X\ ^3\Sigma_g^-$	0	1580.36	12.073	0.0546	1.4452	0.01534	1.2074	40
N_2	$b'\ ^1\Sigma_u^+$	104481	751.7	4.82	-	1.145	0.002_1	1.450	38
	$b\ ^1\Pi_u$	102283	698	-	-	1.41	-	1.31	38
	$C\ ^3\Pi_u$	89147	2035.1	17.08	-2.15	1.8259	0.0197	1.1482	38
	$B\ ^3\Pi_g$	59626	1733.88	14.35	-0.011	1.6375	0.01794	1.2123	38,40
	$A\ ^3\Sigma_u^+$	50205	1460.6	13.85	0.0065	1.4545	0.01794	1.286	40
	$X\ ^1\Sigma_g^+$	0	2358.07	14.188	-.0124	1.9987	0.0178	1.094	40
N_2^+	$B\ ^2\Sigma_u^+$	25462	2419.8	23.19	-0.5375	2.083	0.0195	1.075	38
	$A\ ^2\Pi_u$	9168.4	1902.8	14.91	-	1.722	0.018	-	39
	$X\ ^2\Sigma_g^+$	0	2207.2	16.146	-.0285	1.9258	.01743	1.116_2	40

Continued

* (Units are cm^{-1}, except r_e in Angstrom)

Table IV. Continued

Molecule	State	T_e	ω_e	$\omega_e x_e$	$\omega_e y_e$	B_e	α_e	r_e	Reference
NO	K $^2\Pi$	64058	2360	15	-	2.01±.02	0.23±04	-	42
	H' $^2\Pi$	62483	2374	17	-	2.017	0.021	1.058	42
	H $^2\Sigma^+$	62470	2369	15	-	2.0030	0.018	1.062	42
	F $^2\Delta$	61818	2370	15	-	2.0245	0.115	-	42
	E $^2\Sigma^+$	60629	2372	15	-	1.9863	0.0181	-	42
	D $^2\Sigma^+$	53083	2323.9	22.885	0.75	2.0026	0.02175	1.062	40
	C $^2\Pi$	52135	2395.	15.0	-	2.002	0.03	1.062	41
	b $^4\Sigma^-$	47430	1230.	14.4	-	1.36	0.024	1.280	40
	B $^2\Pi$	45937	1037.7	7.545	0.0833	1.1245	0.0132	1.448	40
	A $^2\Sigma^+$	43964	2374.8	16.46	-0.28	1.9972	0.0193	1.0637	41
	a $^4\Pi$	39407	1017.	11.0	-	1.17	0.017	1.382	40
**	X $^2\Pi$	62.2	1903.98	14.015	.010	1.7042	0.01725	1.1508	40

** Energies used in the ground state of the β band are averages of $X^2\Pi_{3/2}$ and $X^2\Pi_{1/2}$ states.

Table V. LINE PLANCK MEAN PER MOLECULE (10^{-18} cm^2) - (BY BAND SYSTEM)

BAND MOLECULE	NAME	4000 °K	6000 °K	8000 °K	10000 °K	12000 °K	18000 °K	24000 °K
N_2								
$A^3\Sigma_u^+$-$B'^3\Pi_g$	First Positive	2.006-8	5.890-6	7.279-5	2.626-4	5.083-4	6.574-4	3.311-4
$B^3\Pi_g$-$C^3\Pi_u$	Second Positive	2.842-10	2.337-6	1.444-4	1.330-3	4.810-3	1.857-2	1.728-2
$X^1\Sigma_g^+$-$b'^1\Sigma_u^+$	Birge Hopfield No. 1	4.929-11	2.073-6	2.762-4	3.970-3	1.920-2	1.240-1	1.553-1
$X^1\Sigma_g^+$-$b^1\Pi_u$	Birge Hopfield No. 2	1.744-10	5.746-6	6.839-4	9.246-3	4.314-2	2.672-1	3.336-1
TOTAL	N_2	2.05 -8	1.61 -5	1.18 -3	1.48 -2	6.76 -2	4.10 -1	5.07 -1
O_2								
$X^3\Sigma_g^-$-$B^3\Sigma_u^-$	Schumann Runge	2.311-4	1.573-2	8.079-2	1.604-1	2.080-1	1.769-1	9.902-2
NO								
$X^2\Pi$-$B^2\Pi$	BETA	2.040-5	8.926-4	4.031-3	7.713-3	9.860-3	8.029-3	4.273-3
$X^2\Pi$-$A^2\Sigma^+$	GAMMA	5.56-5	2.10-3	9.34-3	1.87-2	2.58-2	2.69-2	1.77-2
$X^2\Pi$-$C^2\Pi$	DELTA	2.082-5	2.136-3	1.485-2	3.722-2	5.771-2	6.858-2	4.661-2
$X^2\Pi$-$D^2\Sigma^+$	EPSILON	1.485-5	1.716-3	1.301-2	3.483-2	5.692-2	7.563-2	5.554-2
$a^4\Pi$-$b^4\Sigma^-$	OGAWA2	1.17-6	8.63-5	4.74-4	9.40-4	1.15-3	7.27-4	3.05-4
TOTAL		1.13-4	6.93-3	4.17-2	9.94-2	1.51-1	1.80-1	1.24-1

Continued

Table V. Continued

BAND MOLECULE N_2	NAME	4000 °K	6000°K	8000 °K	10000 °K	12000°K	18000 °K	24000°K
Rydbergs- NO								
$K^2\Pi$-$D^2\Sigma^+$		6.78-9	1.96-6	1.81-5	4.67-5	6.68-5	5.37-5	2.62-5
$H'^2\Pi$-$C^2\Pi$	FEAST-HEATH LAGERQUIST	3.98-8	1.24-5	1.32-4	3.93-4	6.48-4	7.32-4	4.46-4
$H^2\Sigma^+$-$C^2\Pi$	FEAST-HEATH LAGERQUIST	3.36-8	1.01-5	1.07-4	3.17-4	5.20-4	5.84-4	3.55-4
$F^2\Delta$-$C^2\Pi$	FEAST-HEATH LAGERQUIST	6.33-8	1.68-5	1.59-4	4.30-4	6.45-4	5.75-4	2.91-4
$H'^2\Pi$-$D^2\Sigma^+$	FEAST-HEATH	4.91-8	1.34-5	1.32-4	3.70-4	5.78-4	5.85-4	3.25-4
$H^2\Sigma^+$-$D^2\Sigma^+$	FEAST-HEATH	2.55-8	6.98-6	6.80-5	1.91-4	2.97-4	2.99-4	1.66-4
$D^2\Sigma^+$-$A^2\Sigma^+$	FEAST 1	5.09-7	4.78-5	2.85-4	6.02-4	7.90-4	6.07-4	2.97-4
$E^2\Sigma^+$-$C^2\Pi$		8.91-9	2.22-6	2.10-5	5.80-5	9.08-5	9.37-5	5.44-5
$C^2\Pi$-$A^2\Sigma^+$	HEATH	1.94-6	1.62-4	8.94-4	1.77-3	2.20-3	1.51-3	6.93-4
TOTAL RYDBERGS		2.68-6	2.74-4	1.82-3	4.18-3	5.84-3	5.04-3	2.65-3
TOTAL NO		1.16-4	7.20-3	4.35-2	1.04-1	1.57-1	1.85-1	1.27-1
N_2^+								
$X^2\Sigma_g^+$-$B^2\Sigma_u^+$	FIRST NEGATIVE	1.32 -1	5.13 -1	7.76 -1	9.07 -1	9.39 -1	6.93 -1	4.08 -1
$X^2\Sigma_g^+$-$A^2\Pi_u$	MEINEL	3.04 -1	1.90 -1	1.05 -1	5.93 -2	3.48 -2	8.40 -3	2.57 -3
TOTAL	N_2^+	4.36 -1	7.03 -1	8.81 -1	9.66 -1	9.74 -1	7.01 -1	4.11 -1

Table V. LINE PLANCK MEAN PER MOLECULE (10^{-18} cm^2) - (RY BAND SYSTEM)

BAND MOLECULE N_2	NAME	4000 °K	6000 °K	8000 °K	10000 °K	12000 °K	18000 °K	24000 °K
$A^3\Sigma_u^+ - B^3\Pi_g$	First Positive	2.006-8	5.890-6	7.279-5	2.626-4	5.083-4	6.574-4	3.311-4
$B^3\Pi_g - C^3\Pi_u$	Second Positive	2.842-10	2.337-6	1.444-4	1.330-3	4.810-3	1.857-2	1.728-2
$X^1\Sigma_g^+ - b'^1\Sigma_u^+$	Birge Hopfield No. 1	4.929-11	2.073-6	2.762-4	3.970-3	1.920-2	1.240-1	1.553-1
$X^1\Sigma_g^+ - b\ ^1\Pi_u$	Birge Hopfield No. 2	1.744-10	5.746-6	6.839-4	9.246-3	4.314-2	2.672-1	3.336-1
TOTAL	N_2	2.05 -8	1.61 -5	1.18 -3	1.48 -2	6.76 -2	4.10 -1	5.07 -1
O_2								
$X^3\Sigma_g^- - B^3\Sigma_u^-$	Schumann Runge	2.311-4	1.573-2	8.079-2	1.604-1	2.080-1	1.769-1	9.902-2
NO								
$X^2\Pi - B^2\Pi$	BETA	2.040-5	8.926-4	4.031-3	7.713-3	9.860-3	8.029-3	4.273-3
$X^2\Pi - A^2\Sigma^+$	GAMMA	5.56-5	2.10-3	9.34-3	1.87-2	2.58-2	2.69-2	1.77-2
$X^2\Pi - C^2\Pi$	DELTA	2.082-5	2.136-3	1.485-2	3.722-2	5.771-2	6.858-2	4.661-2
$X^2\Pi - D^2\Sigma^+$	EPSILON	1.485-5	1.716-3	1.301-2	3.483-2	5.692-2	7.563-2	5.554-2
$a^4\Pi - b^4\Sigma^-$	OGAWA2	1.17-6	8.63-5	4.74-4	9.40-4	1.15-3	7.27-4	3.05-4
TOTAL		1.13-4	6.93-3	4.17-2	9.94-2	1.51-1	1.80-1	1.24-1

Continued

Table V. Continued

BAND MOLECULE N_2	NAME	4000 °K	6000°K	8000 °K	10000 °K	12000°K	18000 °K	24000°K
Rydbergs- NO								
$K^2\Pi$-$D^2\Sigma^+$		6.78-9	1.96-6	1.81-5	4.67-5	6.68-5	5.37-5	2.62-5
$H'^2\Pi$-$C^2\Pi$	FEAST-HEATH LAGERQUIST	3.98-8	1.24-5	1.32-4	3.93-4	6.48-4	7.32-4	4.46-4
$H^2\Sigma^+$-$C^2\Pi$	FEAST-HEATH LAGERQUIST	3.36-8	1.01-5	1.07-4	3.17-4	5.20-4	5.84-4	3.55-4
$F^2\Delta$-$C^2\Pi$	FEAST-HEATH LAGERQUIST	6.33-8	1.68-5	1.59-4	4.30-4	6.45-4	5.75-4	2.91-4
$H'^2\Pi$-$D^2\Sigma^+$	FEAST-HEATH	4.91-8	1.34-5	1.32-4	3.70-4	5.78-4	5.85-4	3.25-4
$H^2\Sigma^+$-$D^2\Sigma^+$	FEAST-HEATH	2.55-8	6.98-6	6.80-5	1.91-4	2.97-4	2.99-4	1.66-4
$D^2\Sigma^+$-$A^2\Sigma^+$	FEAST 1	5.09-7	4.78-5	2.85-4	6.02-4	7.90-4	6.07-4	2.97-4
$E^2\Sigma^+$-$C^2\Pi$		8.91-9	2.22-6	2.10-5	5.80-5	9.08-5	9.37-5	5.44-5
$C^2\Pi$-$A^2\Sigma^+$	HEATH	1.94-6	1.62-4	8.94-4	1.77-3	2.20-3	1.51-3	6.93-4
TOTAL RYDBERGS		2.68-6	2.74-4	1.82-3	4.18-3	5.84-3	5.04-3	2.65-3
TOTAL NO		1.16-4	7.20-3	4.35-2	1.04-1	1.57-1	1.85-1	1.27-1
N_2^+								
$X^2\Sigma_g^+$-$B^2\Sigma_u^+$	FIRST NEGATIVE	1.32 -1	5.13 -1	7.76 -1	9.07 -1	9.39 -1	6.93 -1	4.08 -1
$X^2\Sigma_g^+$-$A^2\Pi_u$	MEINEL	3.04 -1	1.90 -1	1.03 -1	5.93 -2	3.48 -2	8.40 -3	2.57 -3
TOTAL	N_2^+	4.36 -1	7.03 -1	8.81 -1	9.66 -1	9.74 -1	7.01 -1	4.11 -1

Table V. LINE PLANCK MEAN PER MOLECULE (10^{-18} cm^2) - (BY BAND SYSTEM)

BAND MOLECULE N_2	NAME	4000 °K	6000°K	8000°K	10000°K	12000°K	18000°K	24000°K
$A^3\Sigma_u^+ - B^3\Pi_g$	First Positive	2.006-8	5.890-6	7.279-5	2.626-4	5.083-4	6.574-4	3.311-4
$B^3\Pi_g - C^3\Pi_u$	Second Positive	2.842-10	2.337-6	1.444-4	1.330-3	4.810-3	1.857-2	1.728-2
$X^1\Sigma_g^+ - b'^1\Sigma_u^+$	Birge Hopfield No. 1	4.929-11	2.073-6	2.762-4	3.970-3	1.920-2	1.240-1	1.553-1
$X^1\Sigma_g^+ - b\ ^1\Pi_u$	Birge Hopfield No. 2	1.744-10	5.746-6	6.839-4	9.246-3	4.314-2	2.672-1	3.336-1
TOTAL	N_2	2.05 -8	1.61 -5	1.18 -3	1.48 -2	6.76 -2	4.10 -1	5.07 -1
O_2								
$X^3\Sigma_g^- - B^3\Sigma_u^-$	Schumann Runge	2.311-4	1.573-2	8.079-2	1.604-1	2.080-1	1.769-1	9.902-2
NO								
$X^2\Pi - B^2\Pi$	BETA	2.040-5	8.926-4	4.031-3	7.713-3	9.860-3	8.029-3	4.273-3
$X^2\Pi - A^2\Sigma^+$	GAMMA	5.56-5	2.10-3	9.34-3	1.87-2	2.58-2	2.69-2	1.77-2
$X^2\Pi - C^2\Pi$	DELTA	2.082-5	2.136-3	1.485-2	3.722-2	5.771-2	6.858-2	4.661-2
$X^2\Pi - D^2\Sigma^+$	EPSILON	1.485-5	1.716-3	1.301-2	3.483-2	5.692-2	7.563-2	5.554-2
$a^4\Pi - b^4\Sigma^-$	OGAWA2	1.17-6	8.63-5	4.74-4	9.40-4	1.15-3	7.27-4	3.05-4
TOTAL		1.13-4	6.93-3	4.17-2	9.94-2	1.51-1	1.80-1	1.24-1

Continued

Table V. Continued

BAND MOLECULE N_2	NAME	4000 °K	6000°K	8000 °K	10000 °K	12000°K	18000 °K	24000°K
Rydbergs- NO								
$K^2\Pi$-$D^2\Sigma^+$		6.78-9	1.96-6	1.81-5	4.67-5	6.68-5	5.37-5	2.62-5
$H'^2\Pi$-$C^2\Pi$	FEAST-HEATH LAGERQUIST	3.98-8	1.24-5	1.32-4	3.93-4	6.48-4	7.32-4	4.46-4
$H^2\Sigma^+$-$C^2\Pi$	FEAST-HEATH LAGERQUIST	3.36-8	1.01-5	1.07-4	3.17-4	5.20-4	5.84-4	3.55-4
$F^2\Delta$-$C^2\Pi$	FEAST-HEATH LAGERQUIST	6.33-8	1.68-5	1.59-4	4.30-4	6.45-4	5.75-4	2.91-4
$H'^2\Pi$-$D^2\Sigma^+$	FEAST-HEATH	4.91-8	1.34-5	1.32-4	3.70-4	5.78-4	5.85-4	3.25-4
$H^2\Sigma^+$-$D^2\Sigma^+$	FEAST-HEATH	2.55-8	6.98-6	6.80-5	1.91-4	2.97-4	2.99-4	1.66-4
$D^2\Sigma^+$-$A^2\Sigma^+$	FEAST 1	5.09-7	4.78-5	2.85-4	6.02-4	7.90-4	6.07-4	2.97-4
$E^2\Sigma^+$-$C^2\Pi$		8.91-9	2.22-6	2.10-5	5.80-5	9.08-5	9.37-5	5.44-5
$C^2\Pi$-$A^2\Sigma^+$	HEATH	1.94-6	1.62-4	8.94-4	1.77-3	2.20-3	1.51-3	6.93-4
TOTAL RYDBERGS		2.68-6	2.74-4	1.82-3	4.18-3	5.84-3	5.04-3	2.65-3
TOTAL NO		1.16-4	7.20-3	4.35-2	1.04-1	1.57-1	1.85-1	1.27-1
N_2^+								
$X^2\Sigma_g^+$-$B^2\Sigma_u^+$	FIRST NEGATIVE	1.32 -1	5.13 -1	7.76 -1	9.07 -1	9.39 -1	6.93 -1	4.08 -1
$X^2\Sigma_g^+$-$A^2\Pi_u$	MEINEL	3.04 -1	1.90 -1	1.05 -1	5.93 -2	3.48 -2	8.40 -3	2.57 -3
TOTAL	N_2^+	4.36 -1	7.03 -1	8.81 -1	9.66 -1	9.74 -1	7.01 -1	4.11 -1

Table V. LINE PLANCK MEAN PER MOLECULE (10^{-18} cm^2) - (BY BAND SYSTEM)

BAND MOLECULE N_2	NAME	4000 °K	6000 °K	8000 °K	10000 °K	12000 °K	18000 °K	24000 °K
$A^3\Sigma_u^+ - B^3\Pi g$	First Positive	2.006-8	5.890-6	7.279-5	2.626-4	5.083-4	6.574-4	3.311-4
$B^3\Pi_g - C^3\Pi_u$	Second Positive	2.842-10	2.337-6	1.444-4	1.330-3	4.810-3	1.857-2	1.728-2
$X^1\Sigma_g^+ - b', {}^1\Sigma_u^+$	Birge Hopfield No. 1	4.929-11	2.073-6	2.762-4	3.970-3	1.920-2	1.240-1	1.553-1
$X^1\Sigma_g^+ - b\ {}^1\Pi_u$	Birge Hopfield No. 2	1.744-10	5.746-6	6.839-4	9.246-3	4.314-2	2.672-1	3.336-1
TOTAL	N_2	2.05 -8	1.61 -5	1.18 -3	1.48 -2	6.76 -2	4.10 -1	5.07 -1
O_2								
$X^3\Sigma_g^- - B^3\Sigma_u^-$	Schumann Runge	2.311-4	1.573-2	8.079-2	1.604-1	2.080-1	1.769-1	9.902-2
NO								
$X^2\Pi - B^2\Pi$	BETA	2.040-5	8.926-4	4.031-3	7.713-3	9.860-3	8.029-3	4.273-3
$X^2\Pi - A^2\Sigma^+$	GAMMA	5.56-5	2.10-3	9.34-3	1.87-2	2.58-2	2.69-2	1.77-2
$X^2\Pi - C^2\Pi$	DELTA	2.082-5	2.136-3	1.485-2	3.722-2	5.771-2	6.858-2	4.661-2
$X^2\Pi - D^2\Sigma^+$	EPSILON	1.485-5	1.716-3	1.301-2	3.483-2	5.692-2	7.563-2	5.554-2
$a^4\Pi - b^4\Sigma^-$	OGAWA2	1.17-6	8.63-5	4.74-4	9.40-4	1.15-3	7.27-4	3.05-4
TOTAL		1.13-4	6.93-3	4.17-2	9.94-2	1.51-1	1.80-1	1.24-1

Continued

Table V. Continued

BAND MOLECULE N_2	NAME	4000 °K	6000°K	8000 °K	10000 °K	12000°K	18000 °K	24000°K
Rydbergs- NO								
$K^2\Pi$-$D^2\Sigma^+$		6.78-9	1.96-6	1.81-5	4.67-5	6.68-5	5.37-5	2.62-5
$H'^2\Pi$-$C^2\Pi$	FEAST-HEATH LAGERQUIST	3.98-8	1.24-5	1.32-4	3.93-4	6.48-4	7.32-4	4.46-4
$H^2\Sigma^+$-$C^2\Pi$		3.36-8	1.01-5	1.07-4	3.17-4	5.20-4	5.84-4	3.55-4
$F^2\Delta$-$C^2\Pi$		6.33-8	1.68-5	1.59-4	4.30-4	6.45-4	5.75-4	2.91-4
$H'^2\Pi$-$D^2\Sigma^+$	FEAST-HEATH	4.91-8	1.34-5	1.32-4	3.70-4	5.78-4	5.85-4	3.25-4
$H^2\Sigma^+$-$D^2\Sigma^+$		2.55-8	6.98-6	6.80-5	1.91-4	2.97-4	2.99-4	1.66-4
$D^2\Sigma^+$-$A^2\Sigma^+$	FEAST 1	5.09-7	4.78-5	2.85-4	6.02-4	7.90-4	6.07-4	2.97-4
$E^2\Sigma^+$-$C^2\Pi$		8.91-9	2.22-6	2.10-5	5.80-5	9.08-5	9.37-5	5.44-5
$C^2\Pi$-$A^2\Sigma^+$	HEATH	1.94-6	1.62-4	8.94-4	1.77-3	2.20-3	1.51-3	6.93-4
TOTAL RYDBERGS		2.68-6	2.74-4	1.82-3	4.18-3	5.84-3	5.04-3	2.65-3
TOTAL NC		1.16-4	7.20-3	4.35-2	1.04-1	1.57-1	1.85-1	1.27-1
N_2^+								
$X^2\Sigma_g^+$-$B^2\Sigma_u^+$	FIRST NEGATIVE	1.32 -1	5.13 -1	7.76 -1	9.07 -1	9.39 -1	6.93 -1	4.08 -1
$X^2\Sigma_g^+$-$A^2\Pi_u$	MEINEL	3.04 -1	1.90 -1	1.05 -1	5.93 -2	3.48 -2	8.40 -3	2.57 -3
TOTAL	N_2^+	4.36 -1	7.03 -1	8.81 -1	9.66 -1	9.74 -1	7.01 -1	4.11 -1

Table V. LINE PLANCK MEAN PER MOLECULE (10^{-18} cm^2) - (BY BAND SYSTEM)

BAND	MOLECULE	NAME	4000 °K	6000 °K	8000 °K	10000 °K	12000 °K	18000 °K	24000 °K
	N_2								
$A^3\Sigma_u^+ - B^3\Pi g$		First Positive	2.006-8	5.890-6	7.279-5	2.626-4	5.083-4	6.574-4	3.311-4
$B^3\Pi_g - C^3\Pi_u$		Second Positive	2.842-10	2.337-6	1.444-4	1.330-3	4.810-3	1.857-2	1.728-2
$X^1\Sigma_g^+ - b'^1\Sigma_u^+$		Birge Hopfield No. 1	4.929-11	2.073-6	2.762-4	3.970-3	1.920-2	1.240-1	1.553-1
$X^1\Sigma_g^+ - b\ ^1\Pi_u$		Birge Hopfield No. 2	1.744-10	5.746-6	6.839-4	9.246-3	4.314-2	2.672-1	3.336-1
TOTAL		N_2	2.05 -8	1.61 -5	1.18 -3	1.48 -2	6.76 -2	4.10 -1	5.07 -1
	O_2								
$X^3\Sigma_g^- - B^3\Sigma_u^-$		Schumann Runge	2.311-4	1.573-2	8.079-2	1.604-1	2.080-1	1.769-1	9.902-2
	NO								
$X^2\Pi - B^2\Pi$		BETA	2.040-5	8.926-4	4.031-3	7.713-3	9.860-3	8.029-3	4.273-3
$X^2\Pi - A^2\Sigma^+$		GAMMA	5.56-5	2.10-3	9.34-3	1.87-2	2.58-2	2.69-2	1.77-2
$X^2\Pi - C^2\Pi$		DELTA	2.082-5	2.136-3	1.485-2	3.722-2	5.771-2	6.858-2	4.661-2
$X^2\Pi - D^2\Sigma^+$		EPSILON	1.485-5	1.716-3	1.301-2	3.483-2	5.692-2	7.563-2	5.554-2
$a^4\Pi - b^4\Sigma^-$		OGAWA2	1.17-6	8.63-5	4.74-4	9.40-4	1.15-3	7.27-4	3.05-4
TOTAL			1.13-4	6.93-3	4.17-2	9.94-2	1.51-1	1.80-1	1.24-1

Continued

Table V. Continued

BAND MOLECULE N_2	NAME	4000 °K	6000°K	8000 °K	10000 °K	12000°K	18000 °K	24000°K
Rydbergs- NO								
$K^2\Pi-D^2\Sigma^+$		6.78-9	1.96-6	1.81-5	4.67-5	6.68-5	5.37-5	2.62-5
$H'^2\Pi-C^2\Pi$	FEAST-HEATH LAGERQUIST	3.98-8	1.24-5	1.32-4	3.93-4	6.48-4	7.32-4	4.46-4
$H^2\Sigma^+-C^2\Pi$		3.36-8	1.01-5	1.07-4	3.17-4	5.20-4	5.84-4	3.55-4
$F^2\Delta-C^2\Pi$		6.33-8	1.68-5	1.59-4	4.30-4	6.45-4	5.75-4	2.91-4
$H'^2\Pi-D^2\Sigma^+$	FEAST-HEATH	4.91-8	1.34-5	1.32-4	3.70-4	5.78-4	5.85-4	3.25-4
$H^2\Sigma^+-D^2\Sigma^+$		2.55-8	6.98-6	6.80-5	1.91-4	2.97-4	2.99-4	1.66-4
$D^2\Sigma^+-A^2\Sigma^+$	FEAST 1	5.09-7	4.78-5	2.85-4	6.02-4	7.90-4	6.07-4	2.97-4
$E^2\Sigma^+-C^2\Pi$		8.91-9	2.22-6	2.10-5	5.80-5	9.08-5	9.37-5	5.44-5
$C^2\Pi-A^2\Sigma^+$	HEATH	1.94-6	1.62-4	8.94-4	1.77-3	2.20-3	1.51-3	6.93-4
TOTAL RYDBERGS		2.68-6	2.74-4	1.82-3	4.18-3	5.84-3	5.04-3	2.65-3
TOTAL NO		1.16-4	7.20-3	4.35-2	1.04-1	1.57-1	1.85-1	1.27-1
N_2^+								
$X^2\Sigma_g^+-B^2\Sigma_u^+$	FIRST NEGATIVE	1.32 -1	5.13 -1	7.76 -1	9.07 -1	9.39 -1	6.93 -1	4.08 -1
$X^2\Sigma_g^+-A^2\Pi_u$	MEINEL	3.04 -1	1.90 -1	1.05 -1	5.93 -2	3.48 -2	8.40 -3	2.57 -3
TOTAL	N_2^+	4.36 -1	7.03 -1	8.81 -1	9.66 -1	9.74 -1	7.01 -1	4.11 -1

Table V. LINE PLANCK MEAN PER MOLECULE (10^{-18} cm^2) - (BY BAND SYSTEM)

BAND MOLECULE N_2	NAME	4000 °K	6000 °K	8000 °K	10000 °K	12000 °K	18000 °K	24000 °K
$A^3\Sigma_u^+ - B^3\Pi_g$	First Positive	2.006-8	5.890-6	7.279-5	2.626-4	5.083-4	6.574-4	3.311-4
$B^3\Pi_g - C^3\Pi_u$	Second Positive	2.842-10	2.337-6	1.444-4	1.330-3	4.810-3	1.857-2	1.728-2
$X^1\Sigma_g^+ - b'^1\Sigma_u^+$	Birge Hopfield No. 1	4.929-11	2.073-6	2.762-4	3.970-3	1.920-2	1.240-1	1.553-1
$X^1\Sigma_g^+ - b\ ^1\Pi_u$	Birge Hopfield No. 2	1.744-10	5.746-6	6.839-4	9.246-3	4.314-2	2.672-1	3.336-1
TOTAL	N_2	2.05 -8	1.61 -5	1.18 -3	1.48 -2	6.76 -2	4.10 -1	5.07 -1
O_2								
$X^3\Sigma_g^- - B^3\Sigma_u^-$	Schumann Runge	2.311-4	1.573-2	8.079-2	1.604-1	2.080-1	1.769-1	9.902-2
NO								
$X^2\Pi - B^2\Pi$	BETA	2.040-5	8.926-4	4.031-3	7.713-3	9.860-3	8.029-3	4.273-3
$X^2\Pi - A^2\Sigma^+$	GAMMA	5.56-5	2.10-3	9.34-3	1.87-2	2.58-2	2.69-2	1.77-2
$X^2\Pi - C^2\Pi$	DELTA	2.082-5	2.136-3	1.485-2	3.722-2	5.771-2	6.858-2	4.661-2
$X^2\Pi - D^2\Sigma^+$	EPSILON	1.485-5	1.716-3	1.301-2	3.483-2	5.692-2	7.563-2	5.554-2
$a^4\Pi - b^4\Sigma^-$	OGAWA2	1.17-6	8.63-5	4.74-4	9.40-4	1.15-3	7.27-4	3.05-4
TOTAL		1.13-4	6.93-3	4.17-2	9.94-2	1.51-1	1.80-1	1.24-1

Continued

Table V. Continued

BAND MOLECULE N_2	NAME	4000 °K	6000°K	8000 °K	10000 °K	12000°K	18000 °K	24000°K
Rydbergs- NO								
$K^2\Pi$-$D^2\Sigma^+$		6.78-9	1.96-6	1.81-5	4.67-5	6.68-5	5.37-5	2.62-5
$H'^2\Pi$-$C^2\Pi$	FEAST-HEATH LAGERQUIST	3.98-8	1.24-5	1.32-4	3.93-4	6.48-4	7.32-4	4.46-4
$H^2\Sigma^+$-$C^2\Pi$	FEAST-HEATH LAGERQUIST	3.36-8	1.01-5	1.07-4	3.17-4	5.20-4	5.84-4	3.55-4
$F^2\Delta$-$C^2\Pi$	FEAST-HEATH LAGERQUIST	6.33-8	1.68-5	1.59-4	4.30-4	6.45-4	5.75-4	2.91-4
$H'^2\Pi$-$D^2\Sigma^+$	FEAST-HEATH	4.91-8	1.34-5	1.32-4	3.70-4	5.78-4	5.85-4	3.25-4
$H^2\Sigma^+$-$D^2\Sigma^+$	FEAST-HEATH	2.55-8	6.98-6	6.80-5	1.91-4	2.97-4	2.99-4	1.66-4
$D^2\Sigma^+$-$A^2\Sigma^+$	FEAST 1	5.09-7	4.78-5	2.85-4	6.02-4	7.90-4	6.07-4	2.97-4
$E^2\Sigma^+$-$C^2\Pi$		8.91-9	2.22-6	2.10-5	5.80-5	9.08-5	9.37-5	5.44-5
$C^2\Pi$-$A^2\Sigma^+$	HEATH	1.94-6	1.62-4	8.94-4	1.77-3	2.20-3	1.51-3	6.93-4
TOTAL RYDBERGS		2.68-6	2.74-4	1.82-3	4.18-3	5.84-3	5.04-3	2.65-3
TOTAL NO		1.16-4	7.20-3	4.35-2	1.04-1	1.57-1	1.85-1	1.27-1
N_2^+								
$X^2\Sigma_g^+$-$B^2\Sigma_u^+$	FIRST NEGATIVE	1.32 -1	5.13 -1	7.76 -1	9.07 -1	9.39 -1	6.93 -1	4.08 -1
$X^2\Sigma_g^+$-$A^2\Pi_u$	MEINEL	3.04 -1	1.90 -1	1.05 -1	5.93 -2	3.48 -2	8.40 -3	2.57 -3
TOTAL	N_2^+	4.36 -1	7.03 -1	8.81 -1	9.66 -1	9.74 -1	7.01 -1	4.11 -1

Table VI. TOTAL PLANCK MEAN (CM^{-1})*- (By Species)

Density $\rho/\rho_o = 1.0$

SPECIES	TEMPERATURE (°K)						
	4000	6000	8000	10,000	12,000	18,000	24,000
N_2	4.14-7	3.24-4	1.82-2	9.92-2	1.05-1	8.96-3	1.69-3
O_2	6.60-4	3.61-3	3.02-3	2.88-3	2.69-3	1.31-4	1.59-5
NO	2.68-4	9.22-3	2.80-2	3.32-2	1.98-2	2.09-3	1.50-4
N_2^+	2.03-11	2.26-6	1.05-3	1.40-2	2.38-2	1.15-2	2.29-3
NO_2	-	2.43-5	2.06-6	-	-	-	-
N^-	-	1.28-6	1.49-4	2.32-3	1.20-2	-	-
N	-	3.26-4	1.50-1	3.41	1.60+1	9.55+1	1.43+2
N^+	-	-	2.58.6	1.3-3	3.73-2	3.37	2.78+1
O^-	-	6.17-4	2.81-3	1.06-2	3.06-2	-	-
O	-	6.75-4	2.48-2	2.04-1	8.61-1	7.78	1.75+1
O^+	-	-	-	2.7-5	9.65-4	1.94-1	2.65
TOTAL**		1.51-2	2.29-1	3.78	1.78+1	1.07+2	1.92+2

** Includes Free-free and higher degrees of ionization

* 6.75-4 denotes 6.75×10^{-4}

Table VII. TOTAL PLANCK MEAN (CM^{-1})* - (By Species)

Density $\rho/\rho_o = 10^{-1}$

SPECIES	TEMPERATURE (°K)						
	4000	6000	8000	10,000	12,000	18,000	24,000
N_2	4.22-8	3.11-5	9.68-4	1.66-3	1.15-3	1.04-4	1.74-6
O_2	3.10-5	4.55-5	3.33-5	3.02-5	2.66-5	8.21-7	2.08-8
NO	1.79-5	3.21-4	6.79-4	4.58-4	2.06-4	1.17-5	1.77-7
N_2^+	5.10-12	1.14-6	2.63-4	8.34-4	8.32-4	2.15-4	1.30-5
NO_2	-	9.50-8	5.23-9	-	-	-	-
N^-	-	7.57-8	7.36-6	9.47-5	3.89-4	-	-
N	-	9.98-5	3.47-2	4.79-1	1.76	6.95	5.25
N^+	-	-	2.80-6	5.79-4	1.26-2	9.0-1	5.16
O^-	-	1.32-5	6.29-5	3.28-4	9.48-4	-	-
O	-	7.27-5	2.59-3	2.82-3	8.51-2	6.56-1	7.32-1
O^+	-	-	-	9.14-6	3.10-4	5.77-2	5.68-1
TOTAL**		5.94-5	3.93-2	4.86-1	1.86	8.57	1.18+1

** Includes Free-free and higher degrees of ionization

* 6.75-4 denotes 6.75×10^{-4}

Table VIII. TOTAL PLANCK MEAN (CM^{-1})*- By Species

Density $\rho/\rho_o = 10^{-2}$

SPECIES	TEMPERATURE (K)						
	4000	6000	8000	10,000	12,000	18,000	24,000
N_2	4.31-9	2.58-6	2.15-5	1.89-5	9.71-6	6.55-8	6.67-11
O_2	6.33-7	4.84-7	3.41-7	2.97-7	2.39-7	1.76-9	4.65-12
NO	8.15-7	9.51-6	1.03-5	4.66-6	1.81-6	2.07-8	3.68-11
N_2^+	3.50-12	5.30-7	2.10-5	2.82-5	2.34-5	1.57-6	2.14-8
NO_2	-	2.91-10	7.99-12	-	-	-	-
N^-	-	3.87-9	3.05-7	3.04-6	1.08-5	-	-
N	-	2.85-5	5.17-3	4.71-2	1.61-1	2.91-1	8.35-2
N^+	-	-	1.51-6	1.89-4	3.82-3	1.79-1	6.35-1
O^-	-	2.42-7	1.77-6	1.02-5	2.71-5	-	-
O	-	7.47-6	2.63-4	2.08-3	8.01-3	3.24-2	1.25-2
O^+	-	-	1.2-8	2.89-6	9.70-5	1.39-2	7.60-2
TOTAL**		4.95-5	5.49-3	4.95-2	1.73-1	5.17-1	8.12-1

** Includes Free-free and higher degrees of ionization

* 6.75-4 denotes 6.75×10^{-4}

Table IX. TOTAL PLANCK MEAN (CM^{-1})*- (By Species)

Density $\rho/\rho_o = 10^{-3}$

SPECIES	TEMPERATURE (°K)						
	4000	6000	8000	10,000	12,000	18,000	24,000
N_2	4.33-10	1.42-7	2.49-7	1.55-7	1.73-7	1.66-11	7.30-15
O_2	7.58-9	4.92-9	3.38-9	1.18-9	4.60-10	5.65-13	5.14-16
NO	2.83-8	2.26-7	1.10-7	4.22-8	1.14-8	5.90-12	4.07-15
N_2^+	1.89-12	1.62-7	7.82-7	8.17-7	4.85-17	3.13-9	2.30-11
NO_2	-	6.93-13	-	-	-	-	-
N^-	-	1.63-10	1.01-8	8.75-8	-	-	-
N	-	6.70-6	5.55-4	4.41-3	1.16-2	5.11-3	8.94-4
N^+	-	-	5.24-7	5.80-5	1.15-3	2.35-2	6.63-2
O^-	-	4.39-9	5.46-8	2.98-7	-	-	-
O	-	7.45-7	2.60-5	1.97-4	7.06-4	6.42-4	1.36-4
O^+	-	-	3.9-9	9.01-6	3.10-5	2.05-3	7.96-3
TOTAL**		7.98-6	5.83-4	4.68-3	1.35-2	3.13-2	7.54-2

** Includes Free-free and higher degrees of ionization

* 6.75-4 denotes 6.75×10^{-4}

Table X. TOTAL PLANCK MEAN (CM^{-1})* - (By Species)

Density $\rho/\rho_o = 10^{-4}$

SPECIES	TEMPERATURE (°K)						
	4000	6000	8000	10,000	12,000	18,000	24,000
N_2	4.37-11	3.36-9	2.52-9	1.06-9	1.15-10	4.43-15	3.79-18
O_2	7.90-11	4.96-11	2.04-11	8.86-12	1.34-12	6.77-17	5.19-20
NO	9.06-10	3.49-9	1.07-9	2.98-10	2.75-11	6.94-16	4.12-19
N_2^+	1.04-12	1.69-8	2.44-8	1.90-8	4.57-9	3.47-12	2.30-14
NO_2	-	-	-	-	-	-	-
N^-	-	-	-	-	-	-	-
N	-	1.03-6	5.40-5	3.55-4	5.20-4	5.49-5	7.8-6
N^+	-	3.9-11	1.63-7	1.63-5	2.11-4	2.46-3	4.5-3
O^-	-	-	-	-	-	-	-
O	-	7.52-8	2.71-6	1.83-5	3.58-5	6.97-6	1.5-6
O^+	-	-	1.31-9	2.89-7	7.66-6	2.21-4	7.5-4
TOTAL**		1.13-6	5.69-5	3.90-4	7.74-4	2.75-3	6.90-3

** Includes Free-free and higher degrees of ionization

* 6.75-4 denotes 6.75×10^{-4}

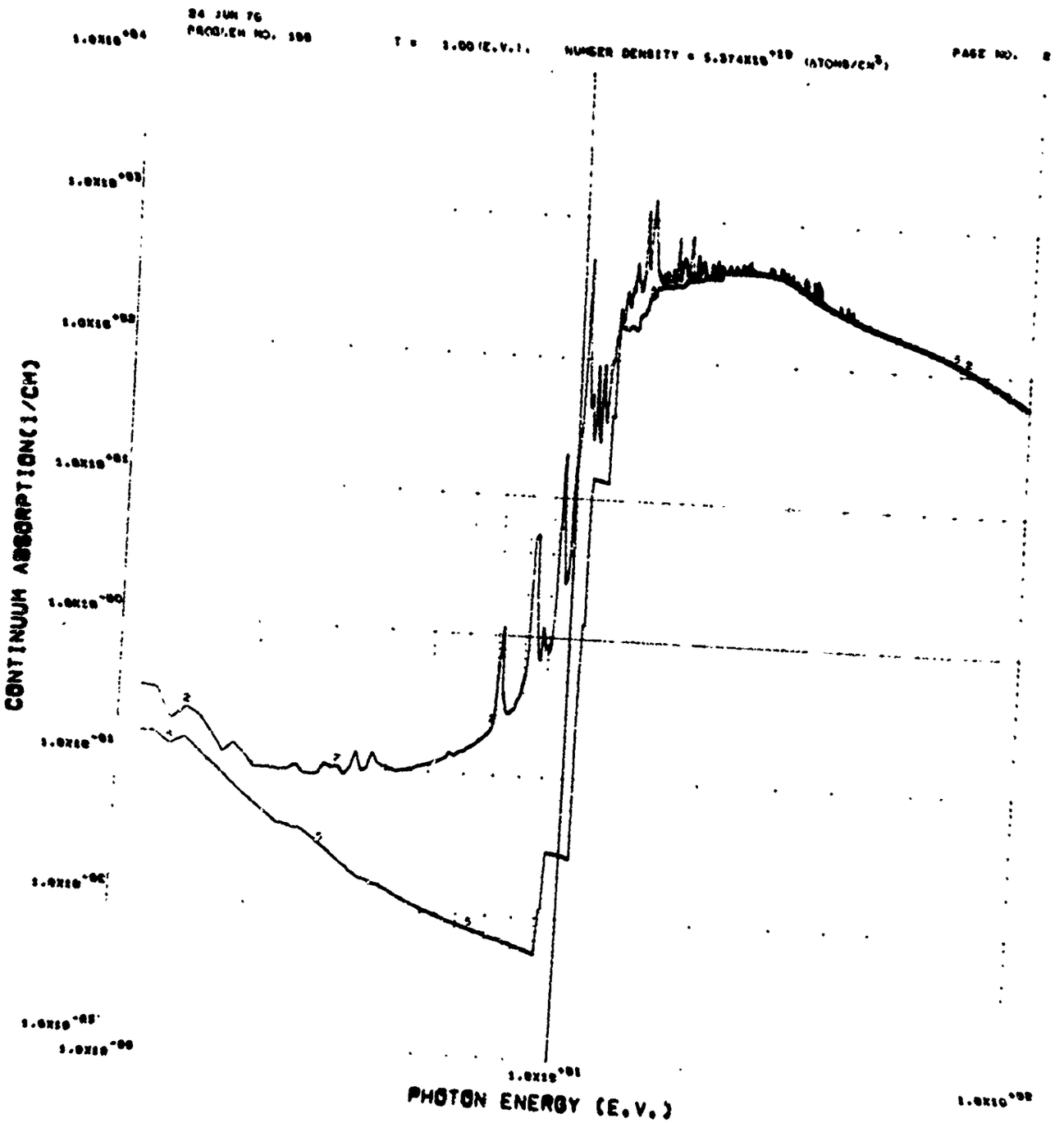
24 JUN 76
PROBLEM NO. 198
T = 1.00(E.V.)
NUMBER DENSITY = 5.374X10**19 (ATOMS/CM**3)
PAGE NO. 2
CONTINUUM ABSORPTION(1/CM)
PHOTON ENERGY (E.V.)

Figure 1

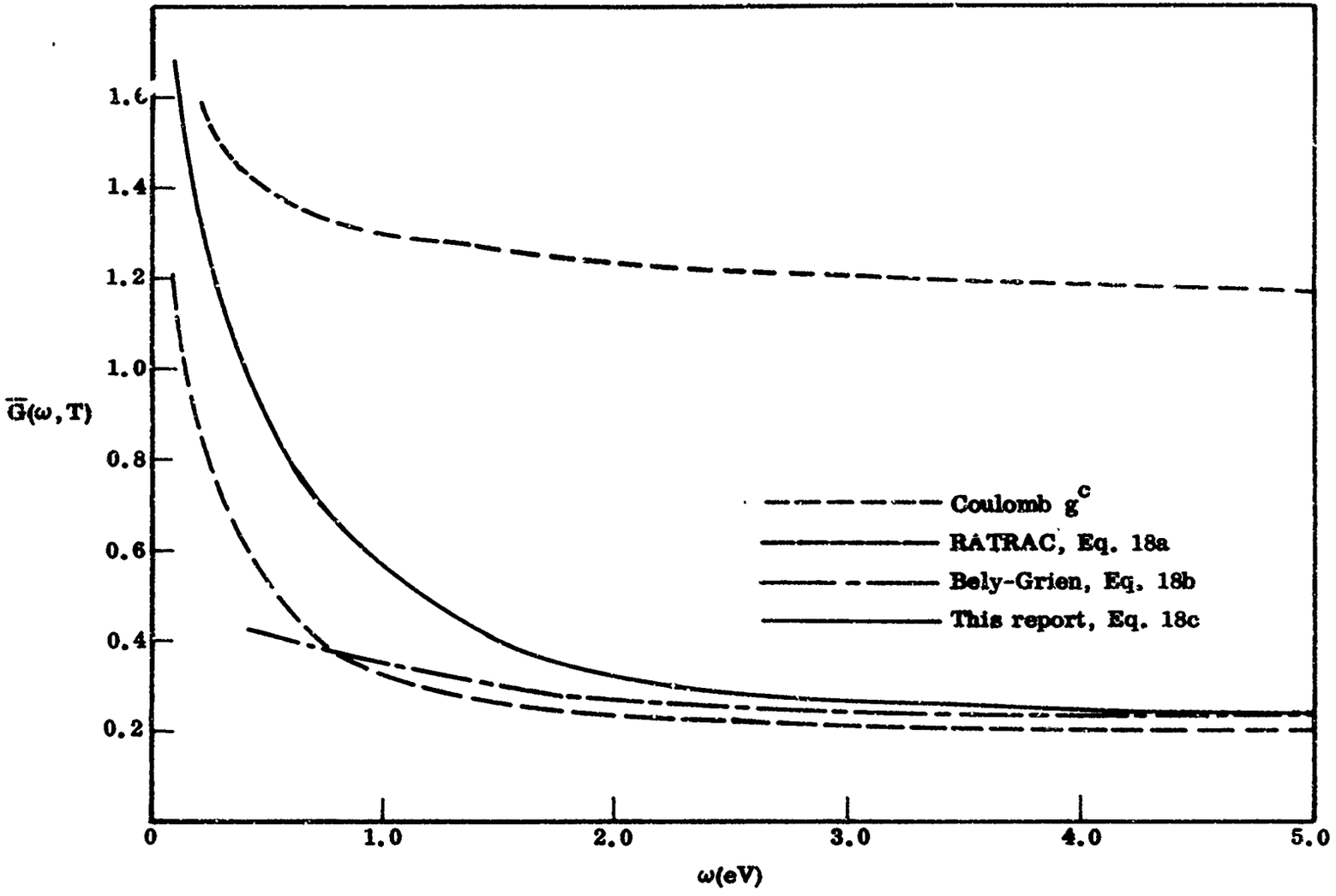

Fig. 2 Thermal Averaged Electron-Ion Collision Broadening Gaunt Factors $\bar{\bar{G}}(\omega, T)$(kT = 2.0 eV)

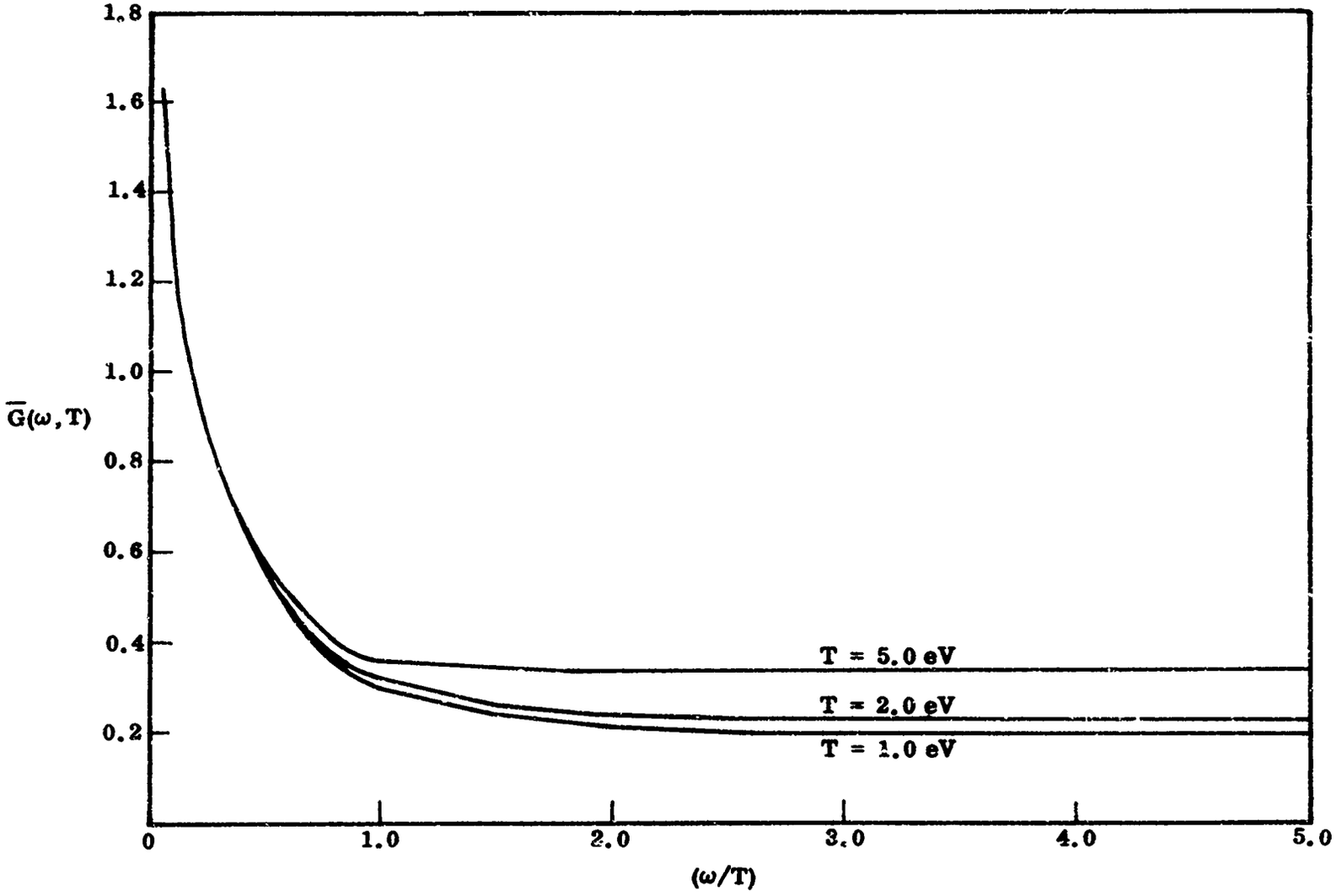

Fig. 3 Thermal Averaged Electron-Ion Collision Broadening Gaunt Factors (Eq. 18c) (for various temperatures)

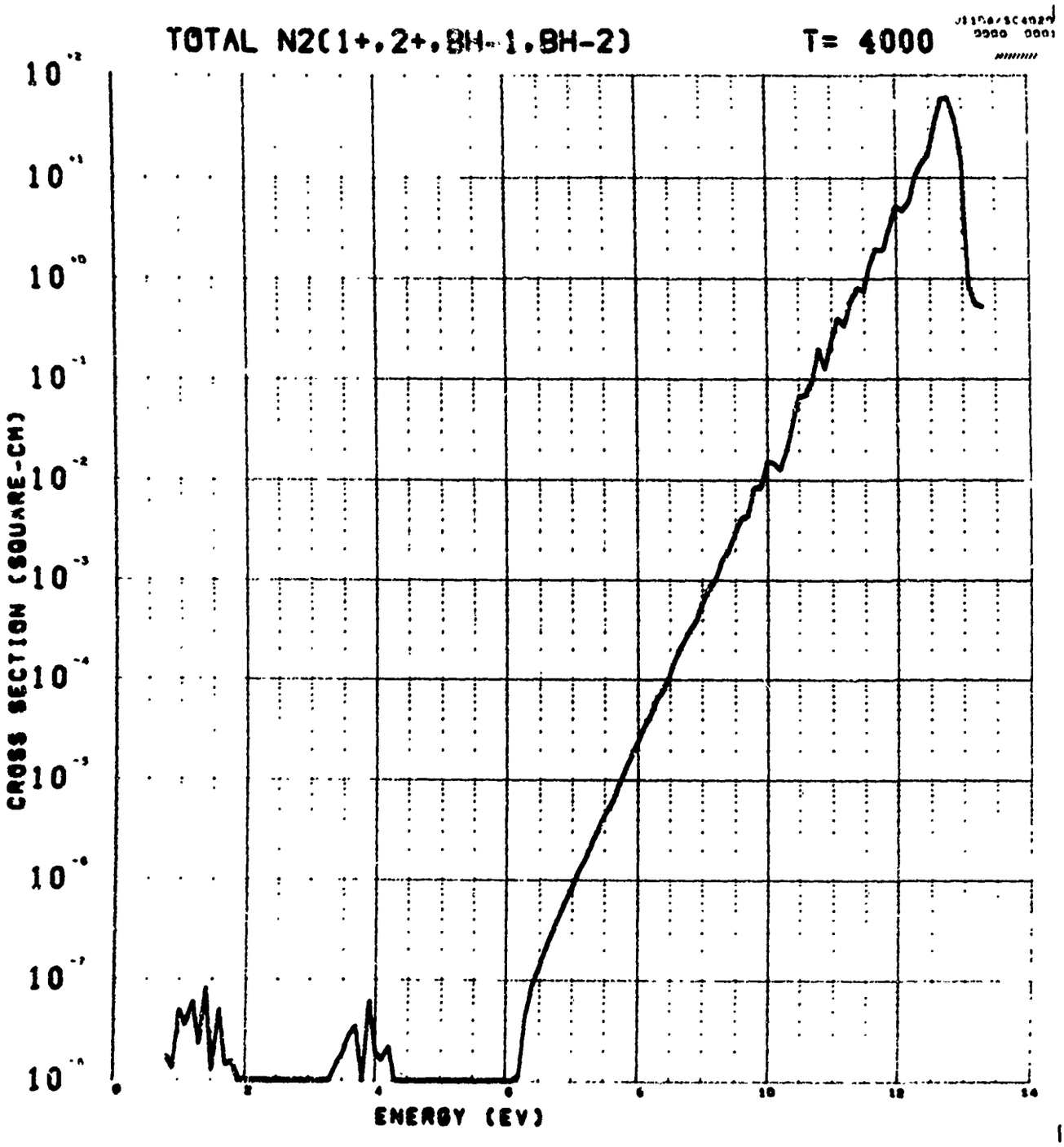

Figure 4

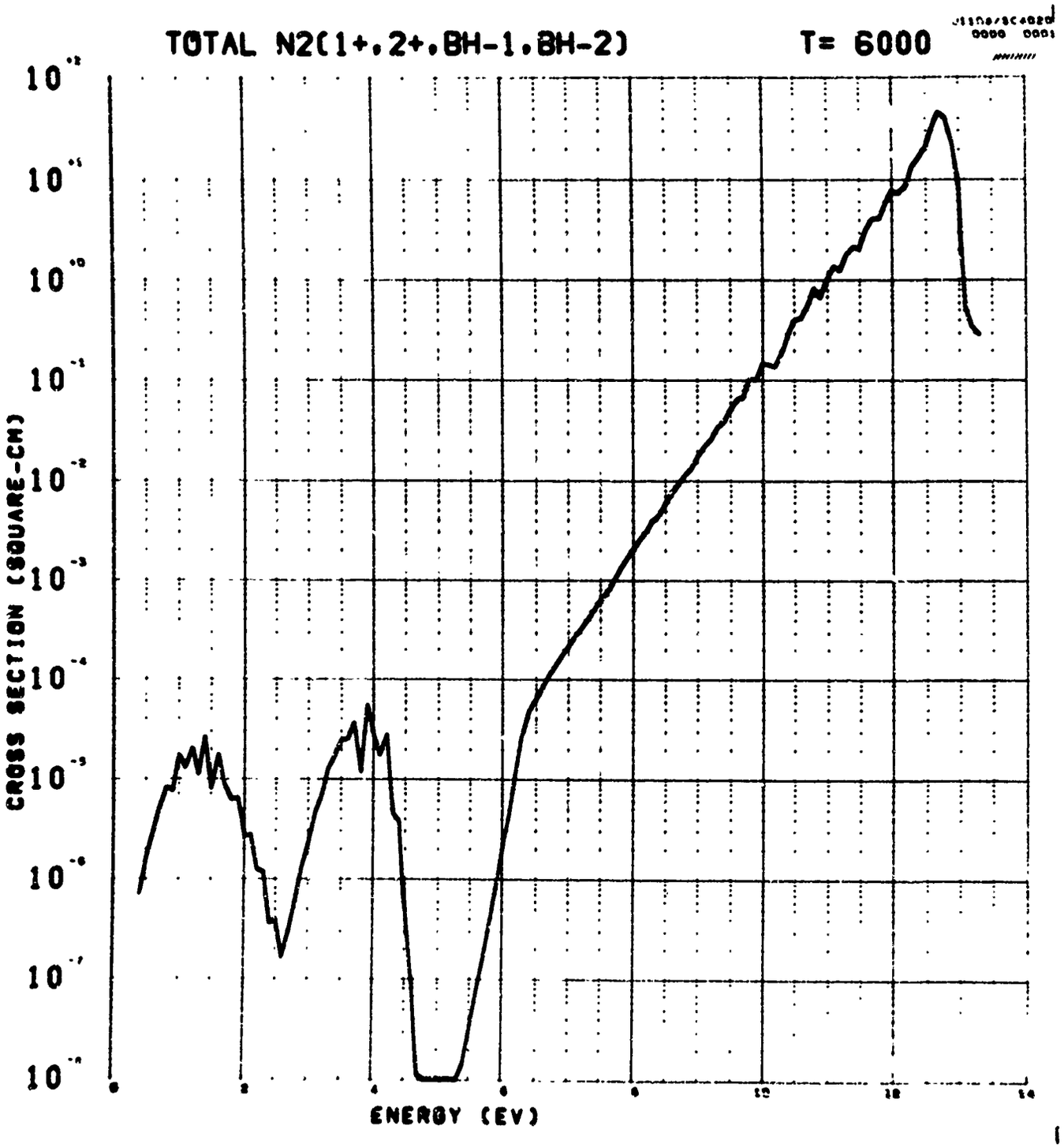

Figure 5

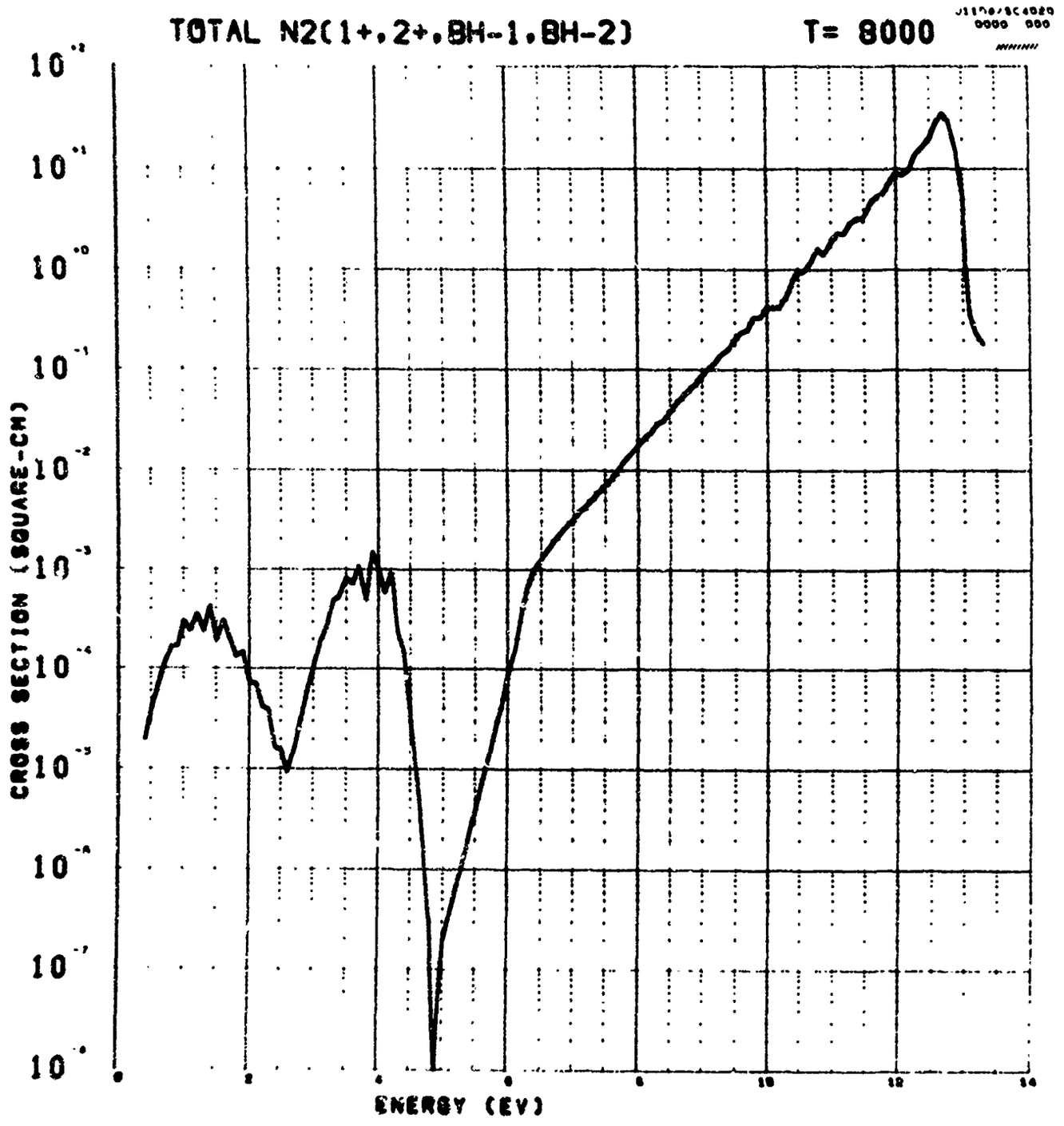

Figure 6

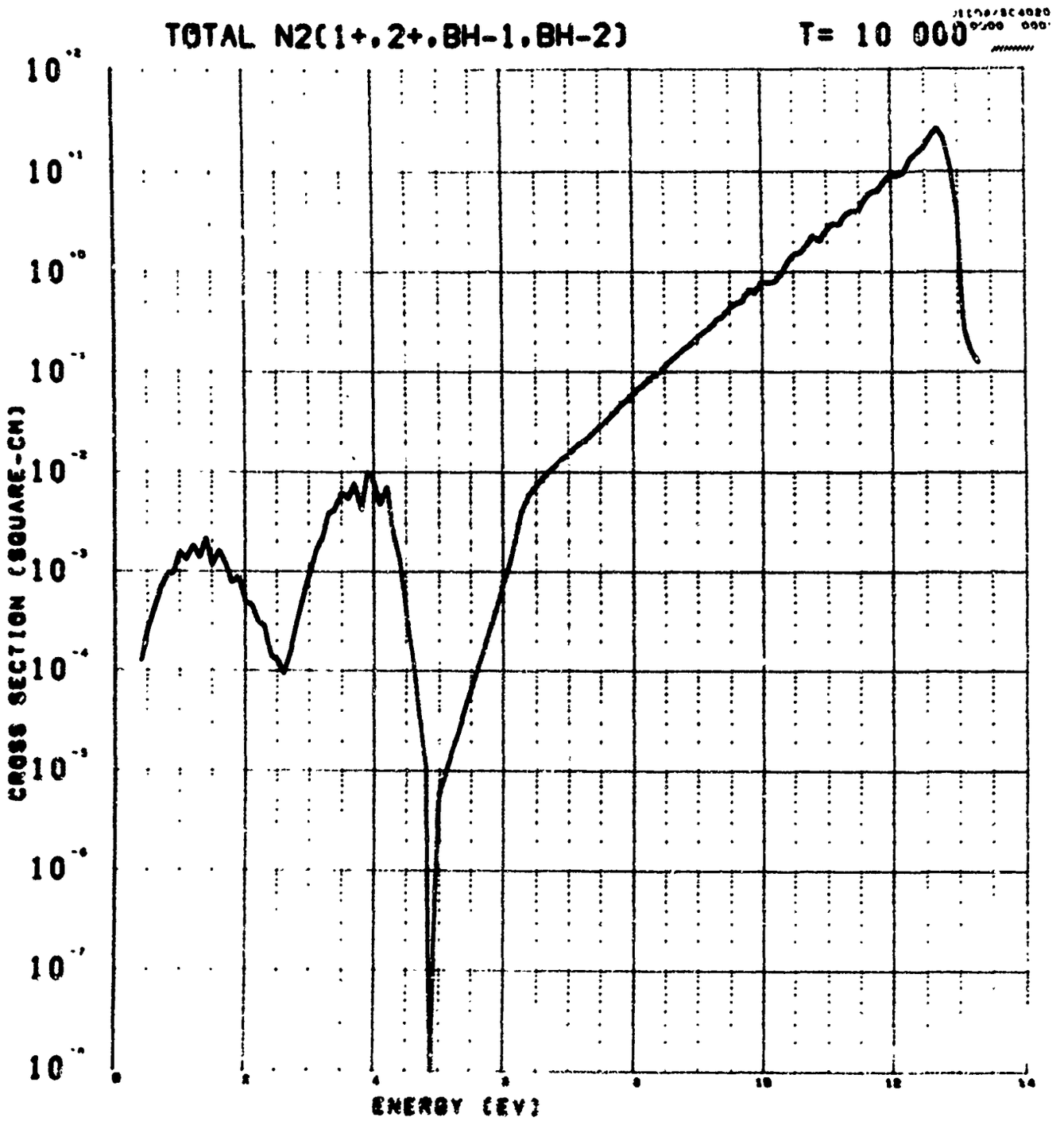

Figure 7

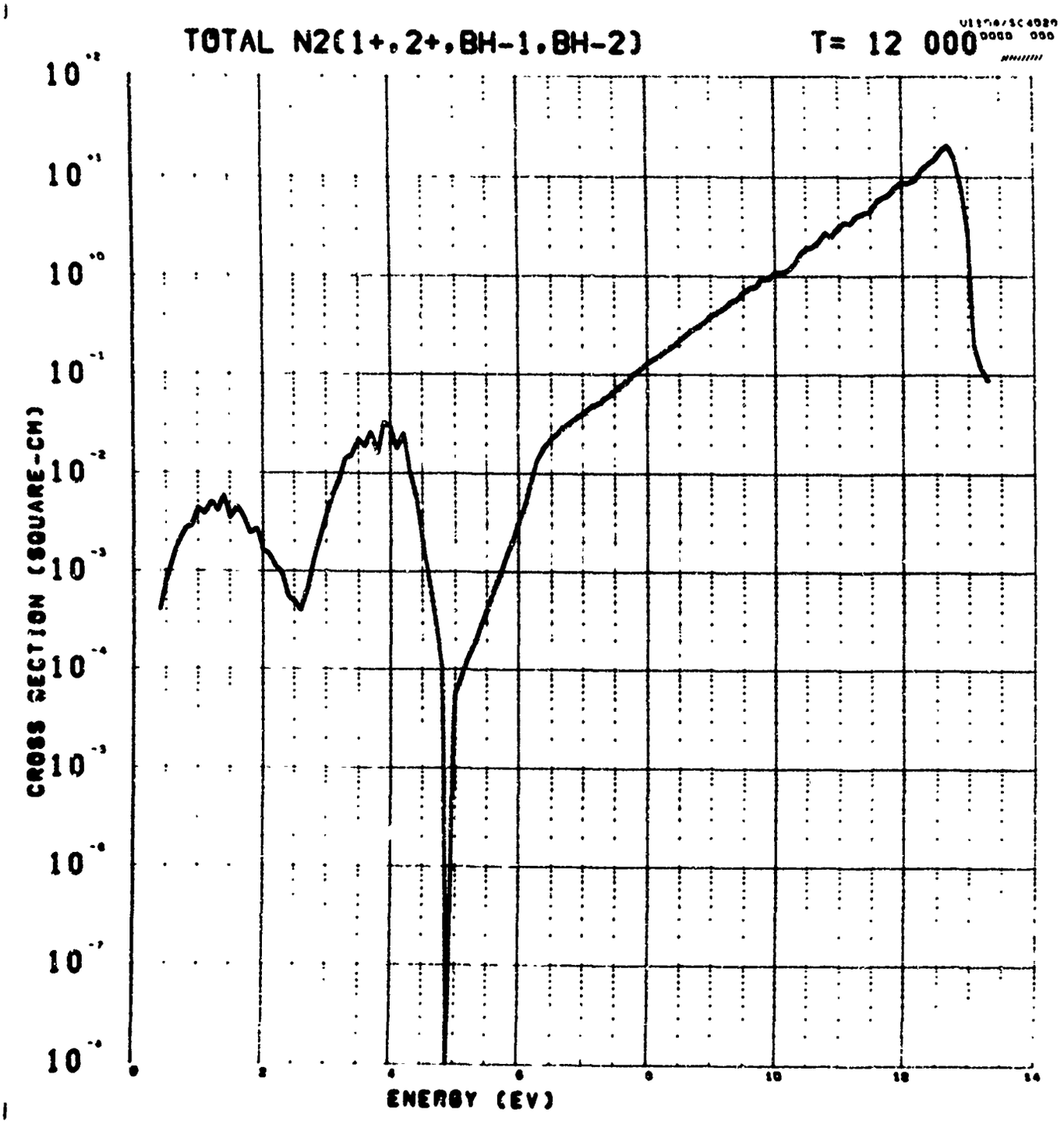

Figure 8

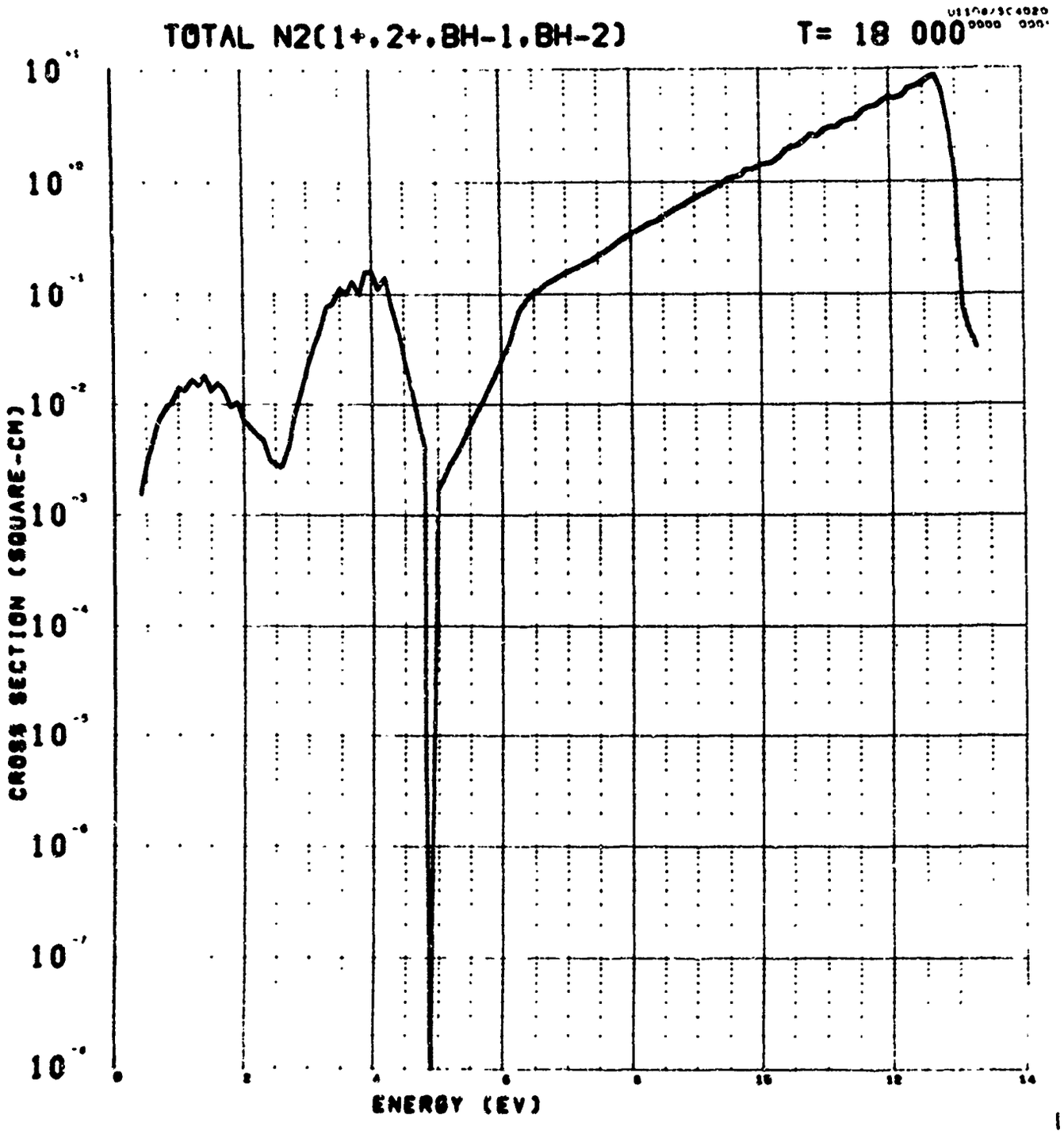

Figure 9

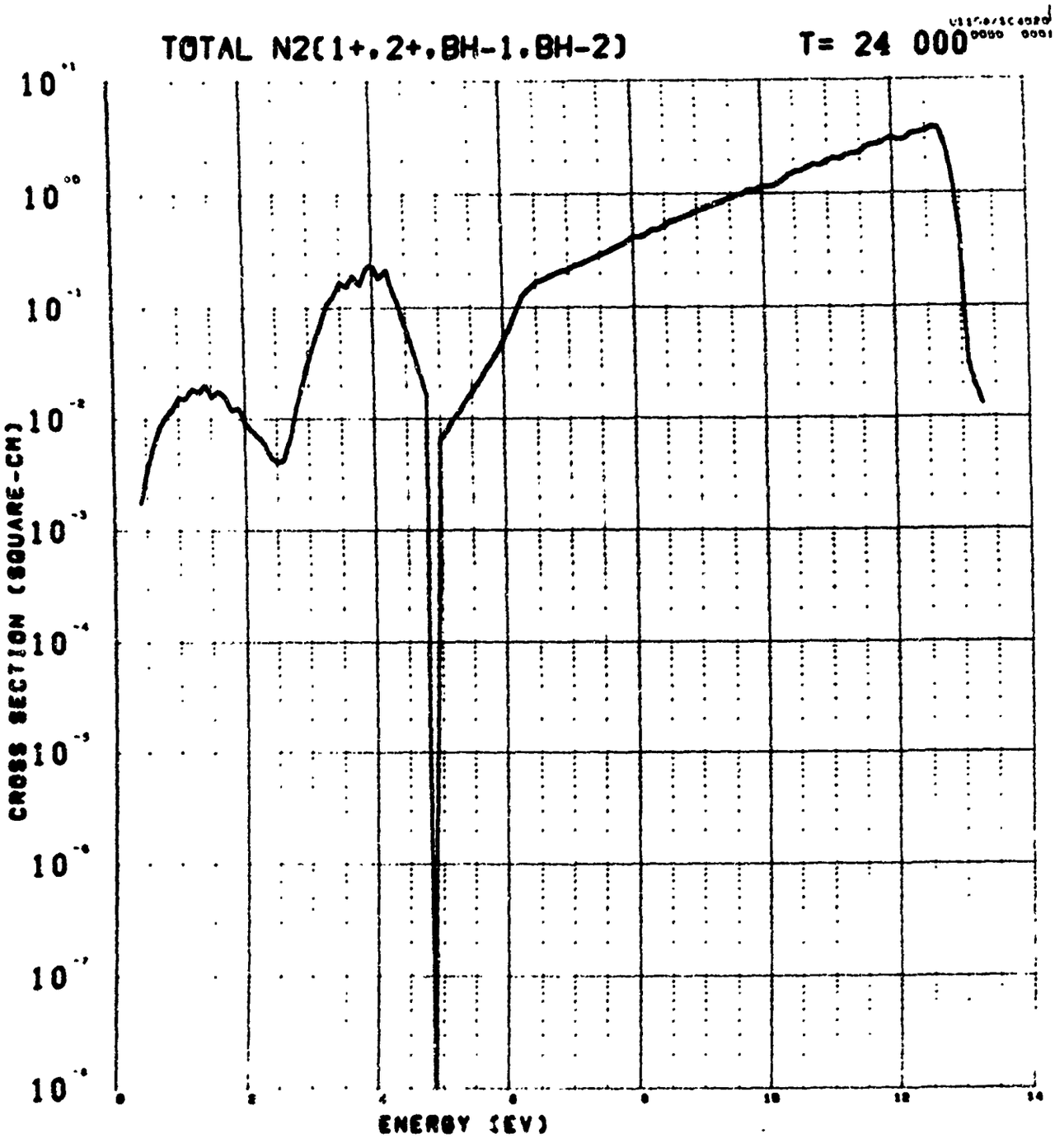

Figure 10

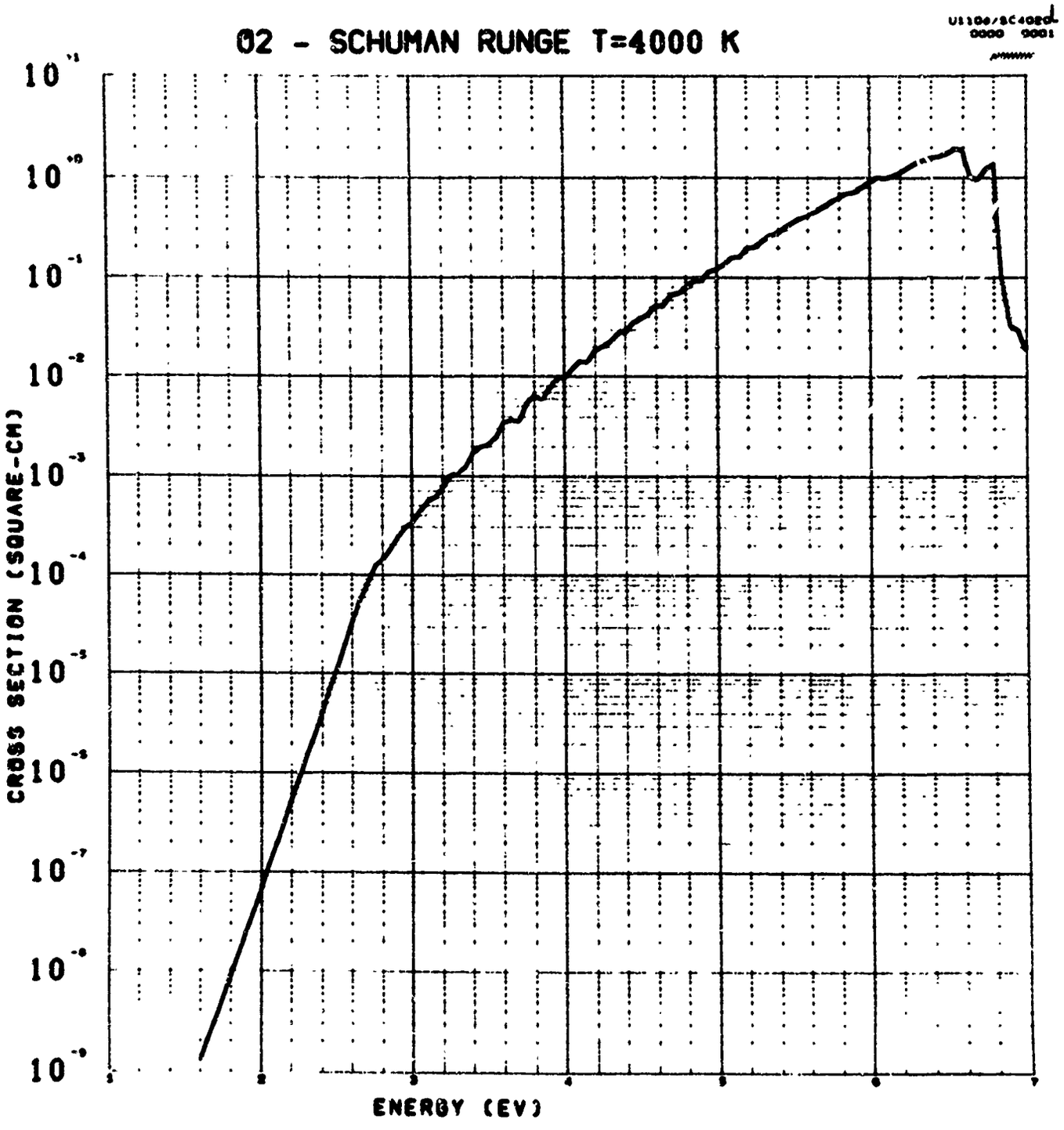

Figure 11

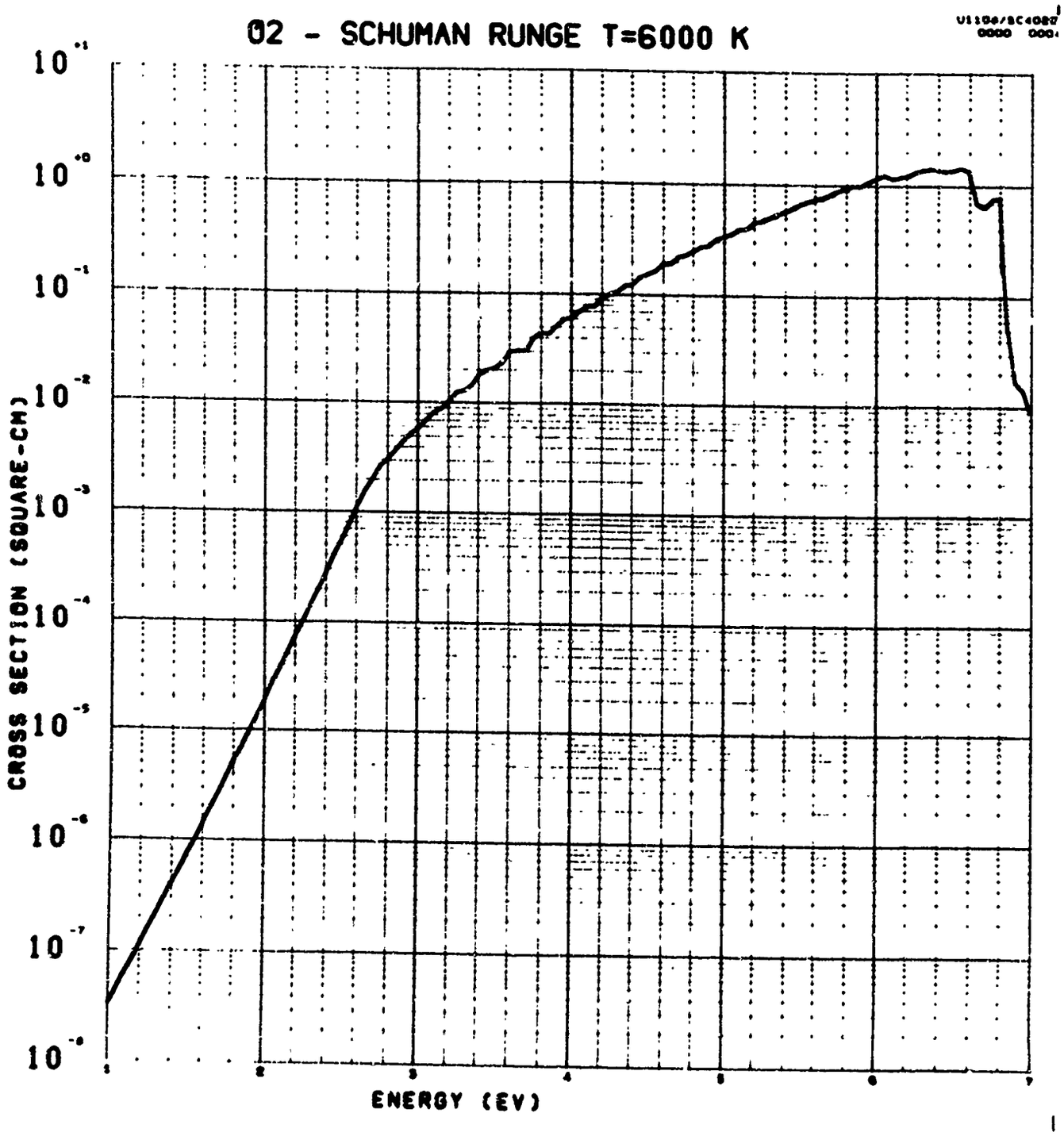

Figure 12

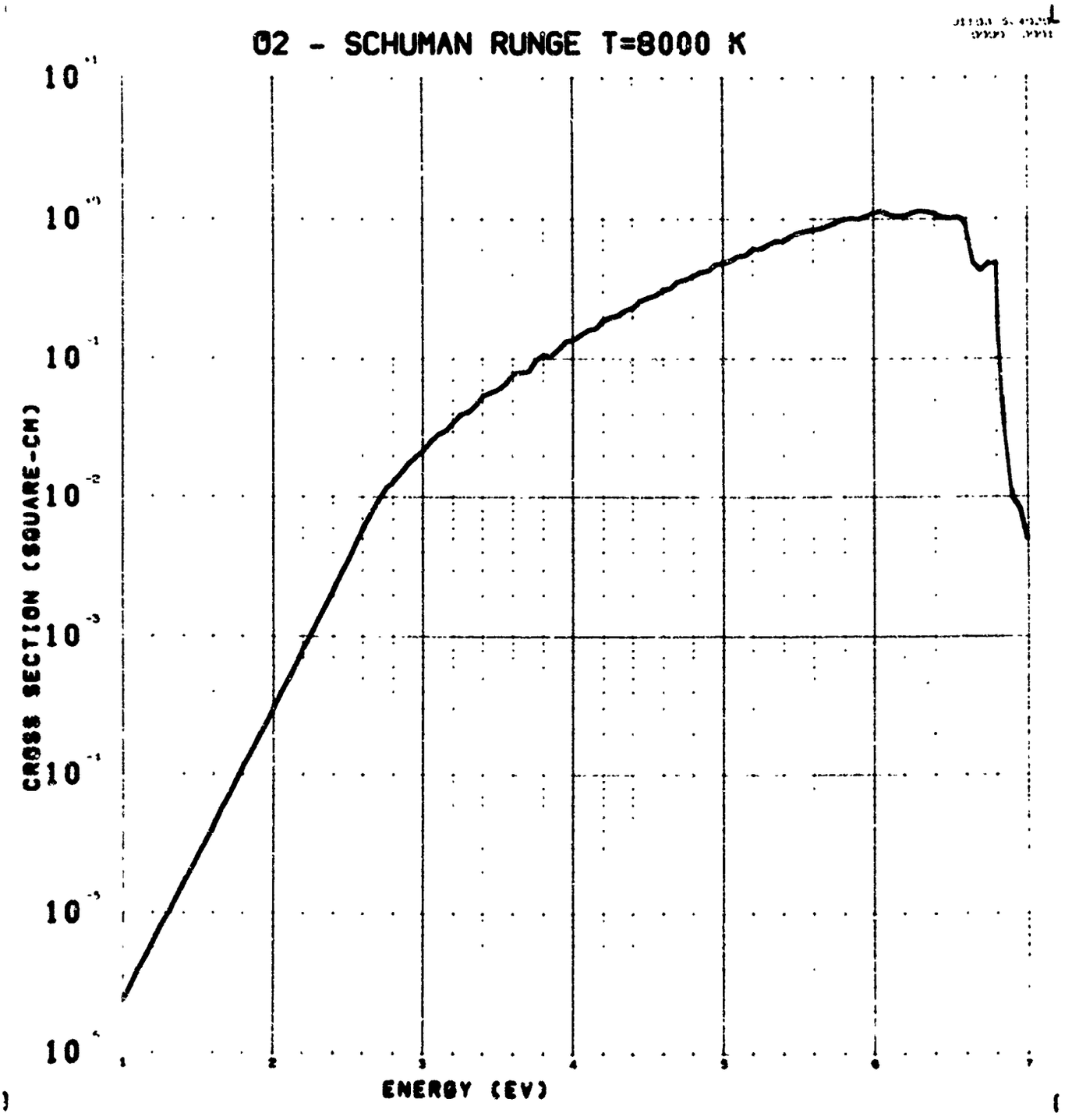

Figure 13

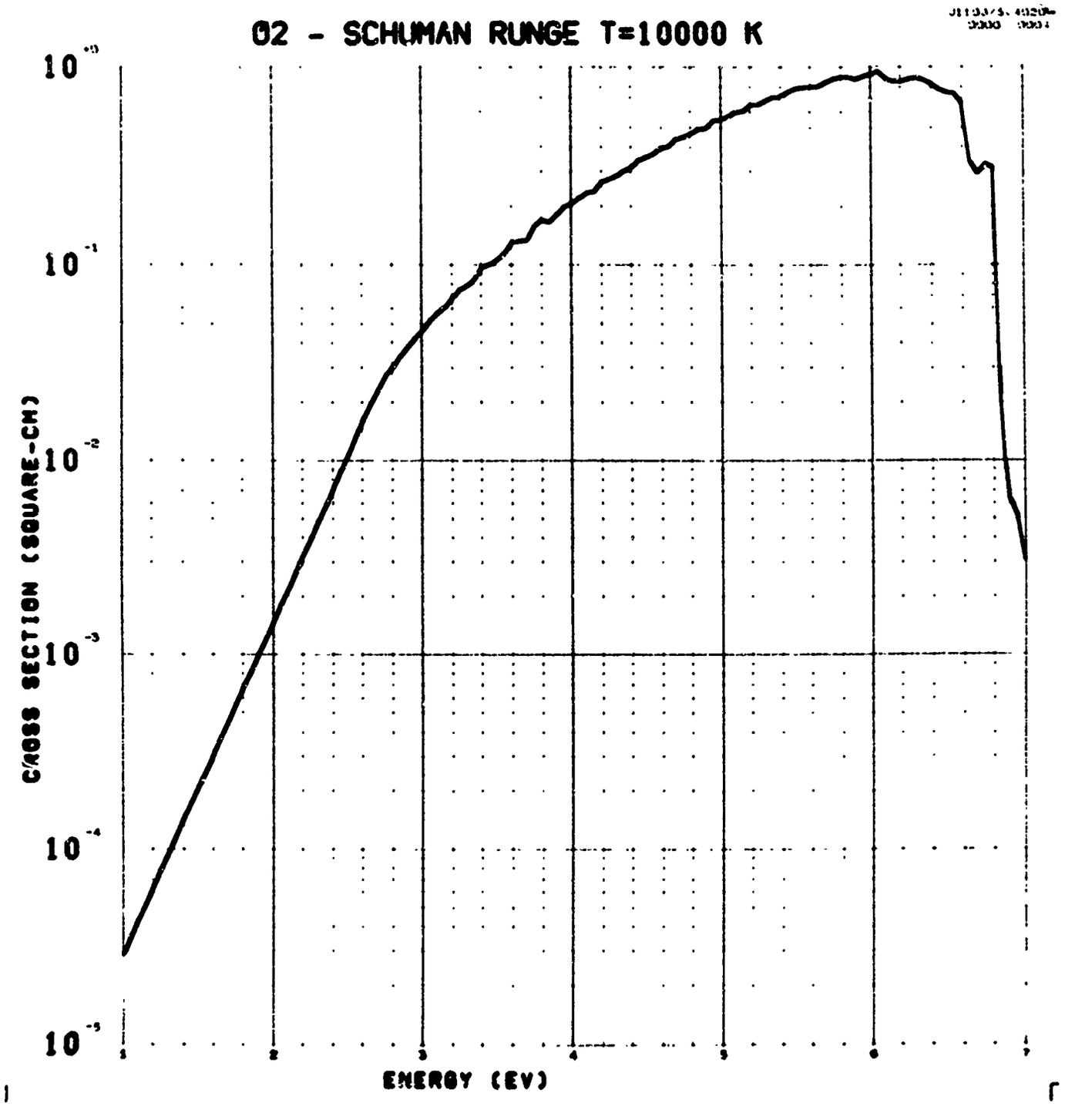

Figure 14

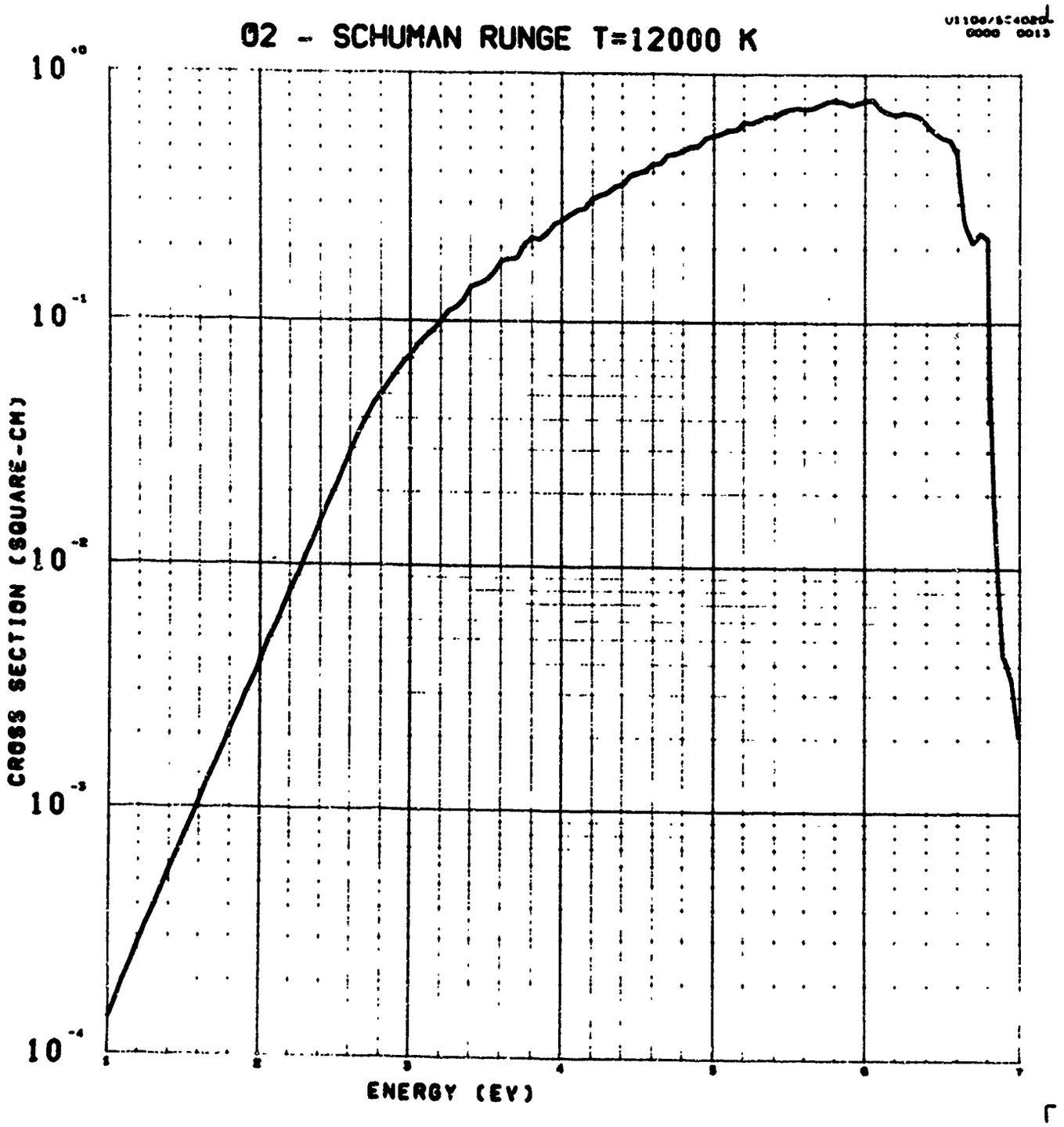

Figure 15

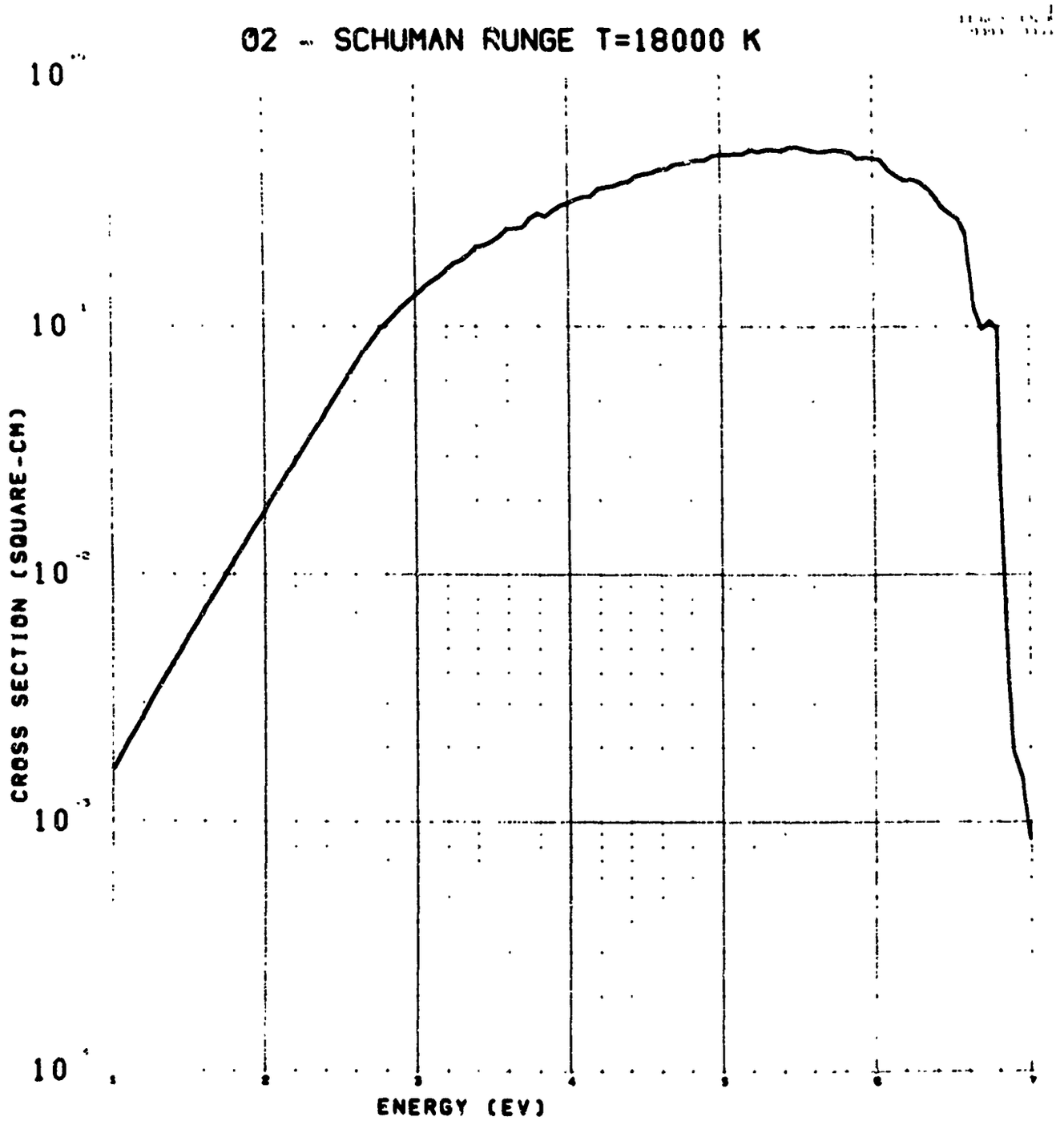

Figure 16

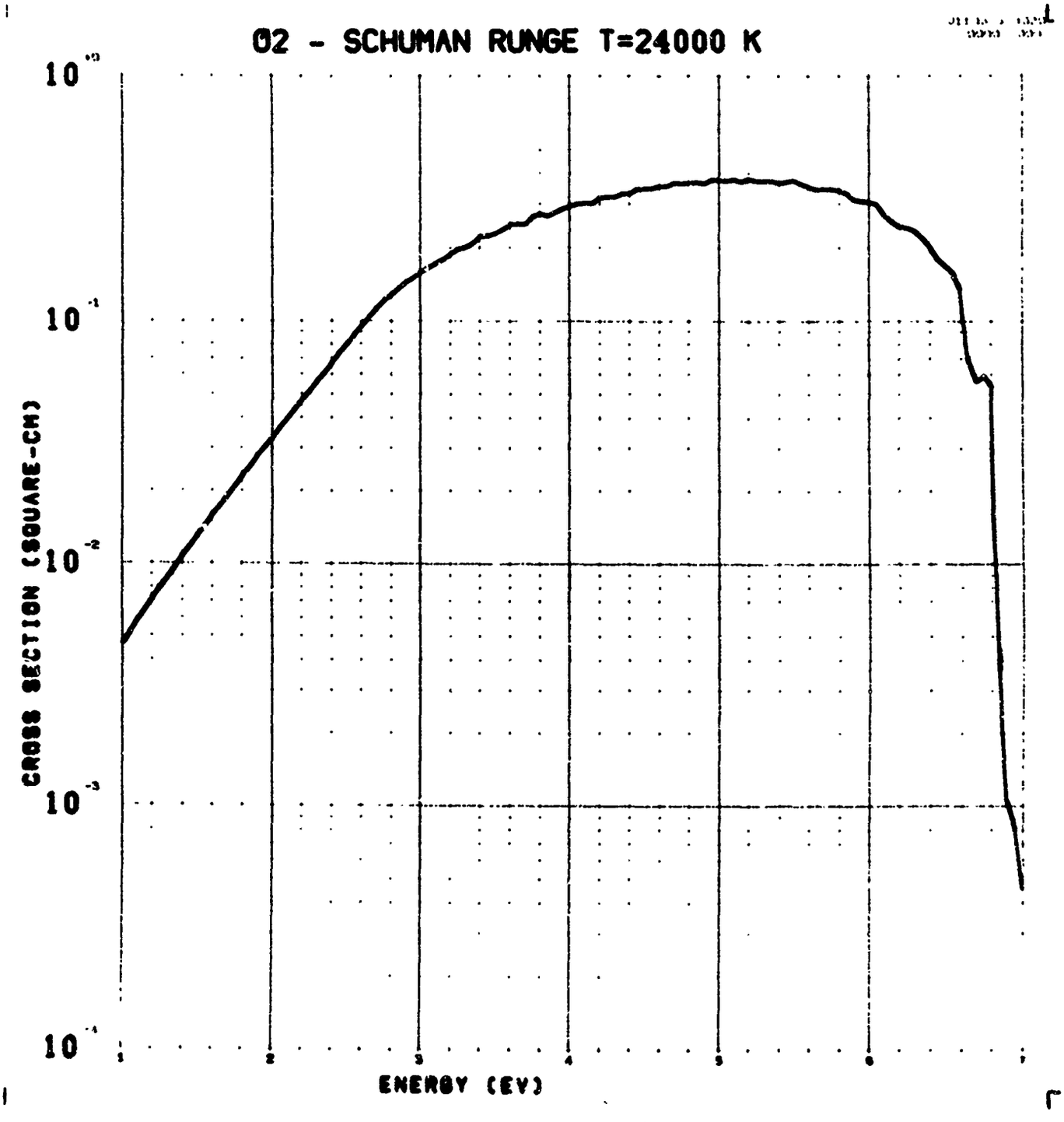

Figure 17

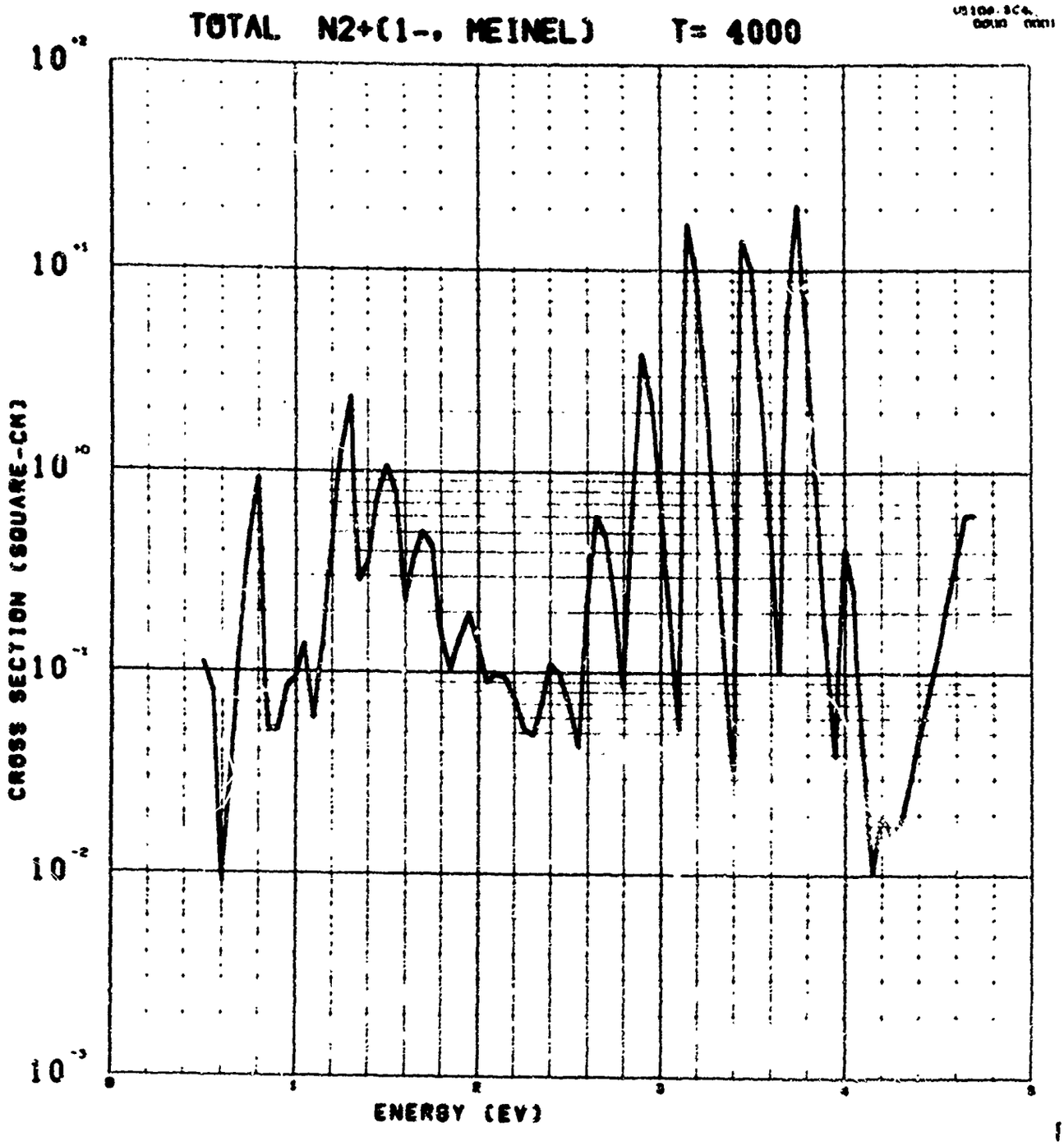

Figure 18

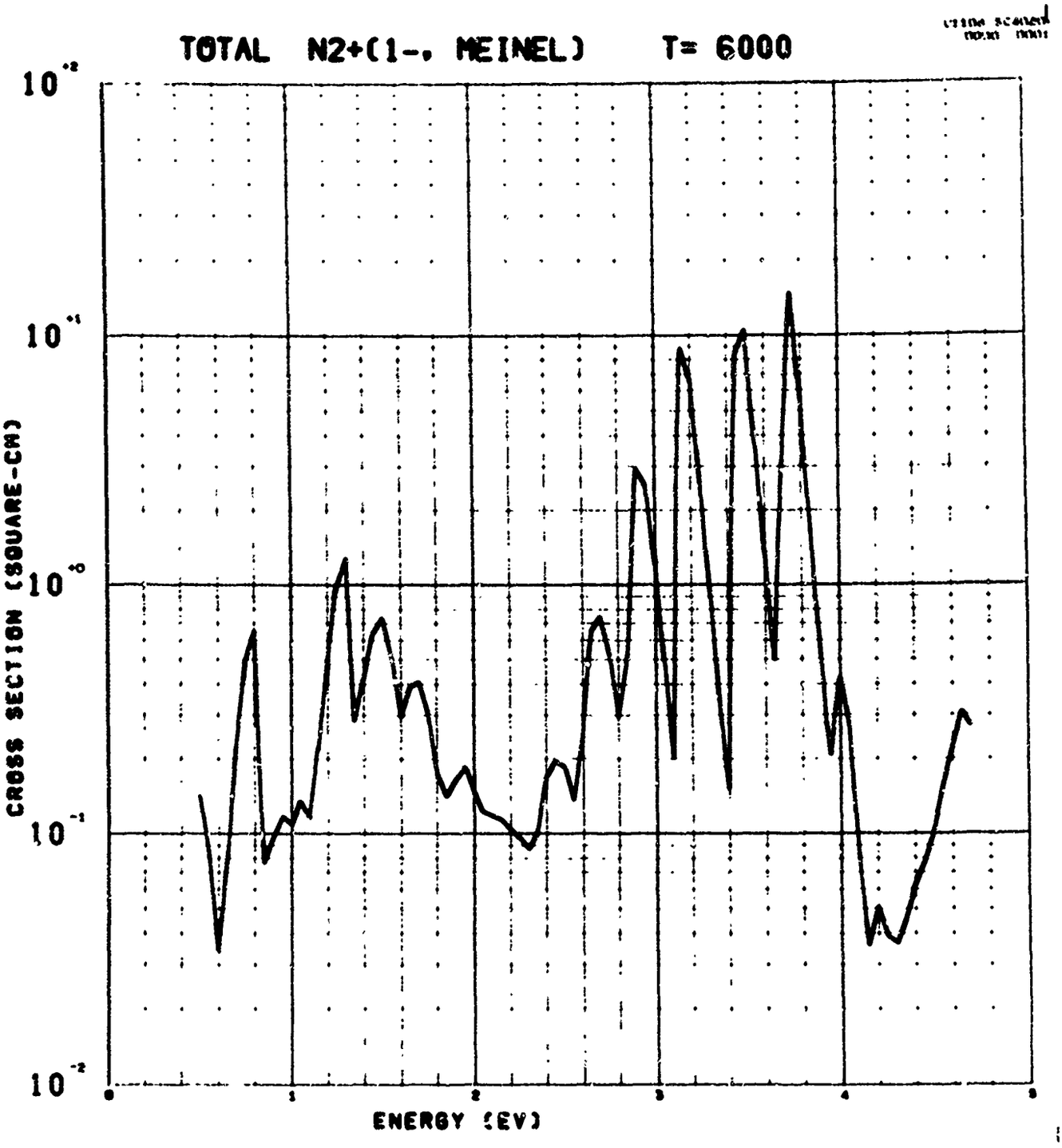

Figure 19

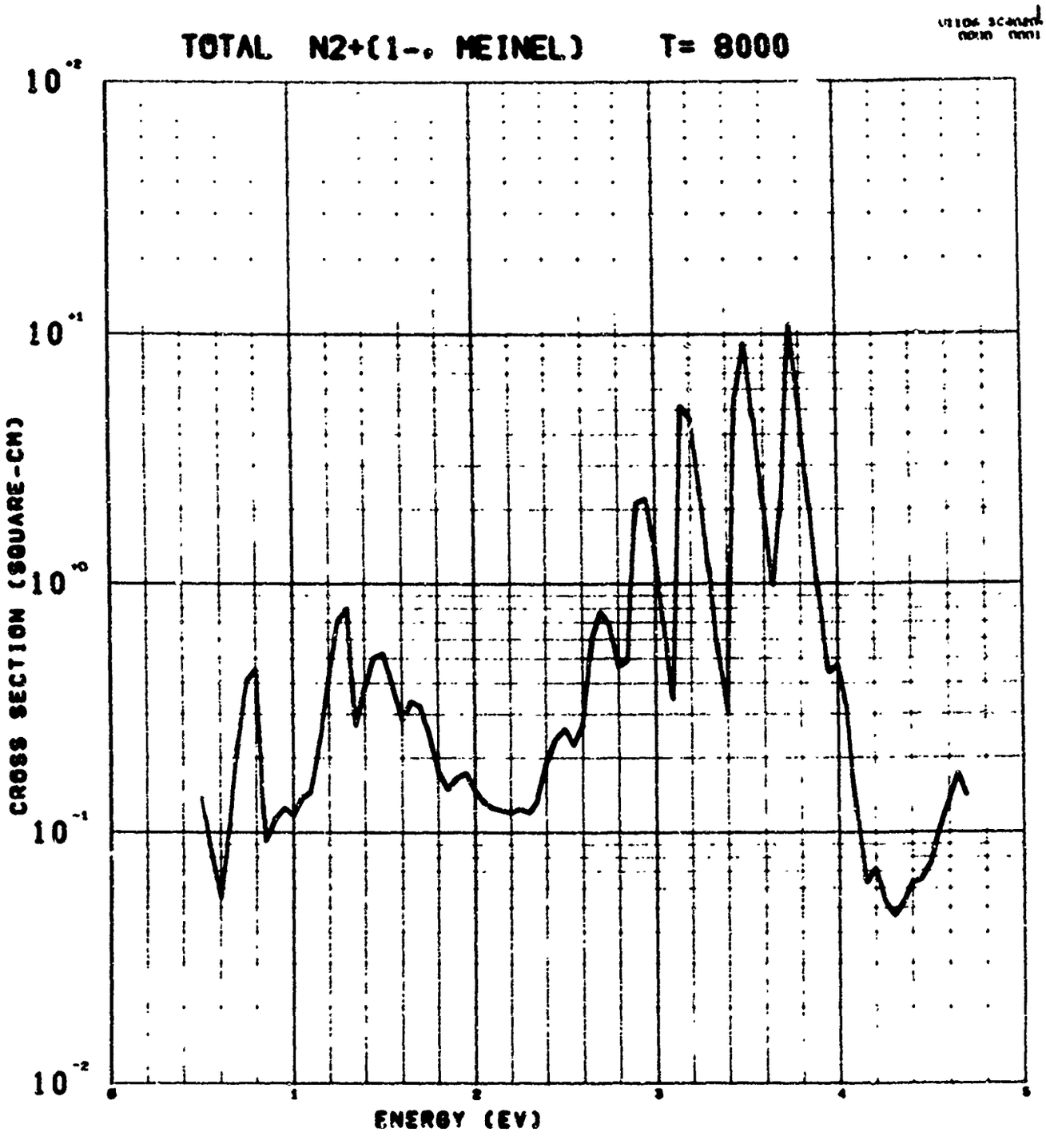

Figure 20

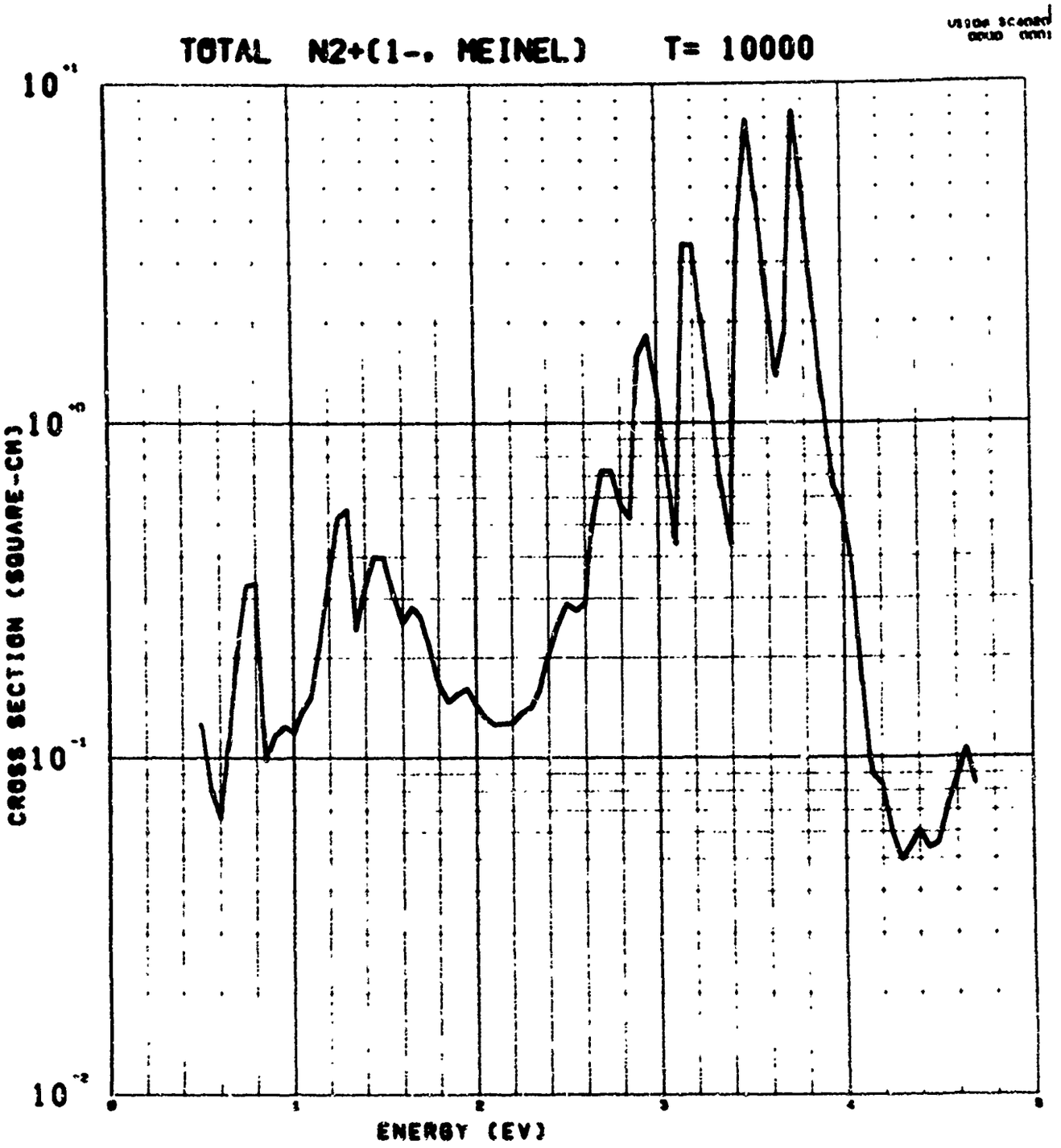

Figure 21

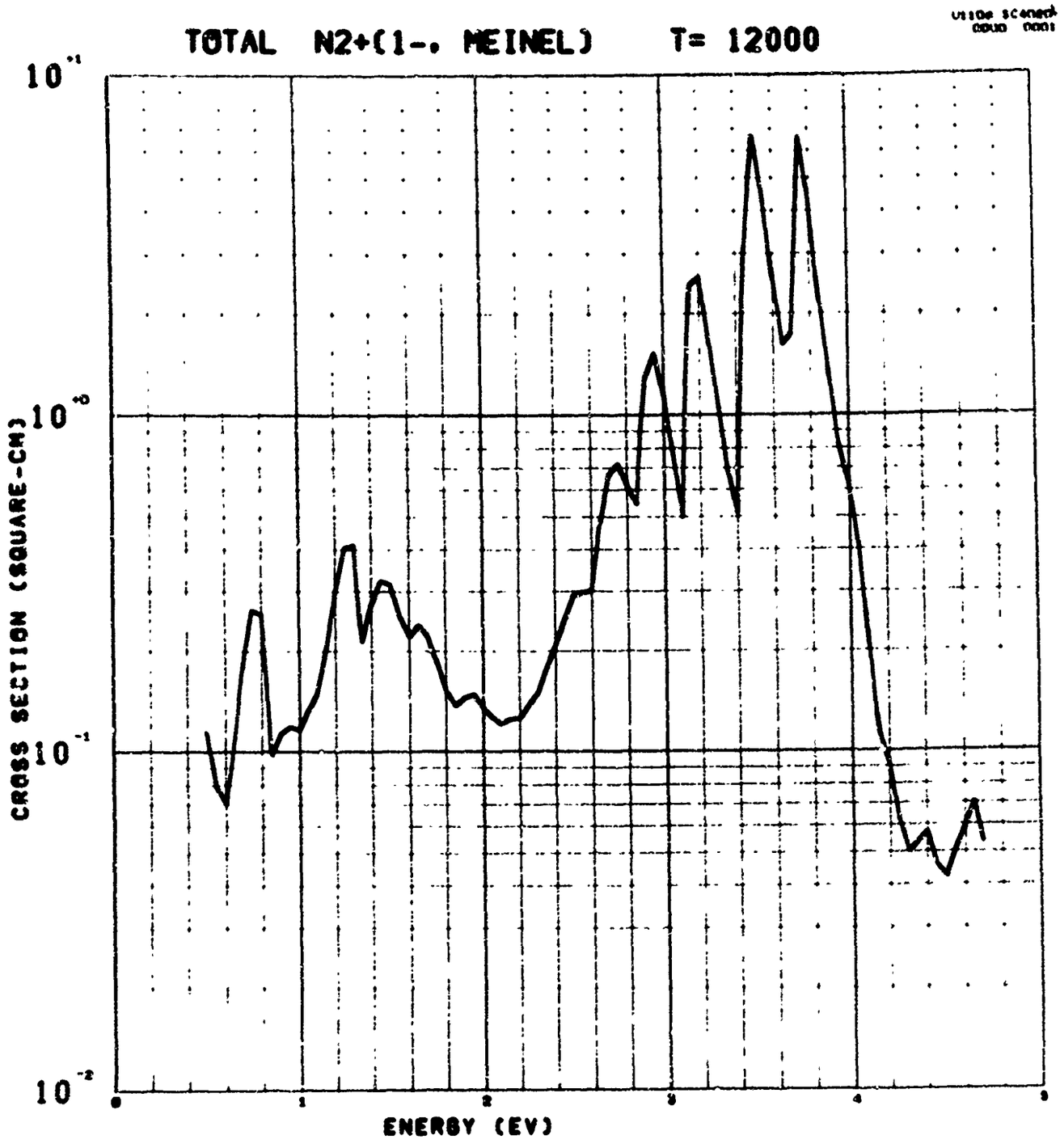

Figure 22

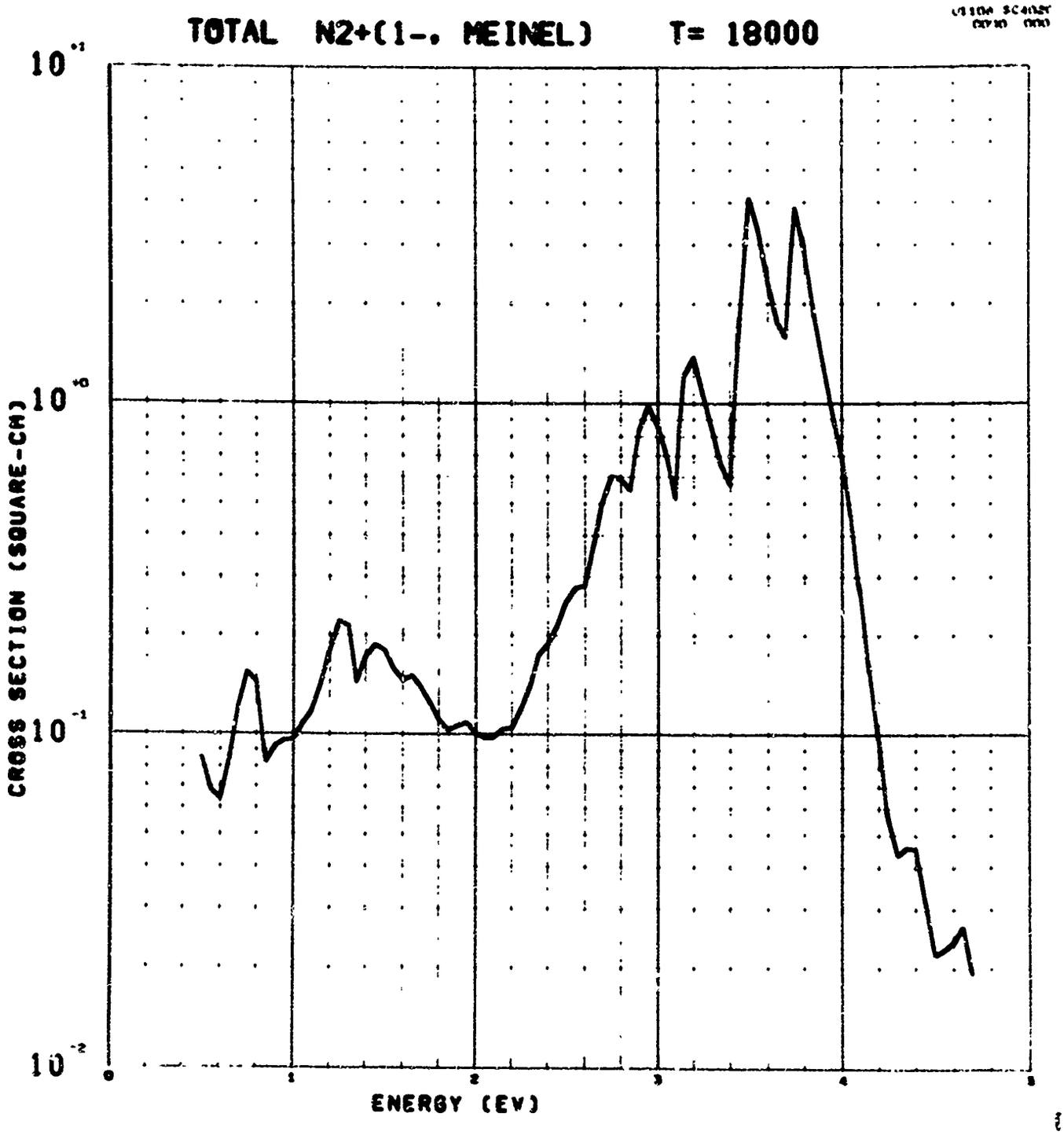

Figure 23

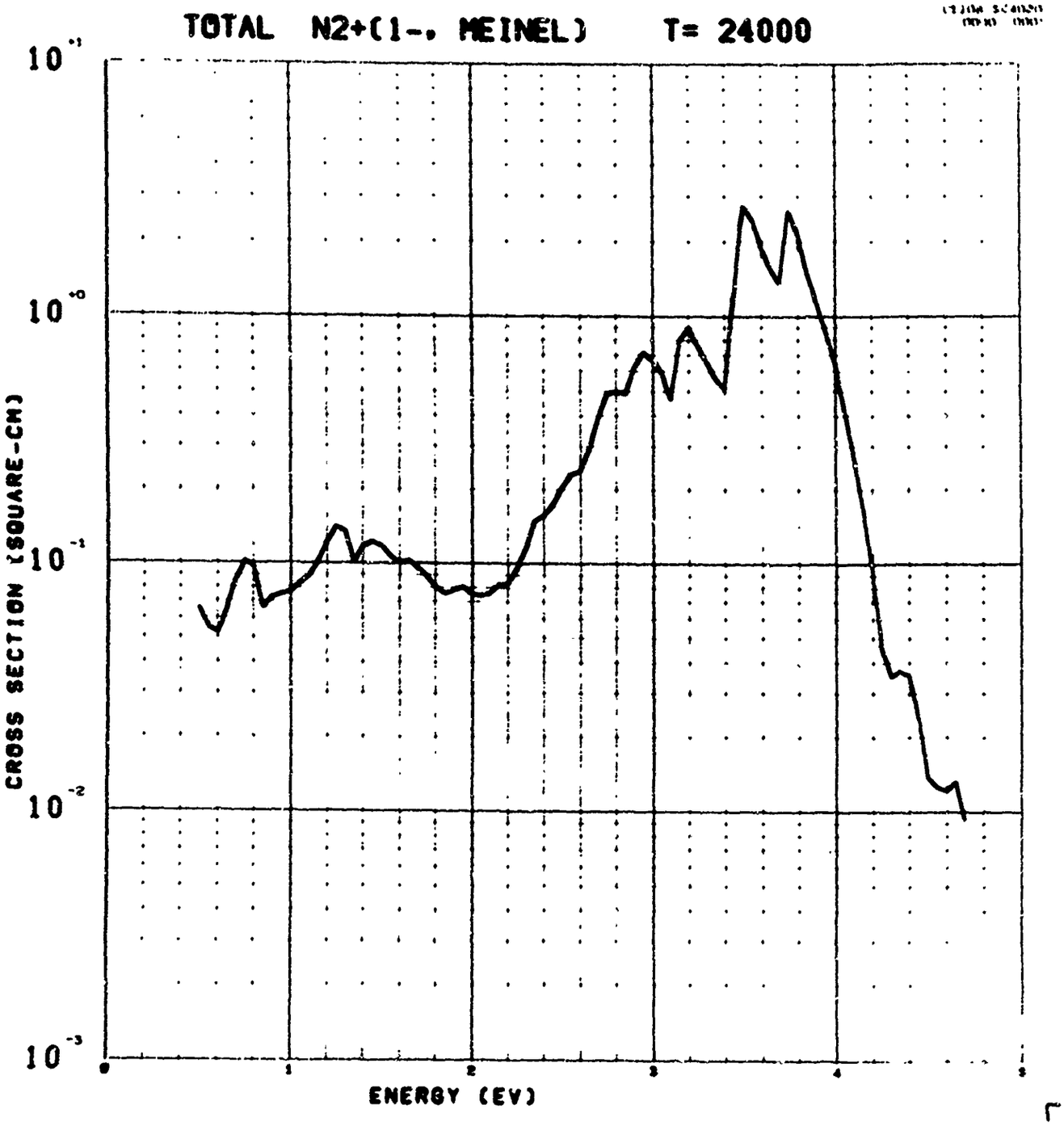
TOTAL N2+(1-, MEINEL) T= 24000
CROSS SECTION (SQUARE-CM)
10^{-1}
10^{0}
10^{-1}
10^{-2}
10^{-3}
0
1
2
3
4
5
ENERGY (EV)

Figure 24

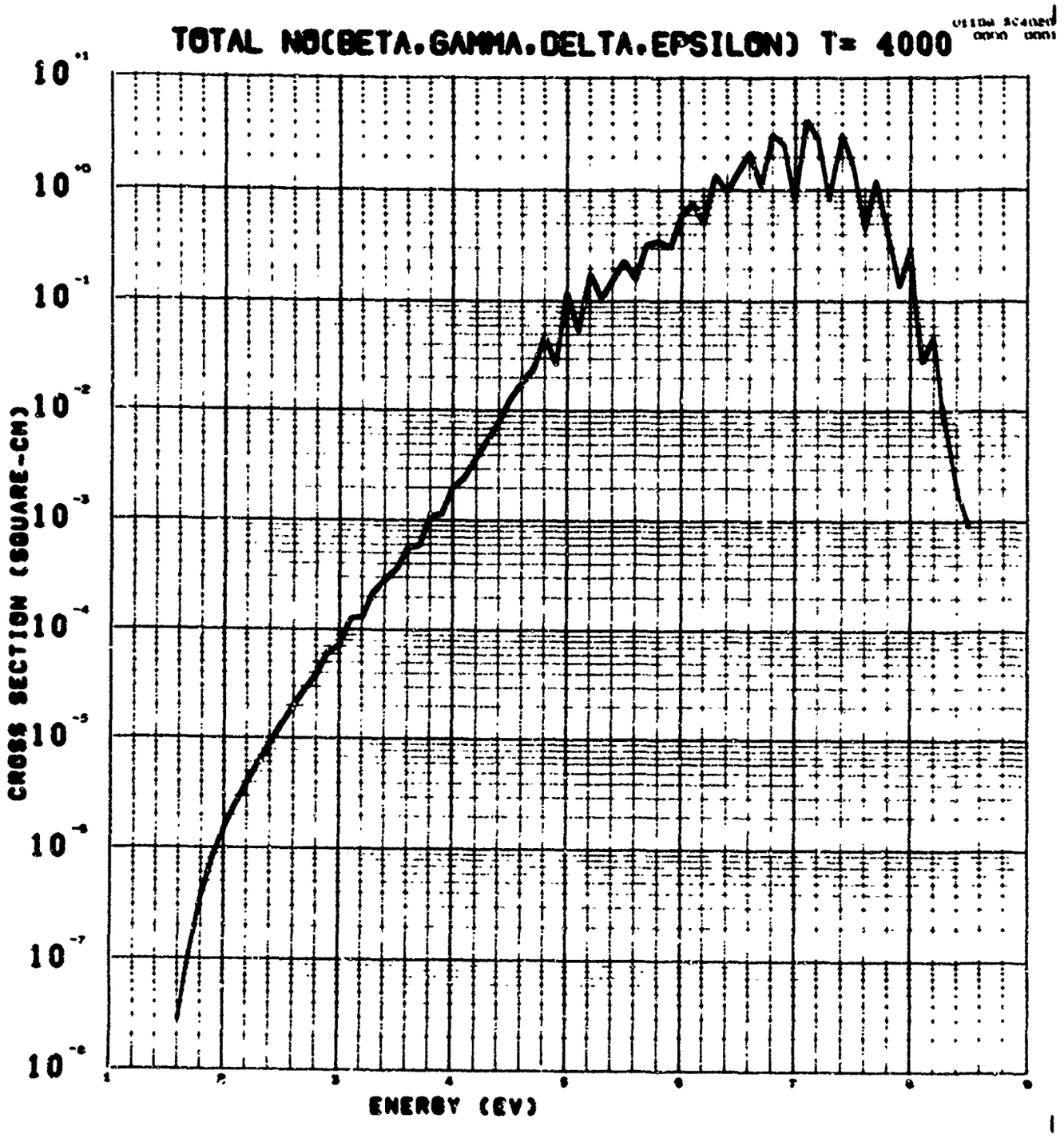
TOTAL NO(BETA.GAMMA.DELTA.EPSILON) T= 4000
CROSS SECTION (SQUARE-CM)
ENERGY (EV)

Figure 25

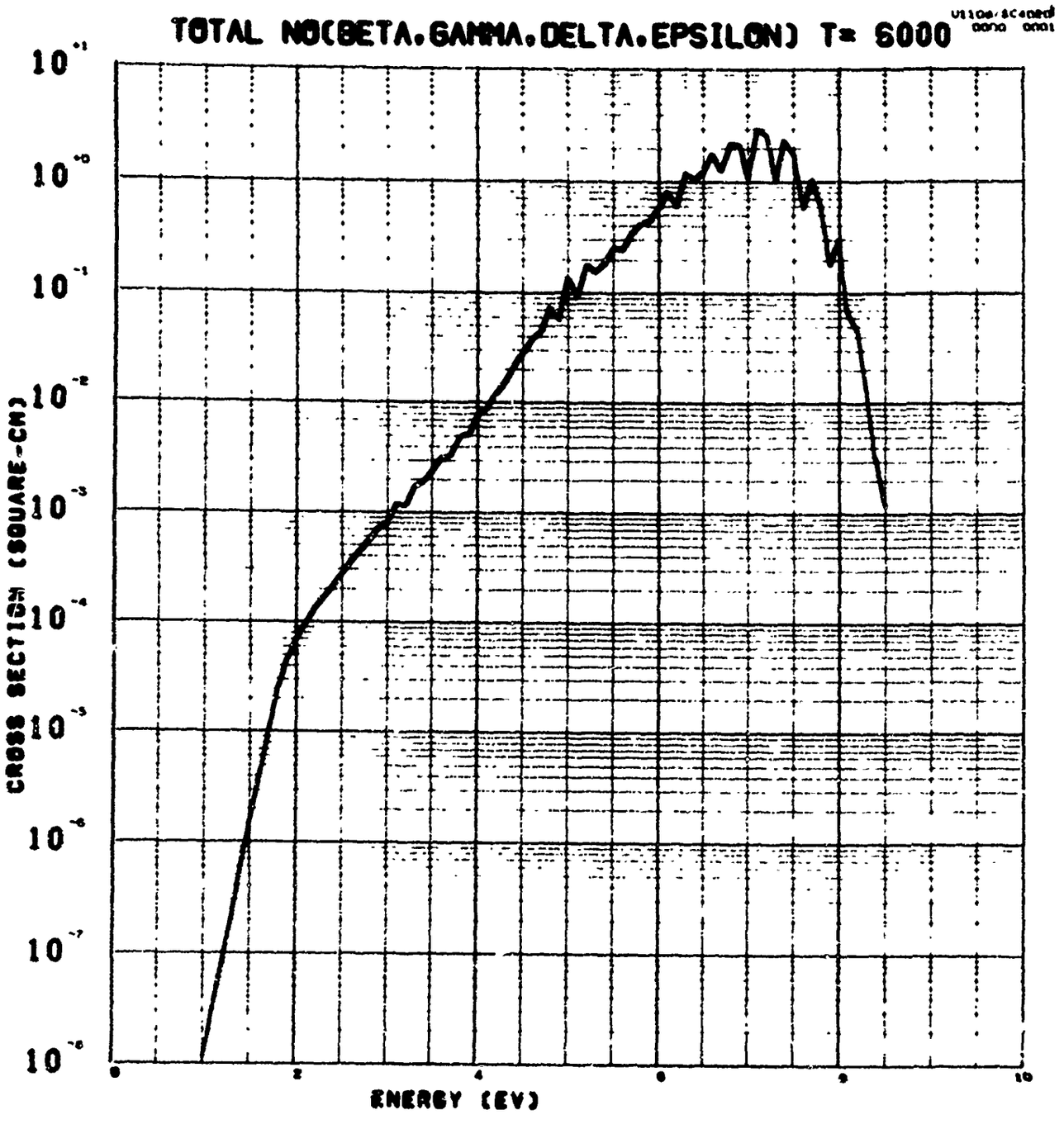
TOTAL NO(BETA.GAMMA.DELTA.EPSILON) T= 6000
CROSS SECTION (SQUARE-CM)
ENERGY (EV)

Figure 26

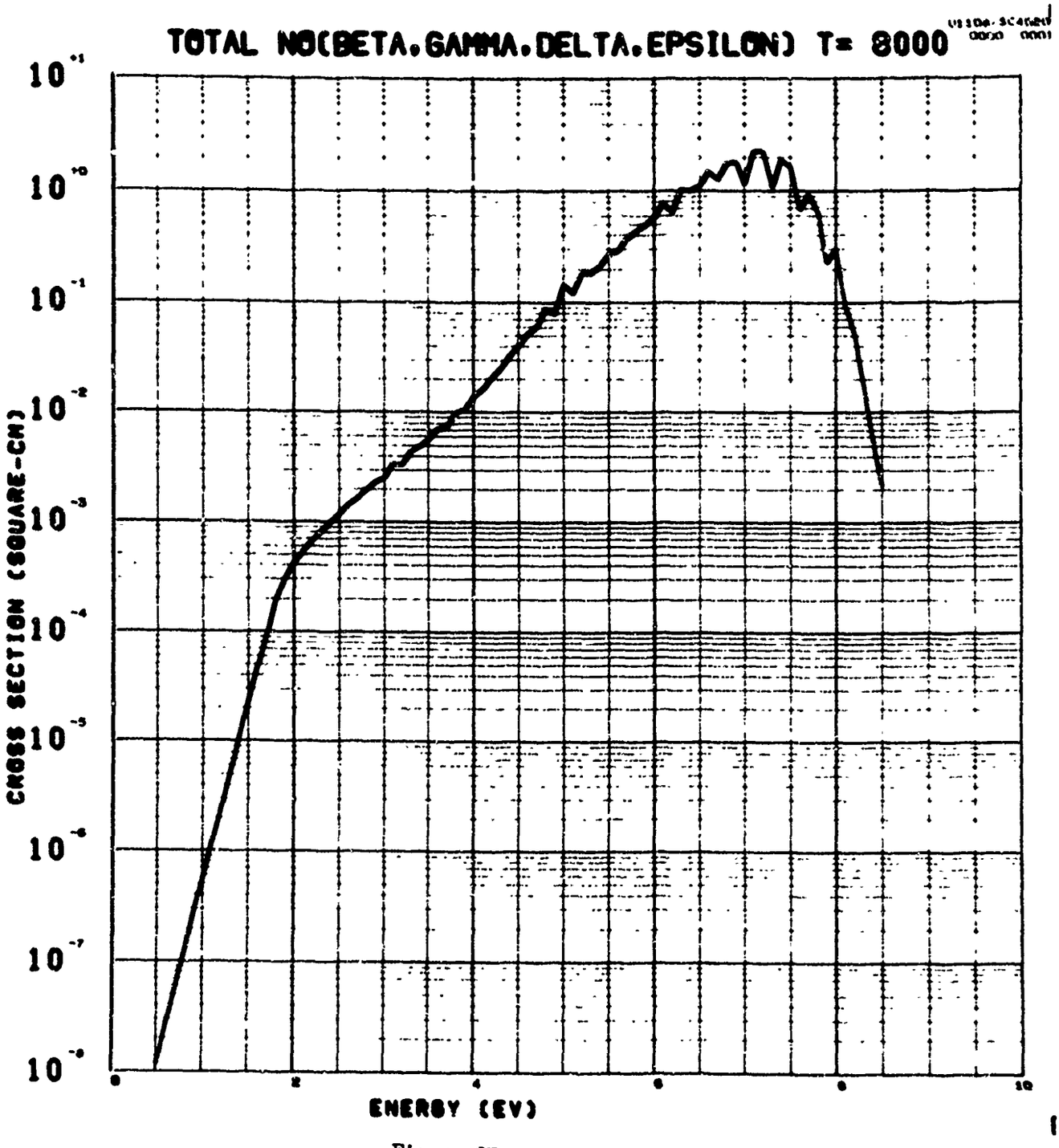
TOTAL NO(BETA.GAMMA.DELTA.EPSILON) T= 8000
CROSS SECTION (SQUARE-CM)
ENERGY (EV)

Figure 27

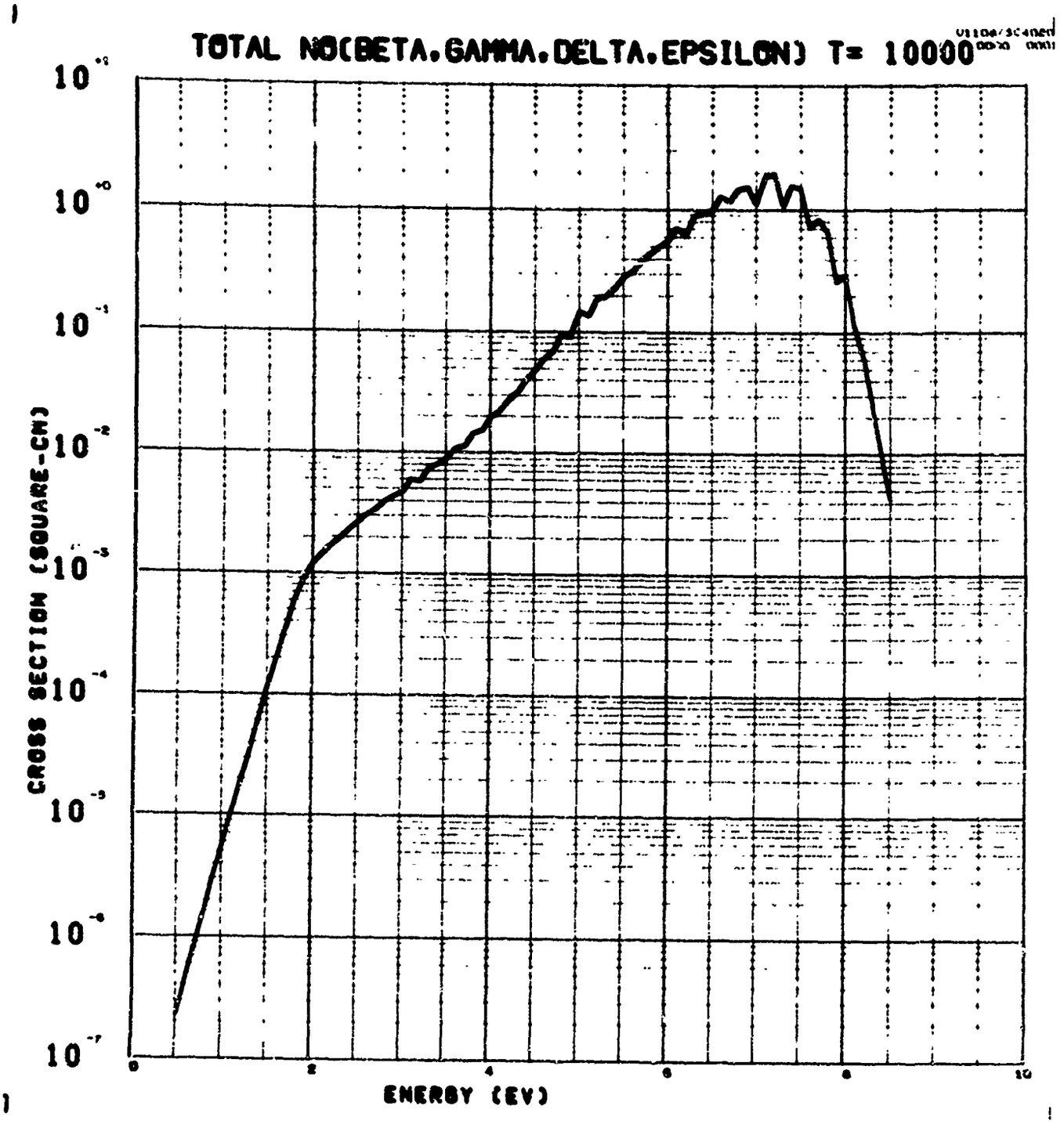
TOTAL NO(BETA.GAMMA.DELTA.EPSILON) T= 10000
CROSS SECTION (SQUARE-CM)
ENERGY (EV)

Figure 28

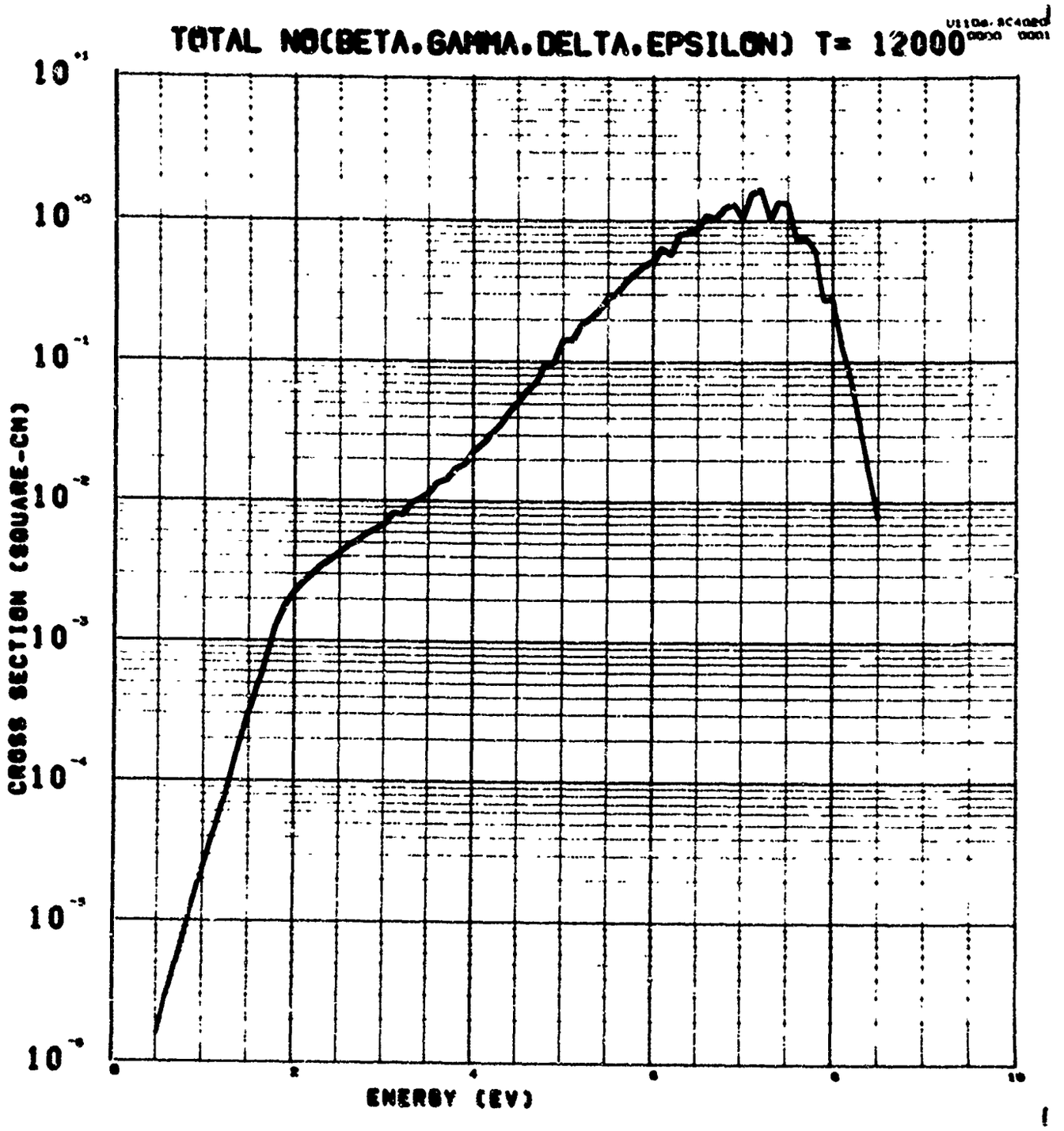
TOTAL NO(BETA.GAMMA.DELTA.EPSILON) T= 12000
CROSS SECTION (SQUARE-CM)
ENERGY (EV)

Figure 29

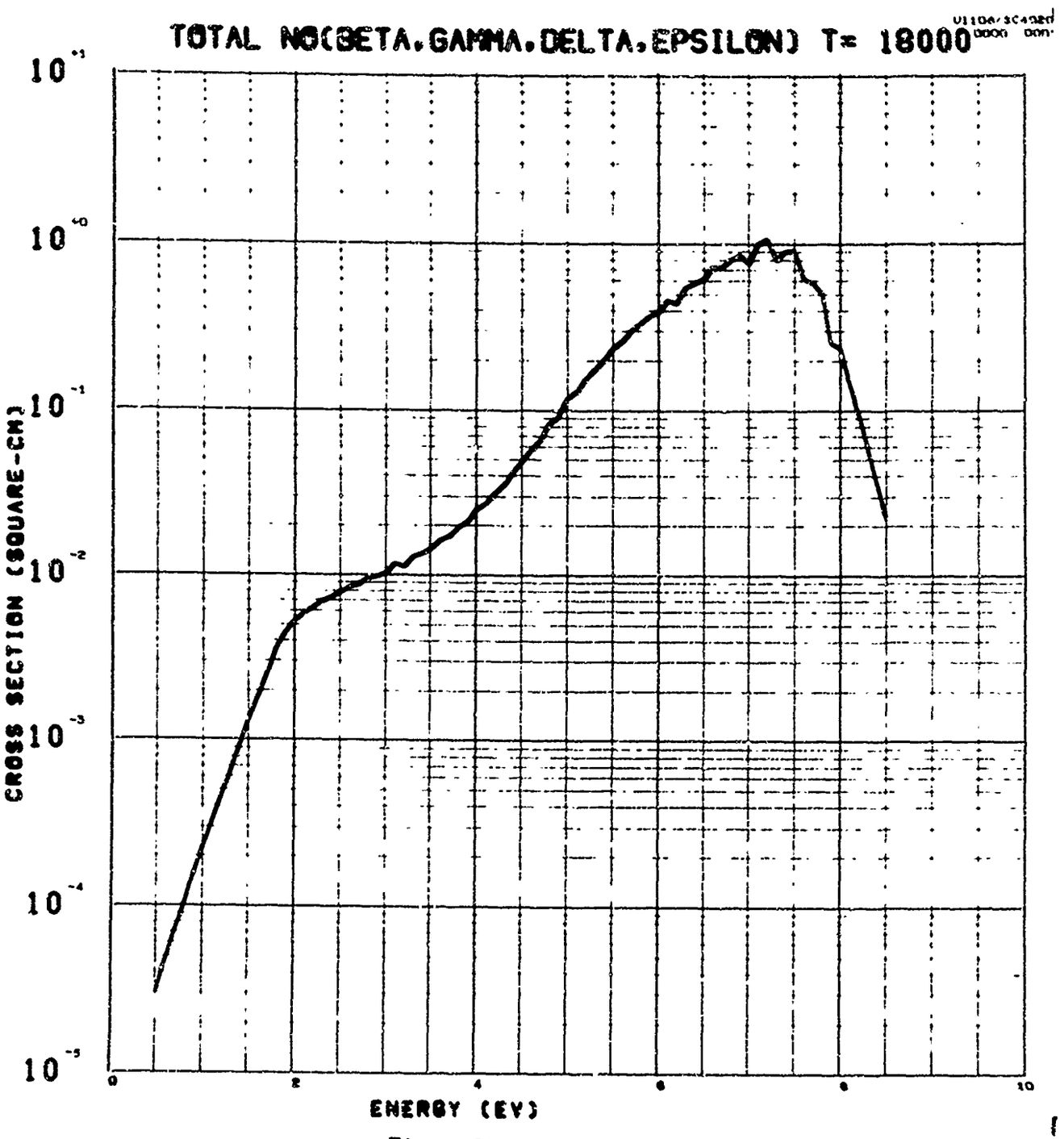
TOTAL NO(BETA,GAMMA,DELTA,EPSILON) T= 18000
CROSS SECTION (SQUARE-CM)
ENERGY (EV)
0
2
4
6
8
10

Figure 30

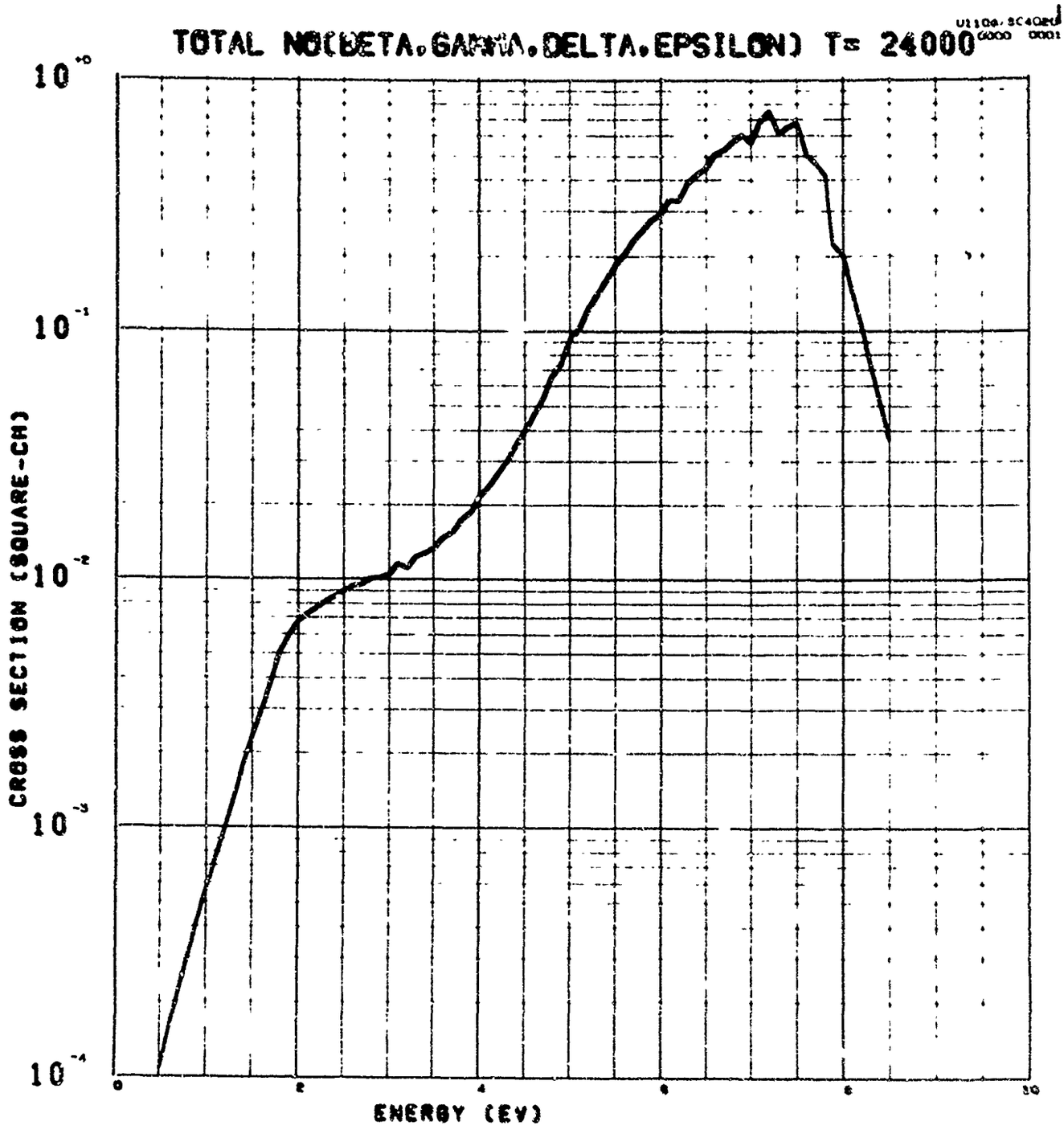
TOTAL NO(BETA.GAMMA.DELTA.EPSILON) T= 24000
CROSS SECTION (SQUARE-CM)
ENERGY (EV)

Figure 31

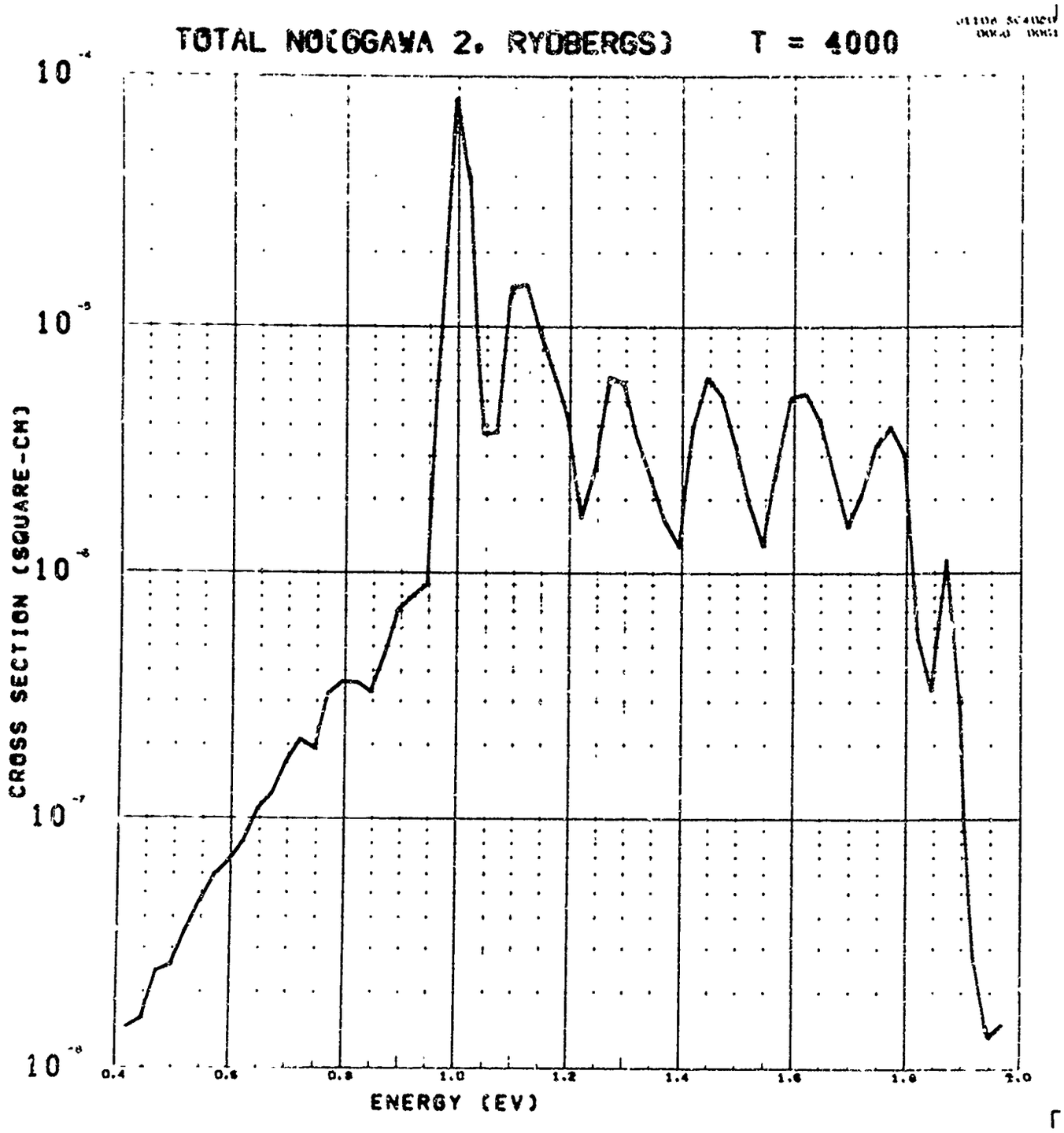
TOTAL NOIOGAWA 2. RYDBERGS) T = 4000
CROSS SECTION (SQUARE-CM)
ENERGY (EV)
0.4
0.6
0.8
1.0
1.2
1.4
1.6
1.8
2.0

Figure 32

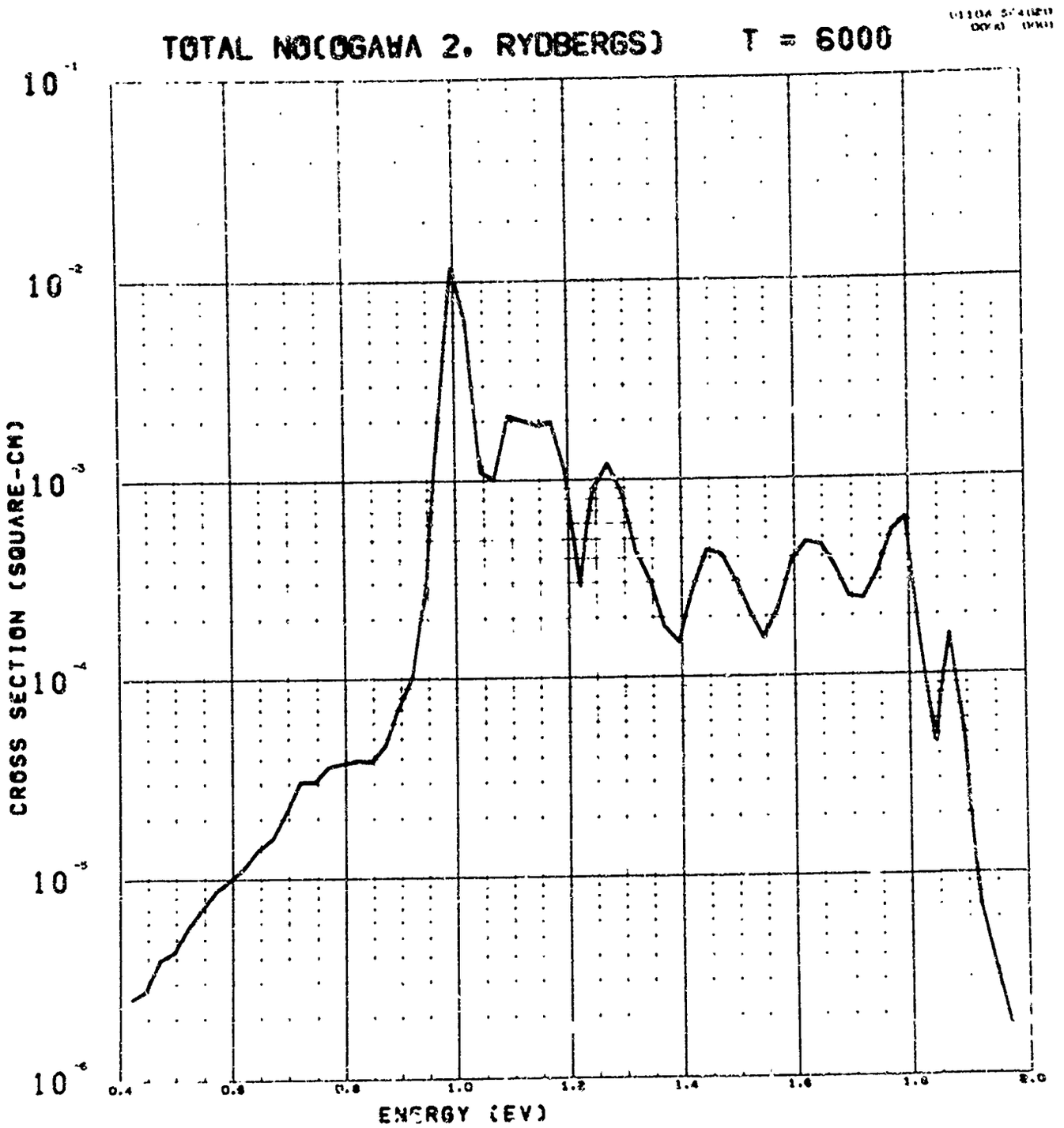
TOTAL NO(OGAWA 2. RYDBERGS) T = 6000
CROSS SECTION (SQUARE-CM)
ENERGY (EV)
10^-1
10^-2
10^-3
10^-4
10^-5
10^-6
0.4
0.6
0.8
1.0
1.2
1.4
1.6
1.8
2.0

Figure 33

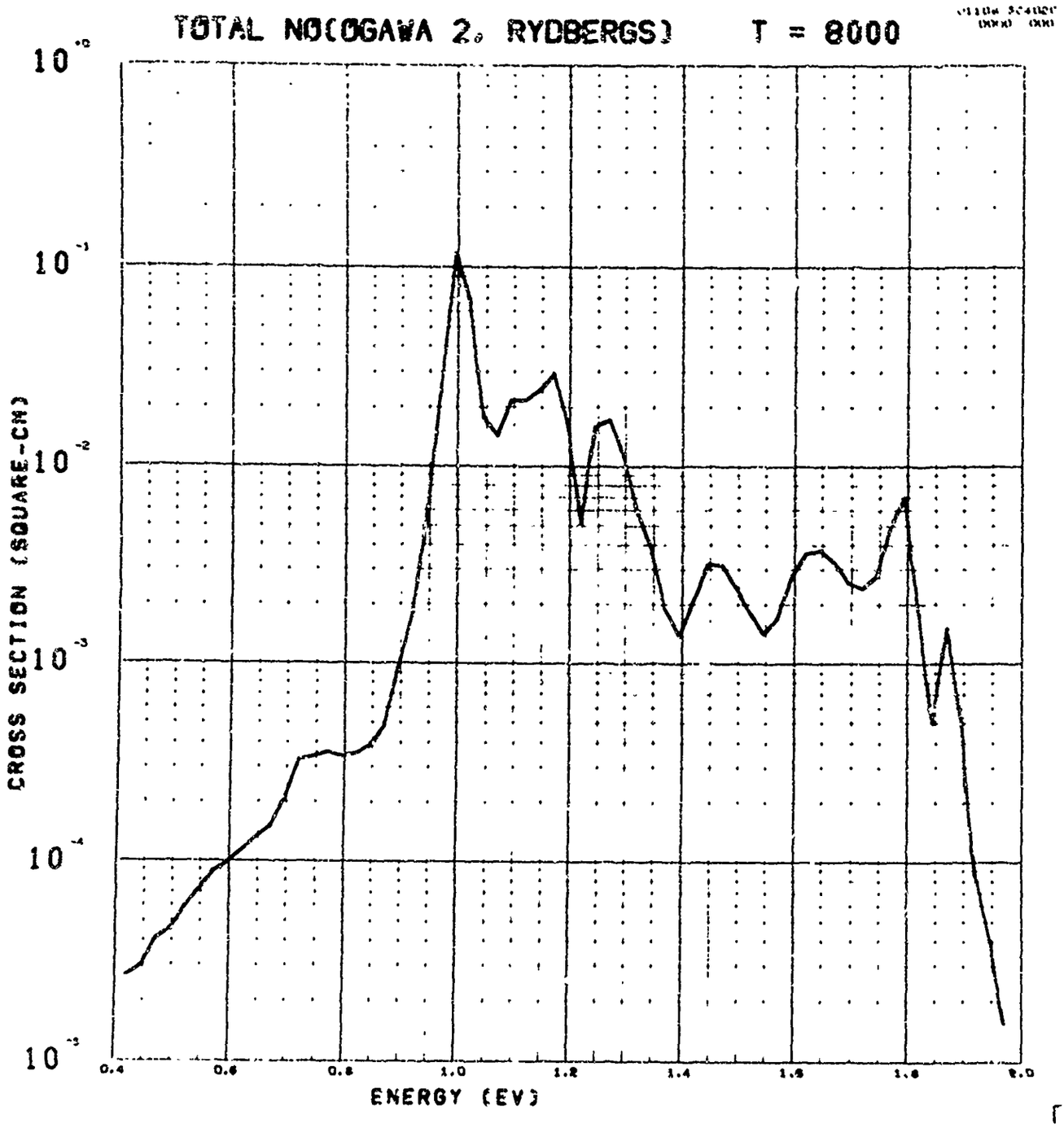
TOTAL NO(OGAWA 2. RYDBERGS) T = 8000
CROSS SECTION (SQUARE-CM)
ENERGY (EV)
0.4
0.6
0.8
1.0
1.2
1.4
1.6
1.8
2.0

Figure 34

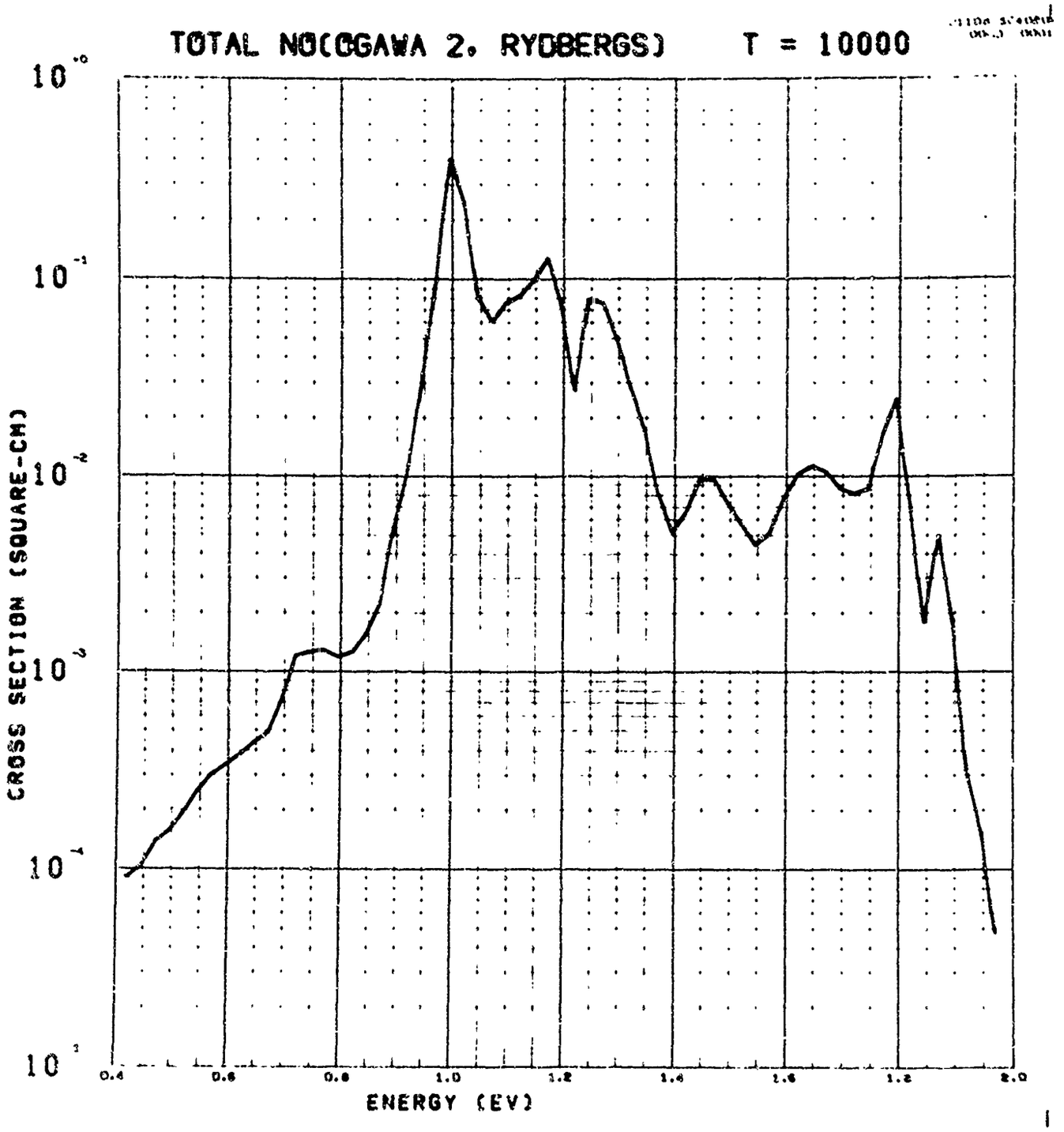
TOTAL NO(OGAWA 2. RYDBERGS) T = 10000
CROSS SECTION (SQUARE-CM)
ENERGY (EV)

Figure 35

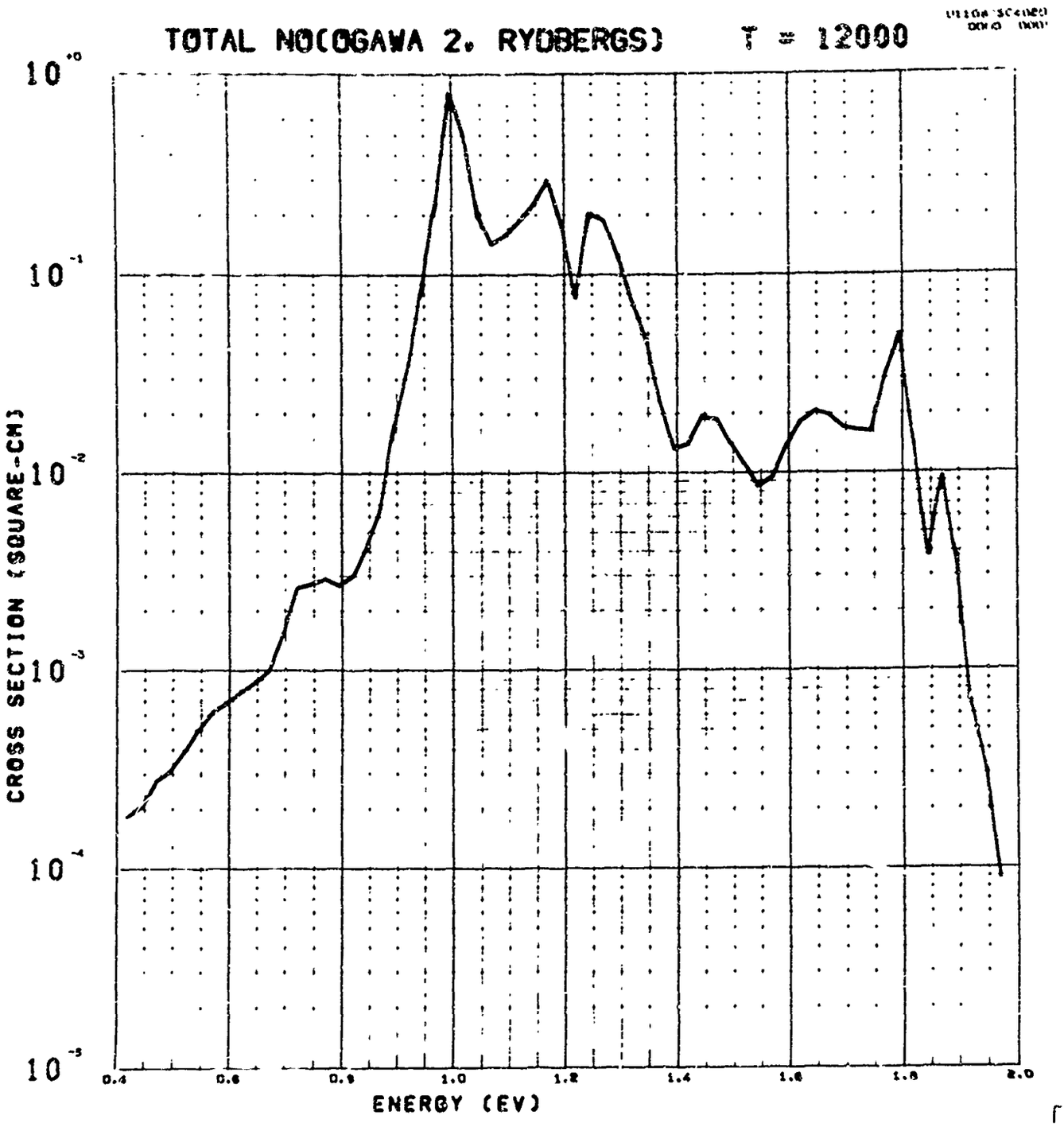
TOTAL NO(OGAWA 2. RYDBERGS)
T = 12000
CROSS SECTION (SQUARE-CM)
ENERGY (EV)
0.4
0.6
0.8
1.0
1.2
1.4
1.6
1.8
2.0

Figure 36

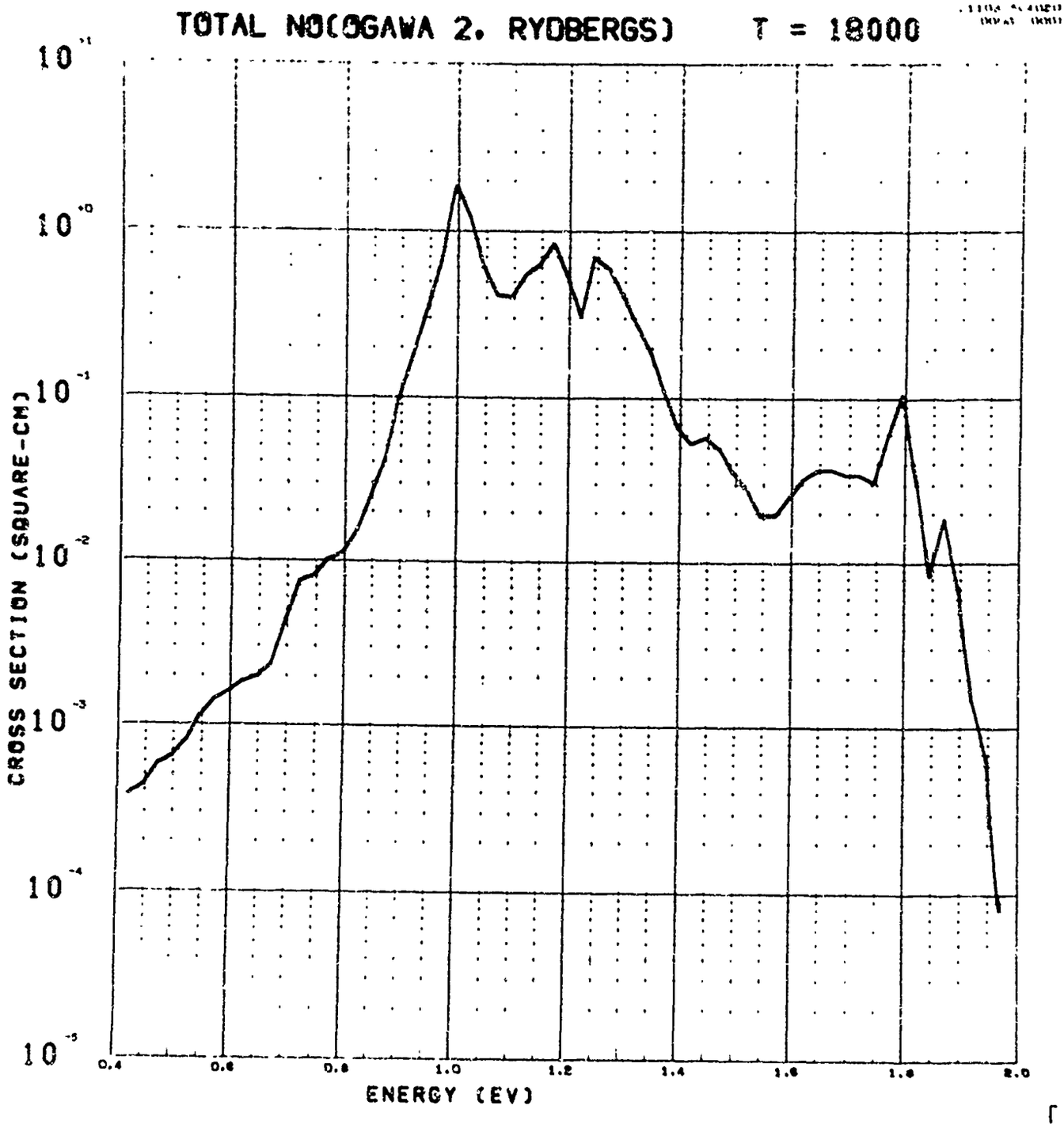
TOTAL NO(OGAWA 2. RYDBERGS)
T = 18000
CROSS SECTION (SQUARE-CM)
ENERGY (EV)
0.4
0.6
0.8
1.0
1.2
1.4
1.6
1.8
2.0

Figure 37

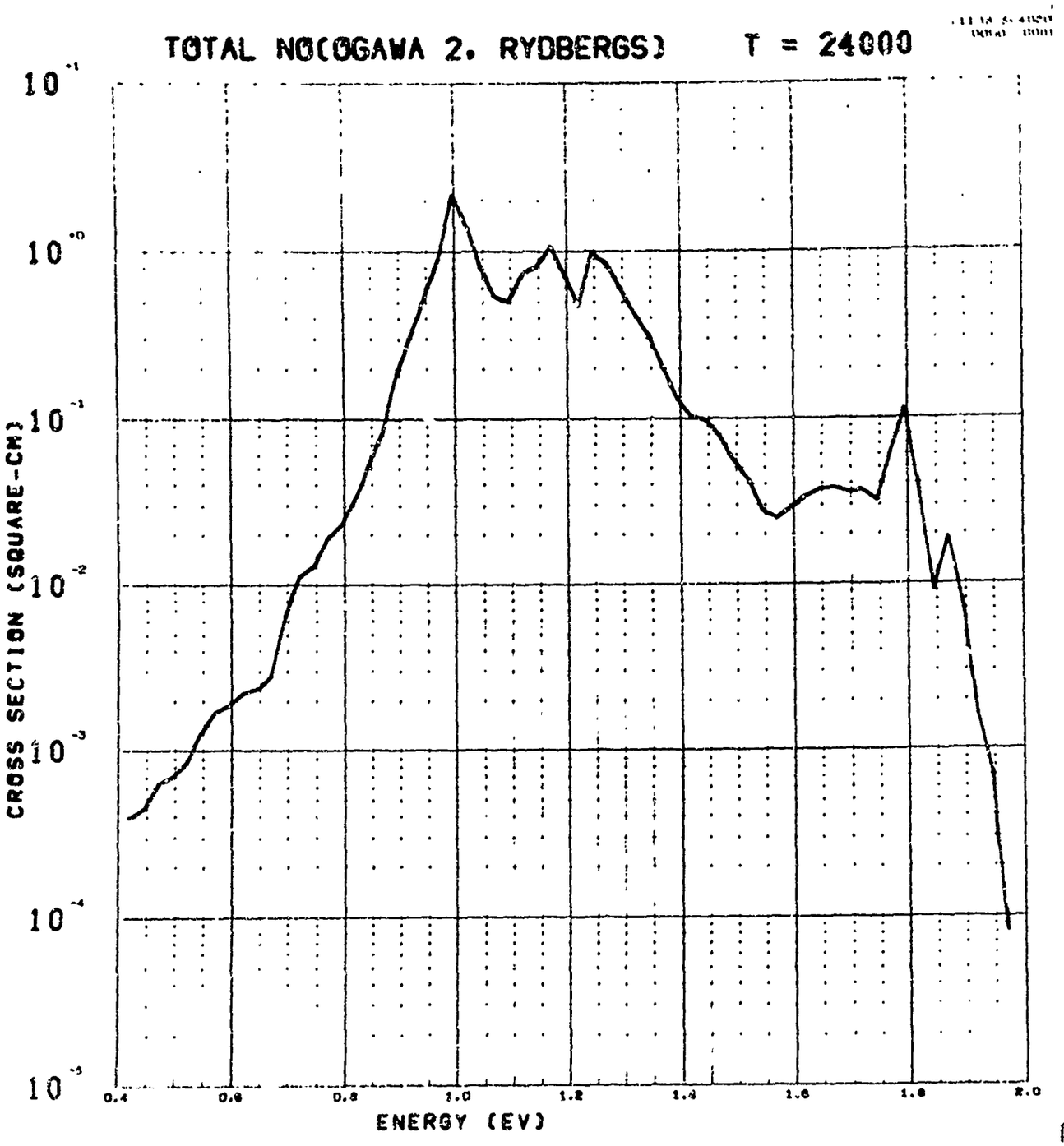
TOTAL NO(OGAWA 2. RYDBERGS)
T = 24000
CROSS SECTION (SQUARE-CM)
ENERGY (EV)
0.4
0.6
0.8
1.0
1.2
1.4
1.6
1.8
2.0

Figure 38

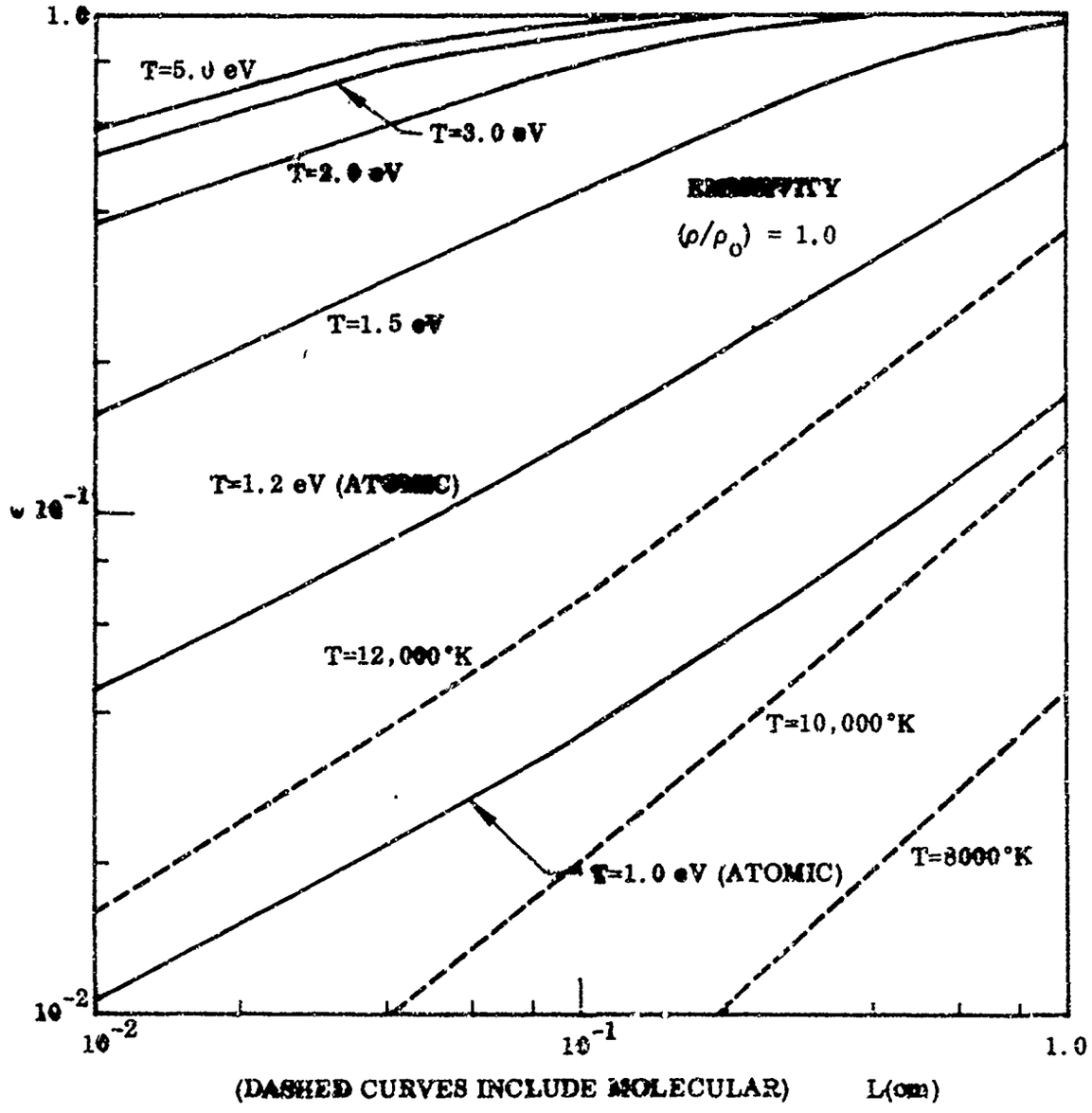
1.0
T=5.0 eV
T=3.0 eV
T=2.0 eV
(ρ/ρ_0) = 1.0
T=1.5 eV
T=1.2 eV (ATOMIC)
10^{-1}
T=12,000°K
T=10,000°K
T=1.0 eV (ATOMIC)
T=8000°K
10^{-2}
10^{-2}
10^{-1}
1.0
(DASHED CURVES INCLUDE MOLECULAR)
L(cm)

Figure 39

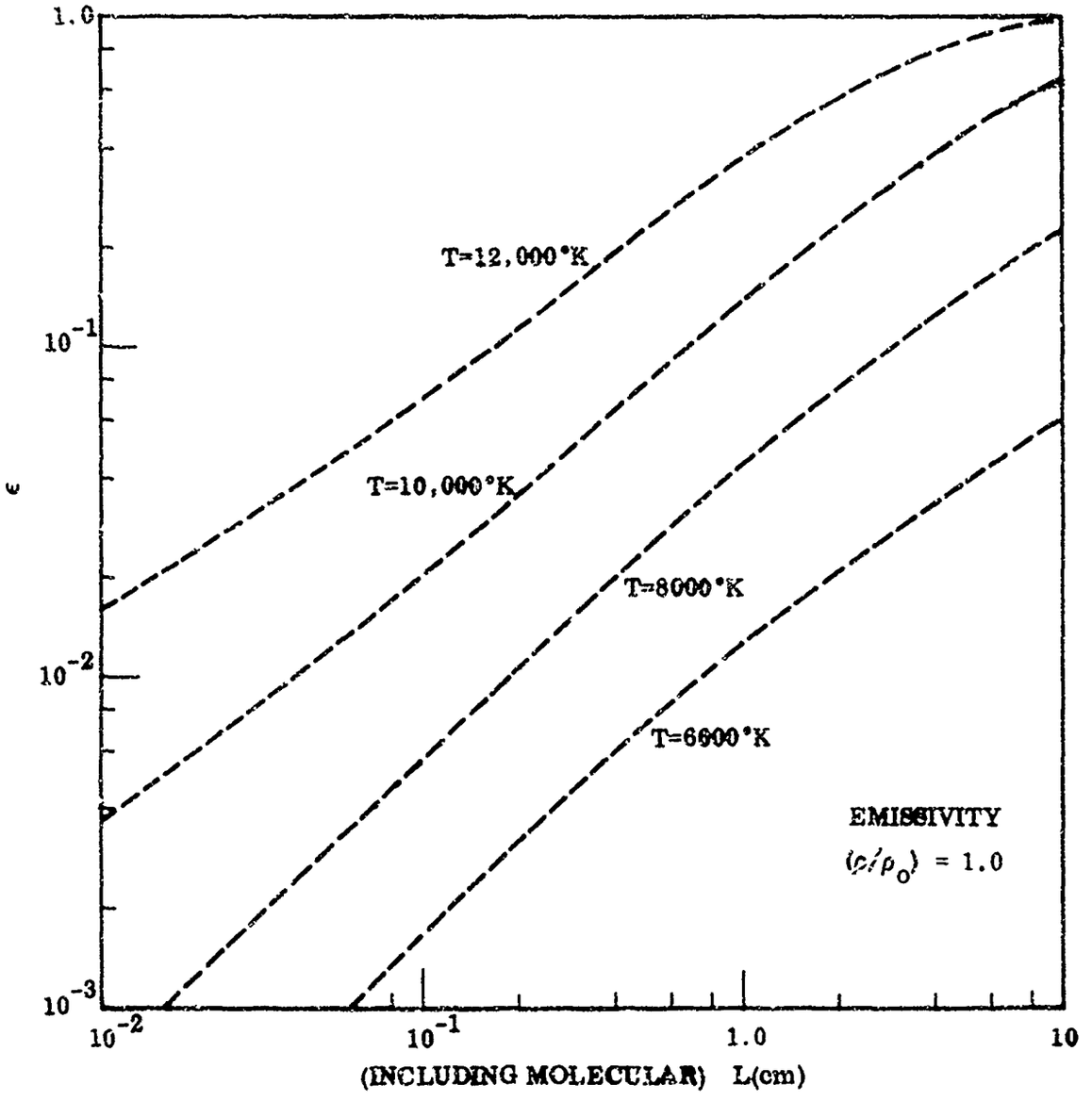
1.0
10^{-1}
10^{-2}
10^{-3}
ε
T=12,000°K
T=10,000°K
T=8000°K
T=6600°K
EMISSIVITY
(ρ/ρ_o) = 1.0
10^{-2}
10^{-1}
1.0
10
(INCLUDING MOLECULAR) L(cm)

Figure 40

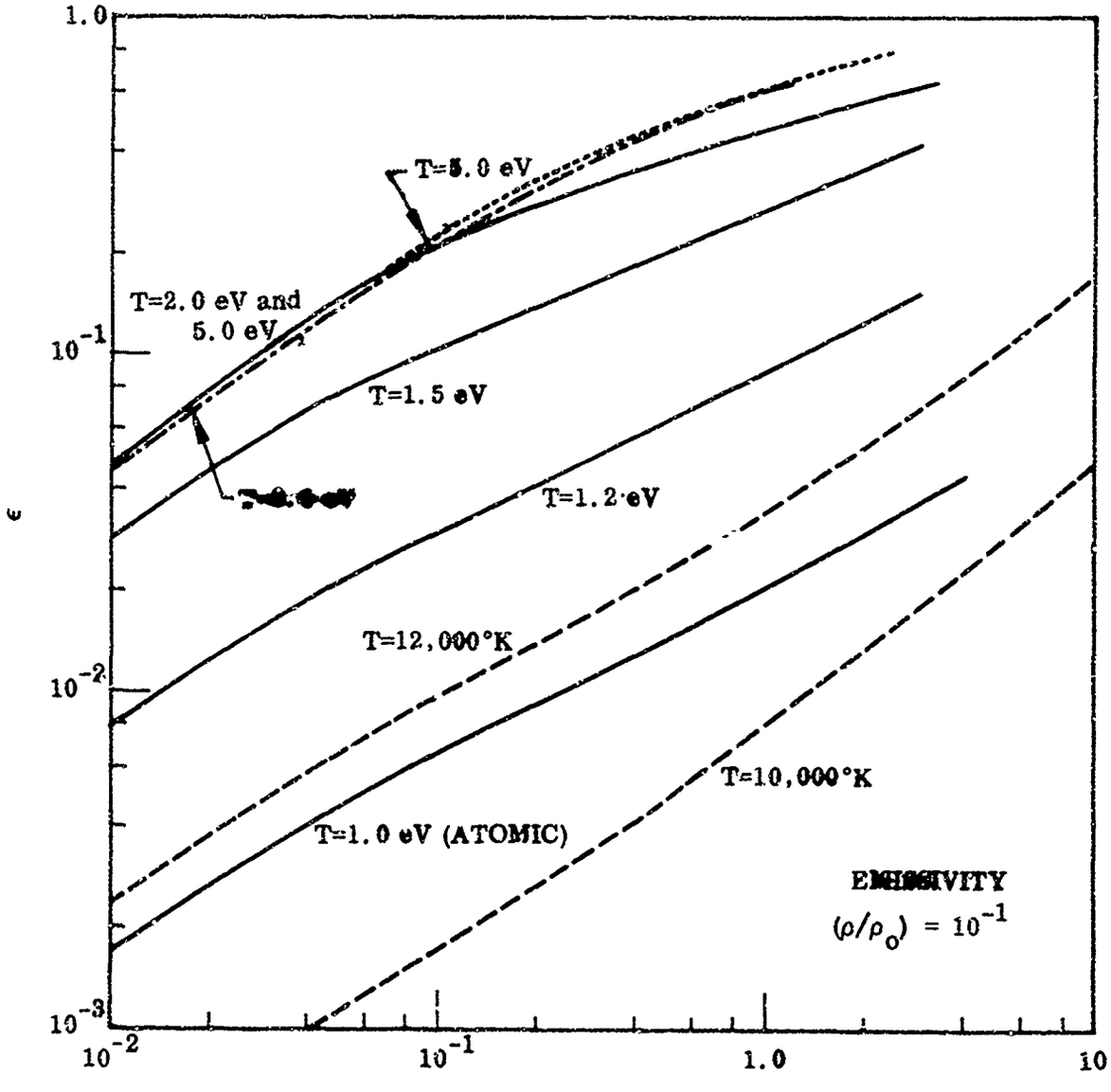
1.0
10^{-1}
10^{-2}
10^{-3}
10^{-2}
10^{-1}
1.0
10
ε
T=5.0 eV
T=2.0 eV and
5.0 eV
T=1.5 eV
T=1.2 eV
T=12,000°K
T=10,000°K
T=1.0 eV (ATOMIC)
EMISSIVITY
$(\rho/\rho_o) = 10^{-1}$
(DASHED CURVES INCLUDE MOLECULAR) L(cm)

Figure 41

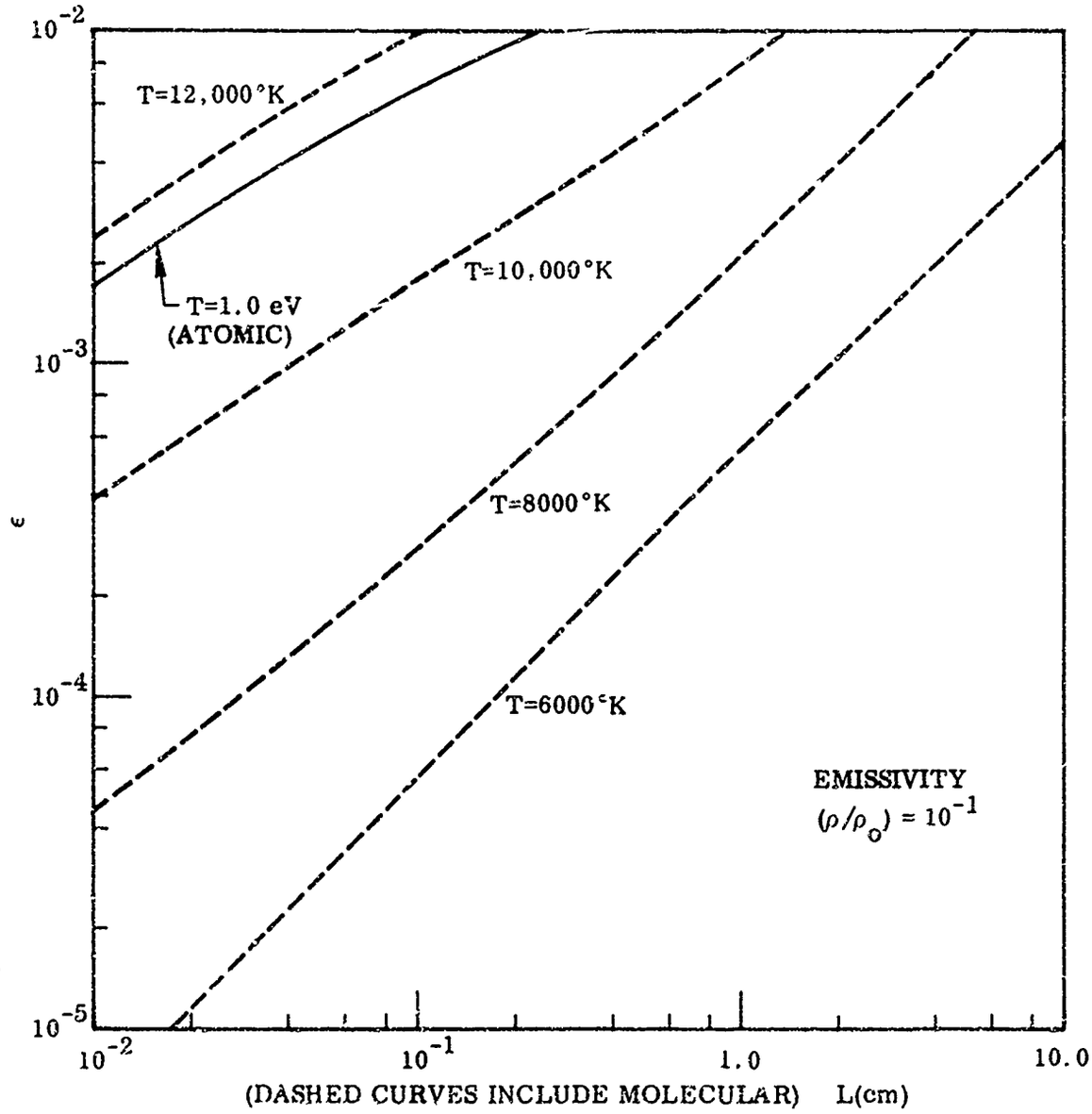
10^{-2}
10^{-3}
10^{-4}
10^{-5}
ε
T=12,000°K
T=1.0 eV
(ATOMIC)
T=10,000°K
T=8000°K
T=6000°K
EMISSIVITY
$(\rho/\rho_o) = 10^{-1}$
10^{-2}
10^{-1}
1.0
10.0
(DASHED CURVES INCLUDE MOLECULAR) L(cm)

Figure 42

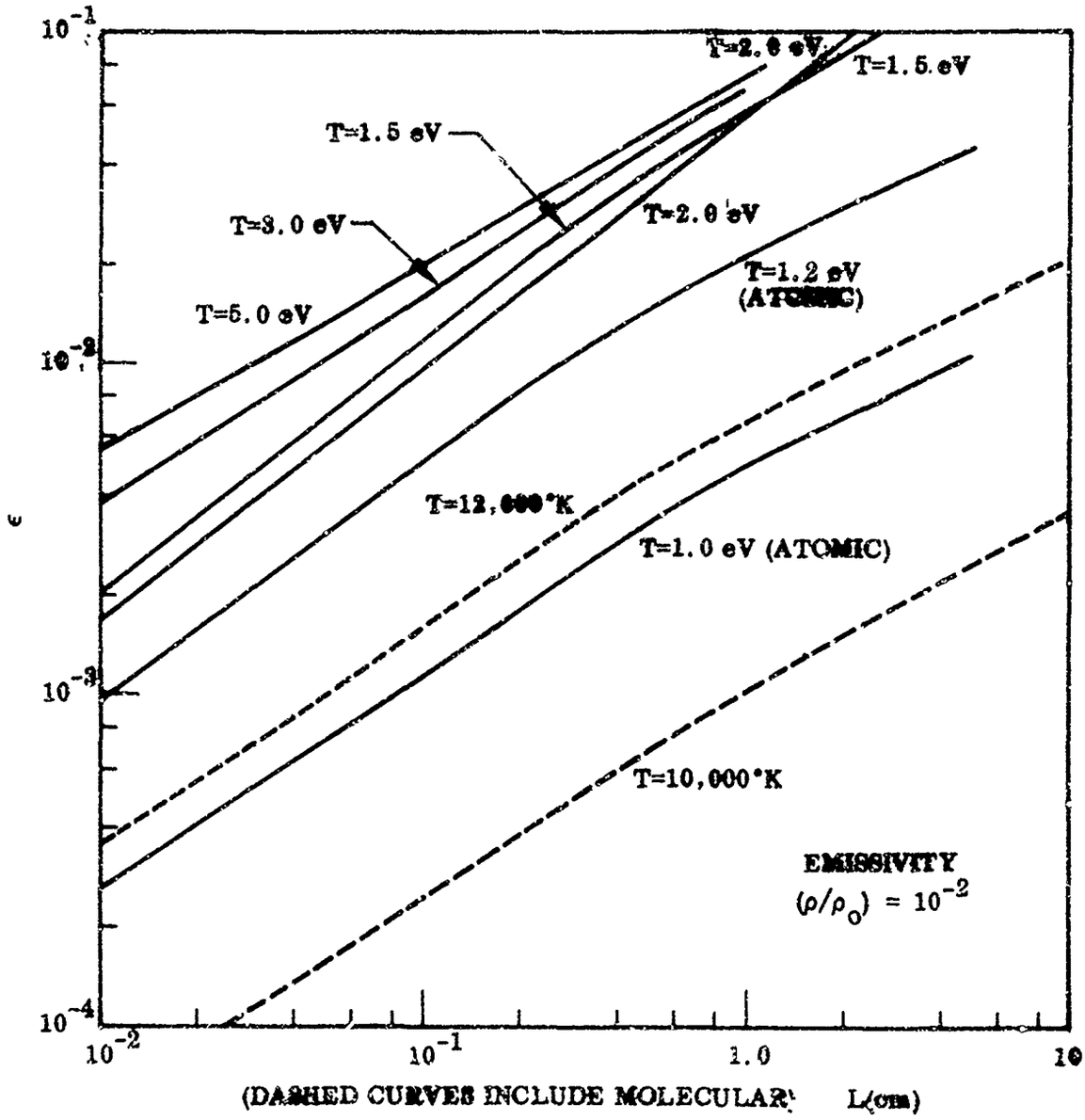
10^{-1}
10^{-2}
10^{-3}
10^{-4}
ε
T=2.0 eV
T=1.5 eV
T=1.5 eV
T=3.0 eV
T=2.0 eV
T=5.0 eV
T=1.2 eV
(ATOMIC)
T=12,000°K
T=1.0 eV (ATOMIC)
T=10,000°K
EMISSIVITY
$(\rho/\rho_o) = 10^{-2}$
10^{-2}
10^{-1}
1.0
10
(DASHED CURVES INCLUDE MOLECULAR
L(cm)

Figure 43

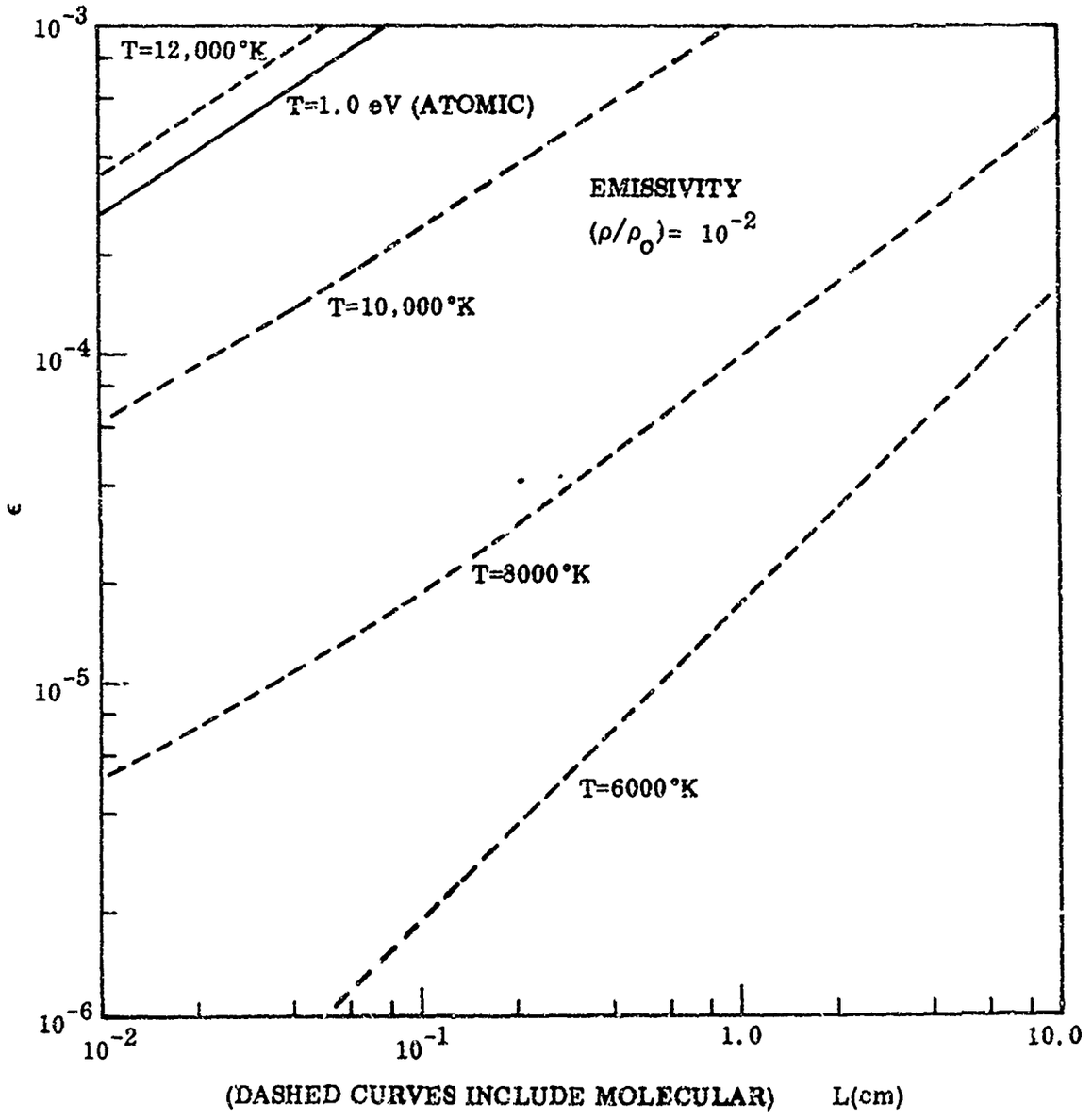
10^{-3}
10^{-4}
10^{-5}
10^{-6}
ϵ
T=12,000°K
T=1.0 eV (ATOMIC)
EMISSIVITY
$(\rho/\rho_o)= 10^{-2}$
T=10,000°K
T=8000°K
T=6000°K
10^{-2}
10^{-1}
1.0
10.0
(DASHED CURVES INCLUDE MOLECULAR)
L(cm)

Figure 44

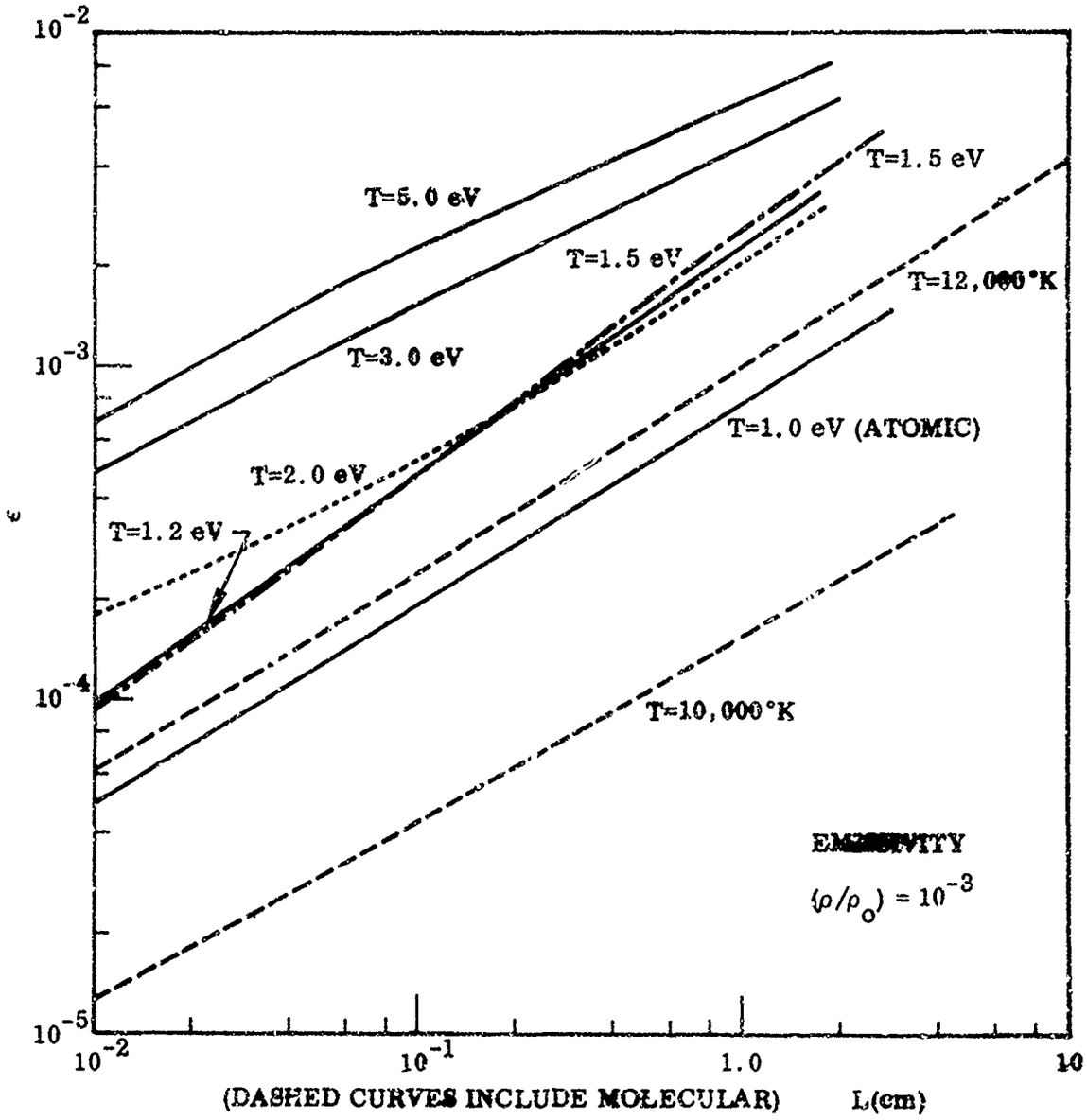
10^{-2}
10^{-3}
10^{-4}
10^{-5}
ϵ
T=5.0 eV
T=1.5 eV
T=3.0 eV
T=1.5 eV
T=12,000°K
T=2.0 eV
T=1.2 eV
T=1.0 eV (ATOMIC)
T=10,000°K
EMISSIVITY
$(\rho/\rho_o) = 10^{-3}$
10^{-2}
10^{-1}
1.0
10
(DASHED CURVES INCLUDE MOLECULAR)
L(cm)

Figure 45

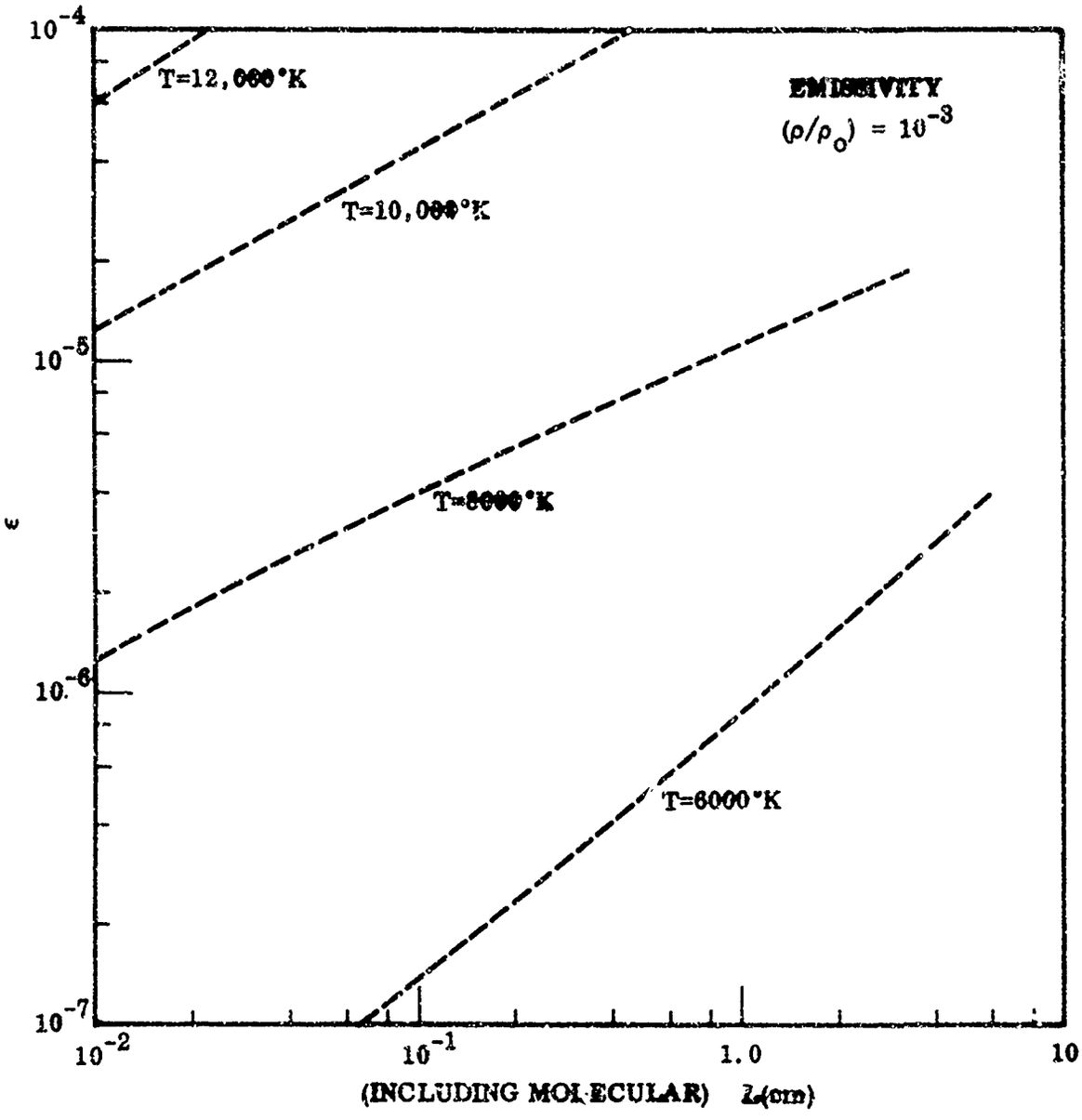
10^{-4}
10^{-5}
10^{-6}
10^{-7}
ε
T=12,000°K
T=10,000°K
T=8000°K
T=6000°K
EMISSIVITY
$(\rho/\rho_o) = 10^{-3}$
10^{-2}
10^{-1}
1.0
10
(INCLUDING MOLECULAR) λ(cm)

Figure 46

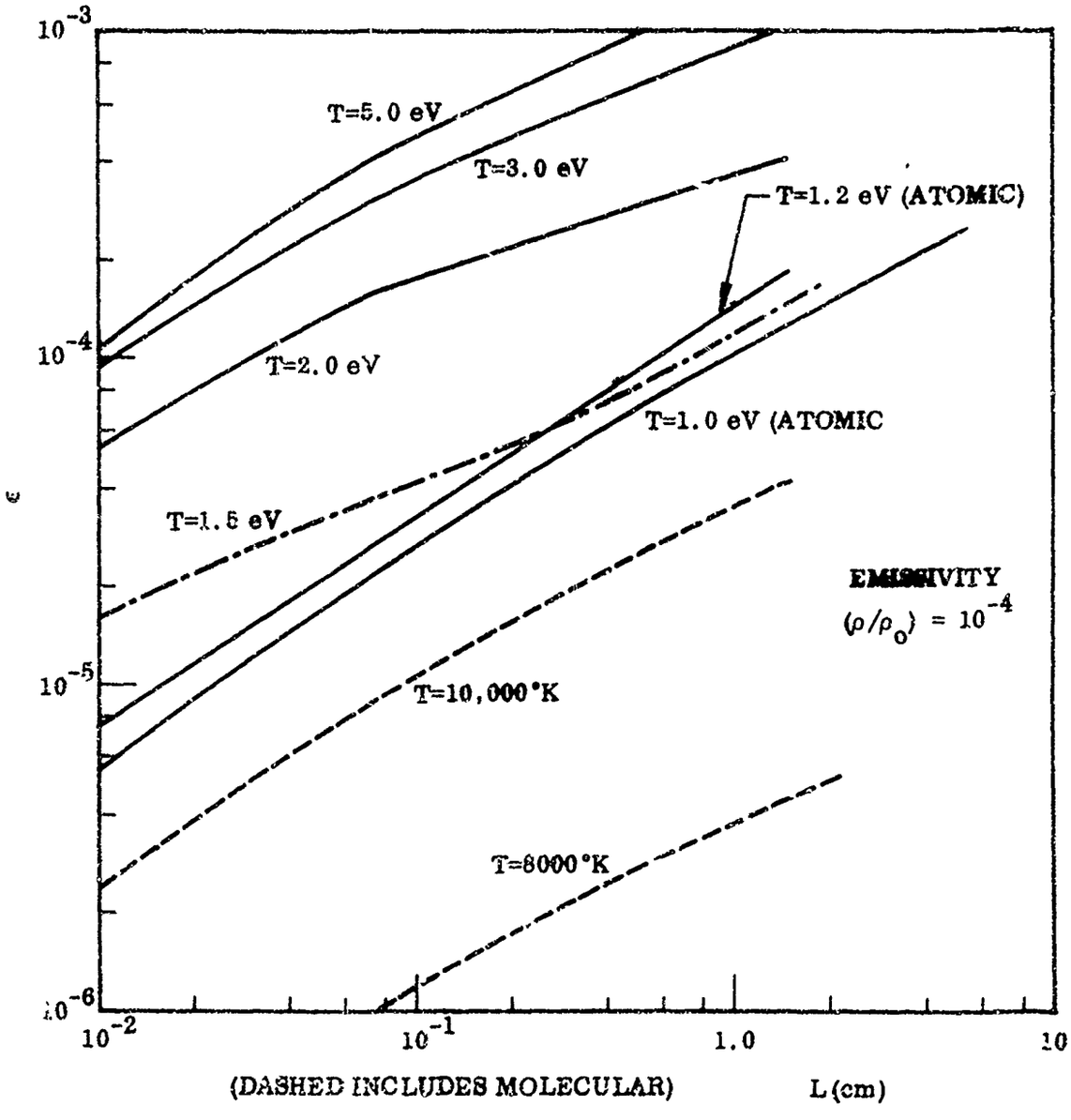
10^{-3}
10^{-4}
10^{-5}
10^{-6}
10^{-2}
10^{-1}
1.0
10
T=5.0 eV
T=3.0 eV
T=1.2 eV (ATOMIC)
T=2.0 eV
T=1.0 eV (ATOMIC
T=1.5 eV
EMISSIVITY
$(\rho/\rho_o) = 10^{-4}$
T=10,000°K
T=8000°K
(DASHED INCLUDES MOLECULAR)
L(cm)

Figure 47

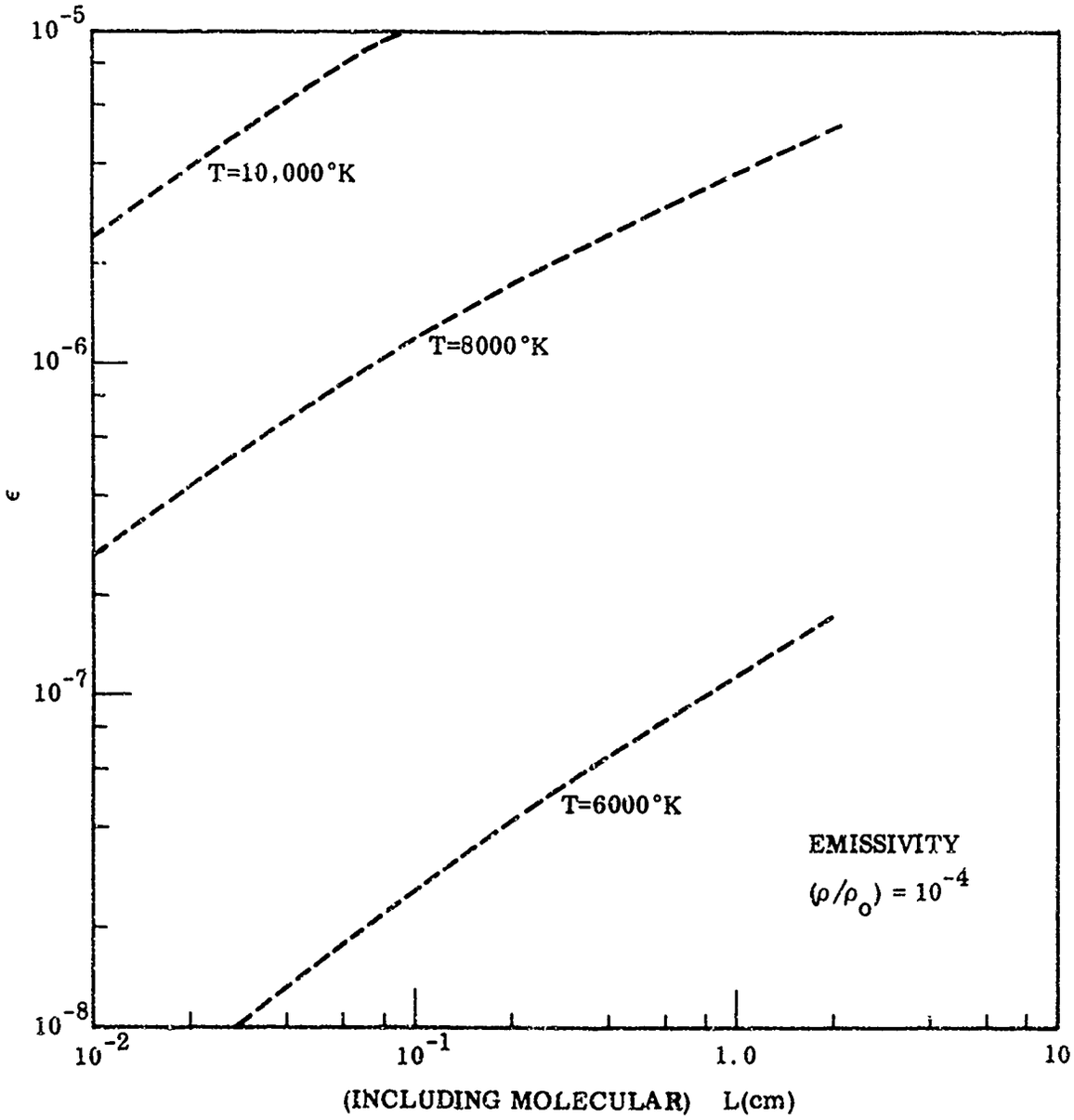
10^{-5}
10^{-6}
10^{-7}
10^{-8}
ϵ
T=10,000°K
T=8000°K
T=6000°K
EMISSIVITY
$(\rho/\rho_o) = 10^{-4}$
10^{-2}
10^{-1}
1.0
10
(INCLUDING MOLECULAR) L(cm)

Figure 48

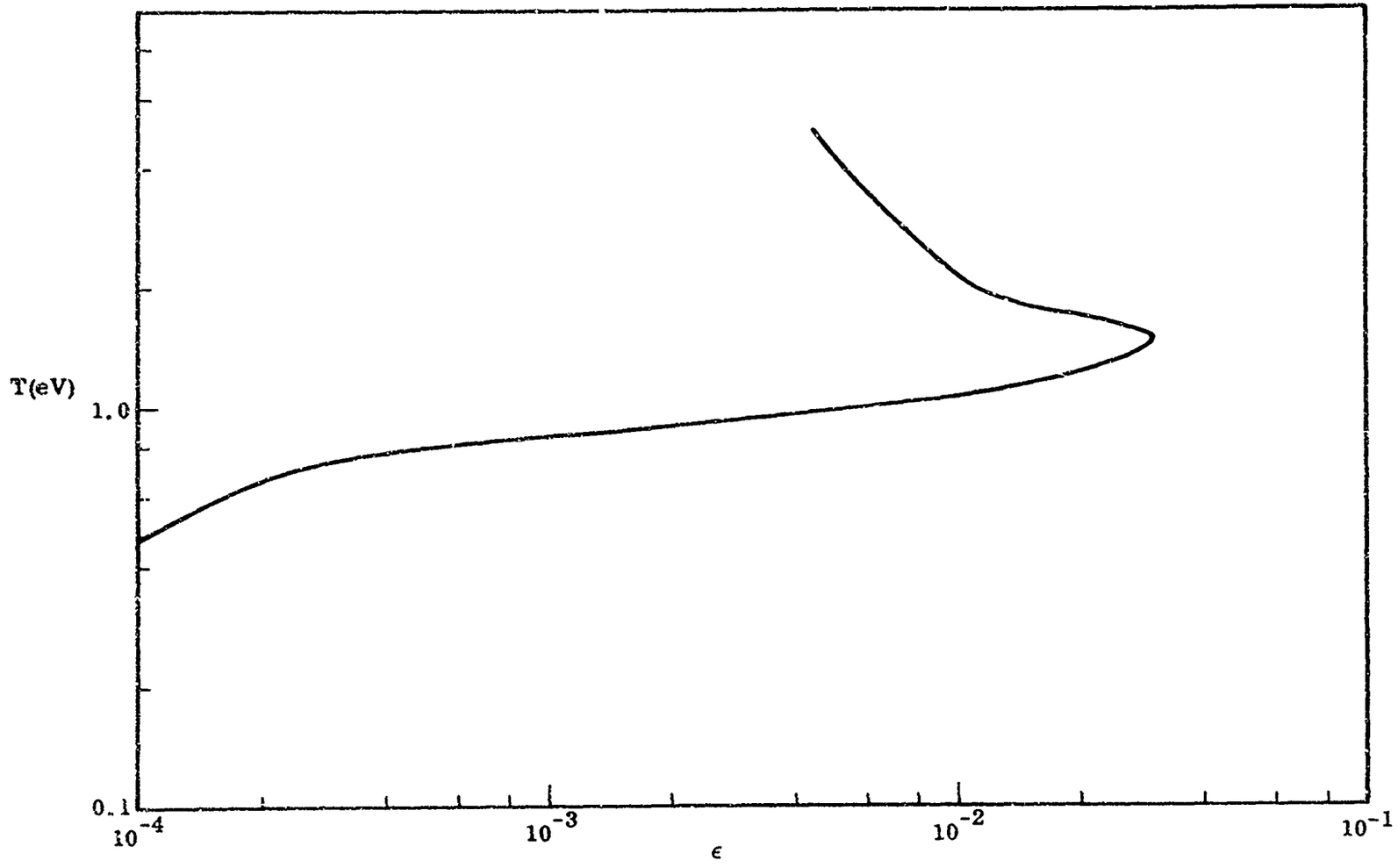

Fig. 49 Emissivity vs. Temperature at Pressure Balance (1.0 atmos.) (L = 1.0 cm)

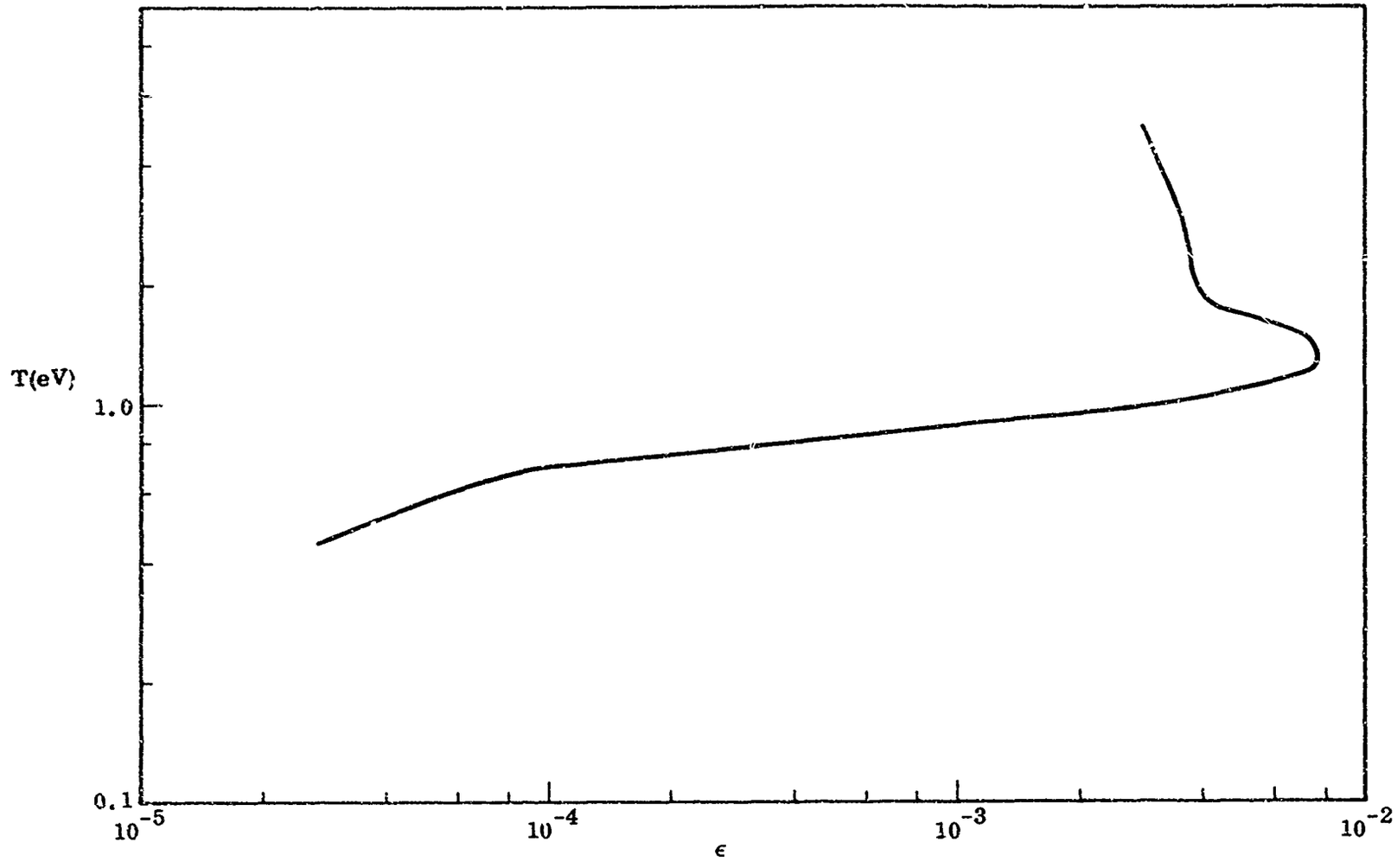

Fig. 50 Emissivity vs. Temperature at Pressure Balance (0.5 atmos.) (L = 1.0 cm)

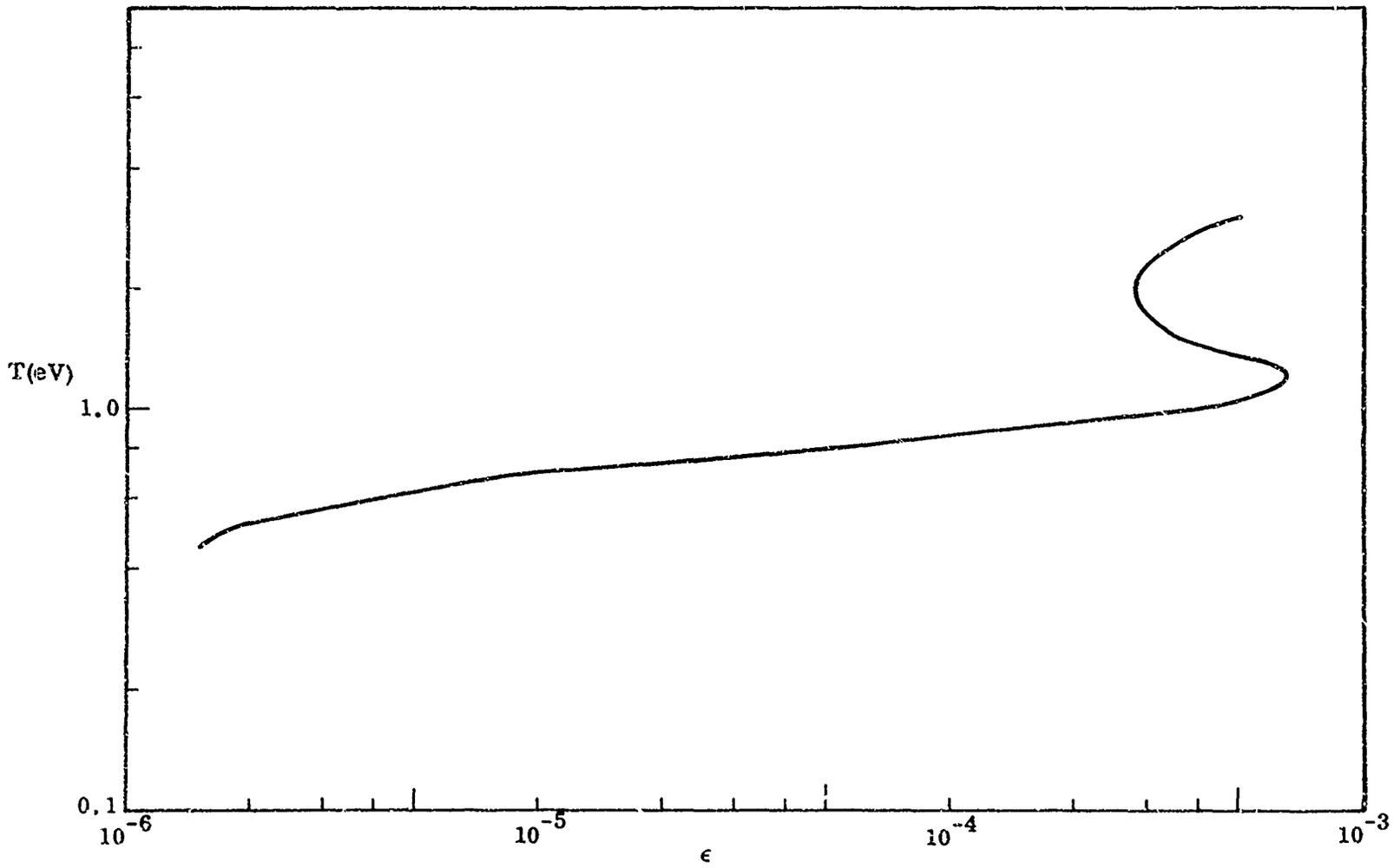

Fig. 51 Emissivity vs. Temperature at Pressure Balance (0.1 atmos.) (L = 1.0 cm)

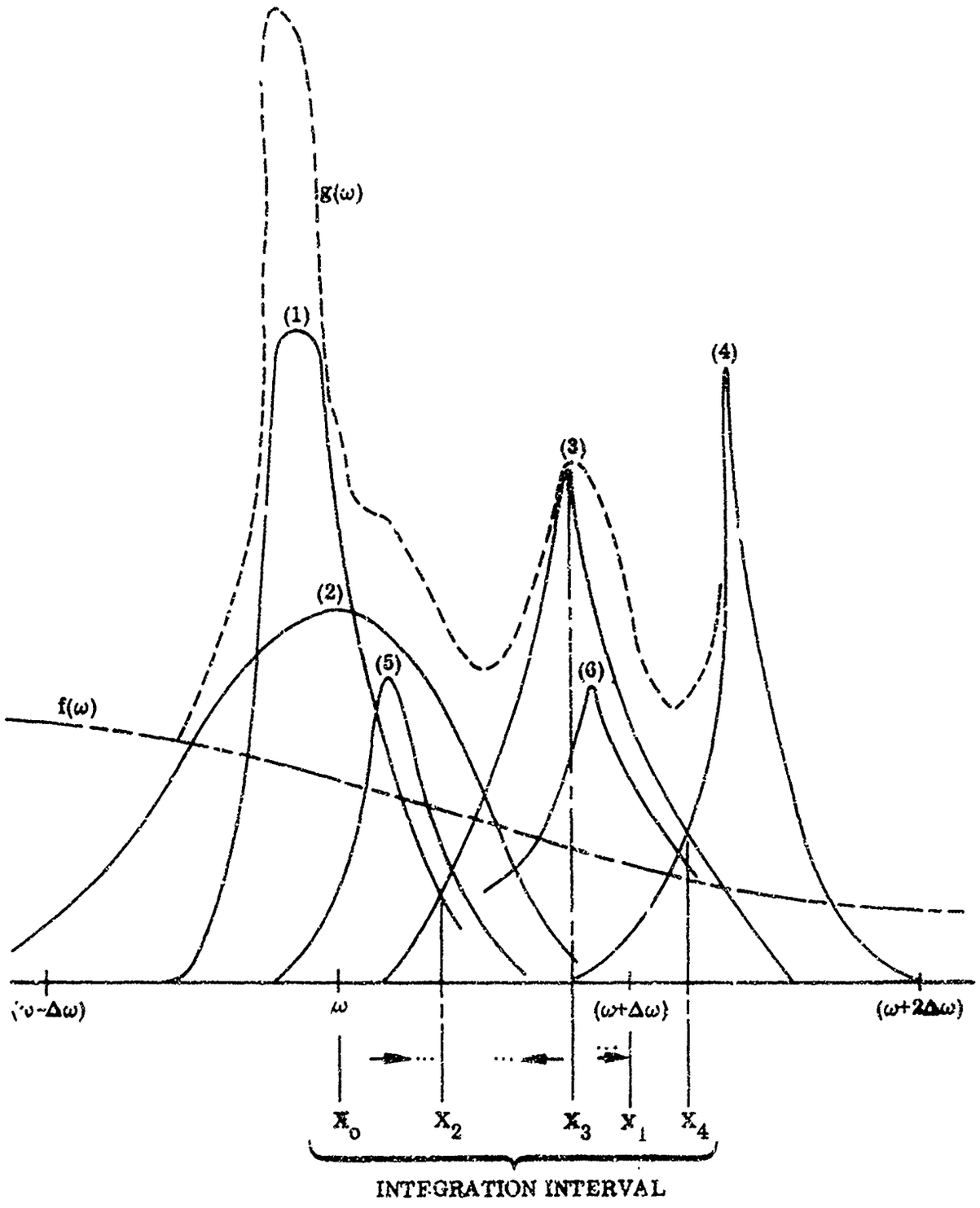
g(ω)
(1)
(2)
(3)
(4)
(5)
(6)
f(ω)
(ω-Δω)
ω
(ω+Δω)
(ω+2Δω)
X0
X2
X3
X1
X4
INTEGRATION INTERVAL

Figure 52

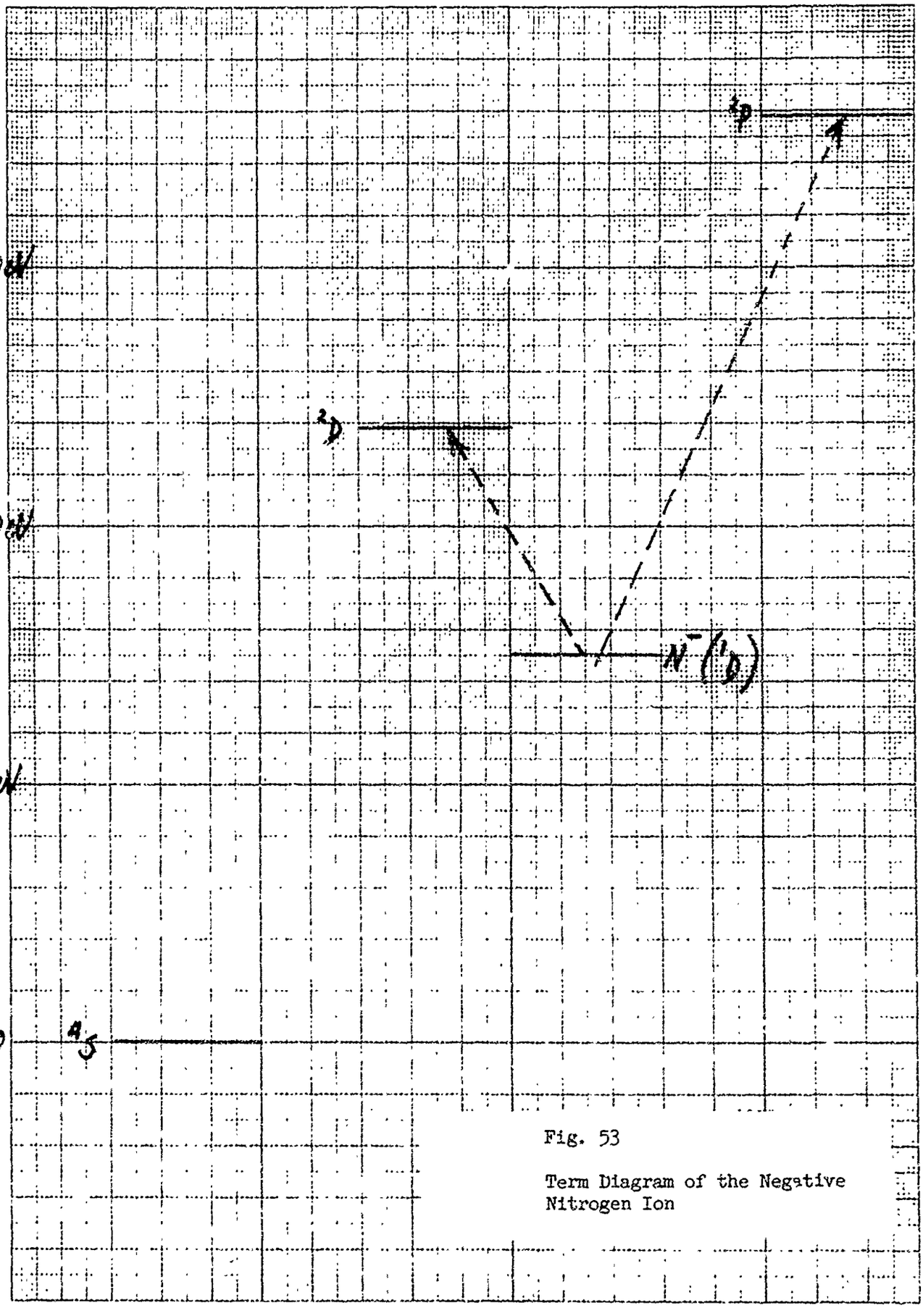

Fig. 53

Term Diagram of the Negative Nitrogen Ion

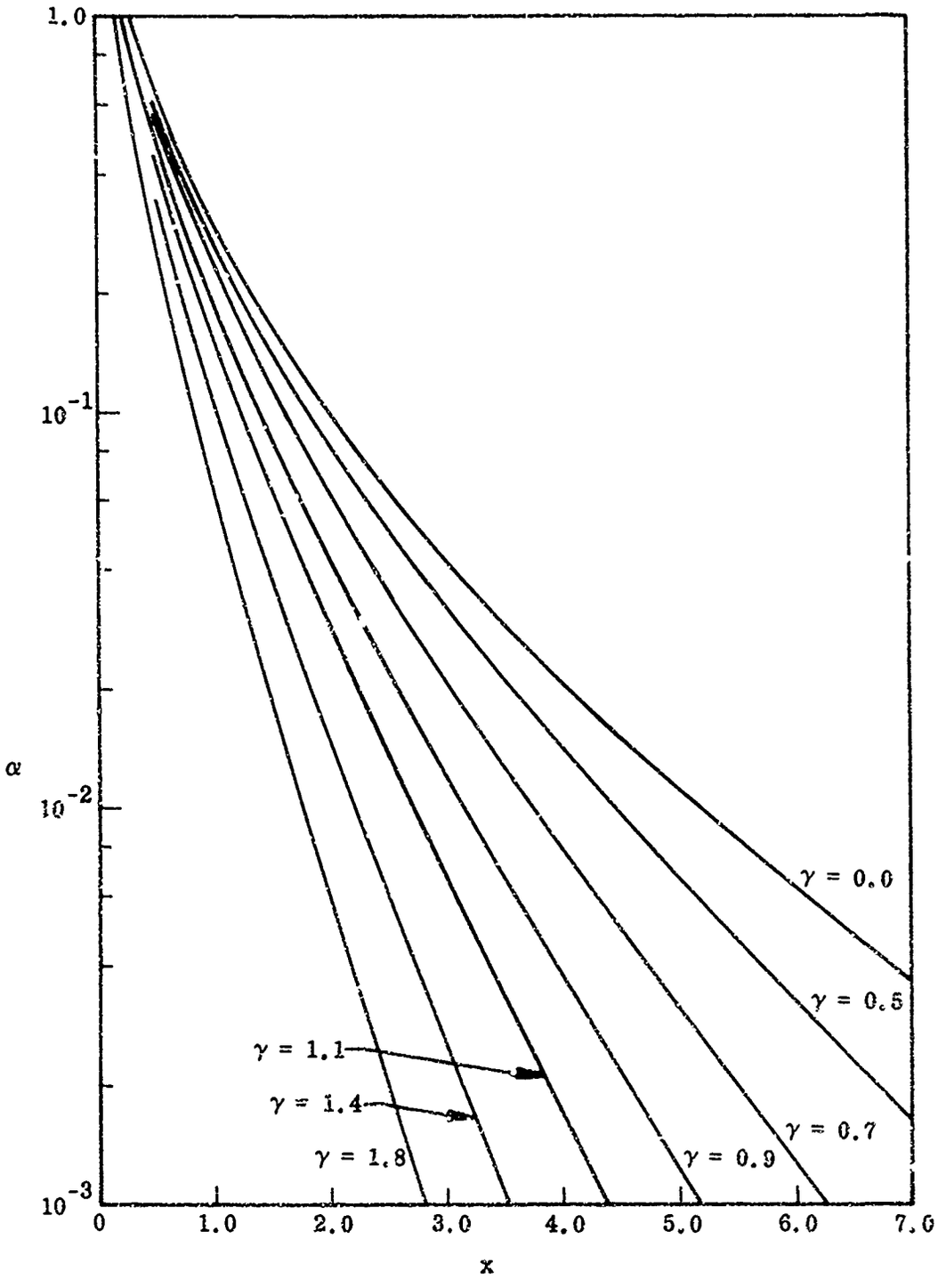

Fig. 54 $\alpha(x, \gamma)$ Wing Thermal Gaunt Factor (Eq. 31)

UNCLASSIFIED
Security Classification

DOCUMENT CONTROL DATA - R & D

(Security classification of title, body of abstract and indexing annotation must be entered when the overall report is classified)

1. ORIGINATING ACTIVITY *(Corporate author)*
Lockheed Palo Alto Research Laboratory
Palo Alto, California

2a. REPORT SECURITY CLASSIFICATION
Unclassified

2b. GROUP

3. REPORT TITLE
Atomic Line Transitions and Radiation from High Temperature Air

4. DESCRIPTIVE NOTES *(Type of report and inclusive dates)*
Annual Report - 15 June 1969 - 15 June 1970

5. AUTHOR(S) *(First name, middle initial, last name)*
Robert R. Johnston, Oscar R. Platas, and Ludwig M. Tannenwald

6. REPORT DATE	7a. TOTAL NO. OF PAGES	7b. NO. OF REFS
1970 July 15	139	60

8a. CONTRACT OR GRANT NO.	9a. ORIGINATOR'S REPORT NUMBER(S)
N00014-68-C-0481	LMSC-N-3L-70-1
b. PROJECT NO. NR 025-390	
c. ARPA Order No. 925	9b. OTHER REPORT NO(S) *(Any other numbers that may be assigned this report)*
d.	

10. DISTRIBUTION STATEMENT
Distribution of this document is unlimited.

11. SUPPLEMENTARY NOTES	12. SPONSORING MILITARY ACTIVITY
	U. S. Office of Naval Research Washington, D. C.

13. ABSTRACT

The status of the current investigation into the radiant emission from high temperature air is described. A treatment of emission by molecular species and some new results in line broadening is included.

Results are presented for air at temperatures 0.5 to 5.0 eV and densities from 1.0 to 10^{-4} times normal.

DD FORM 1 NOV 65 1473

UNCLASSIFIED
Security Classification

14 KEY WORDS	LINK A		LINK B		LINK C	
	ROLE	WT	ROLE	WT	ROLE	WT
High Temperature Air Radiation						
Opacity						
Emissivity						